Politecnico di Milano

SCHOOL OF INDUSTRIAL AND INFORMATION ENGINEERING
Master of Science – Nuclear Engineering

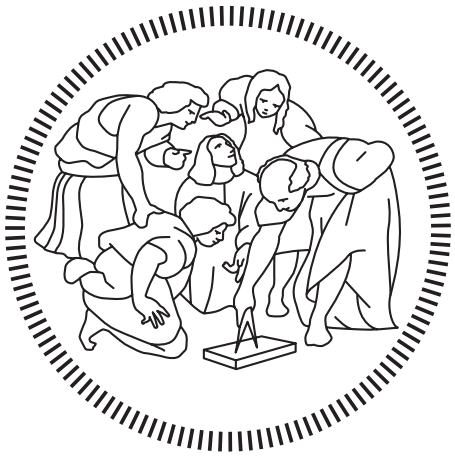

Multi-Objective Topology Optimization with Application to MSFR

Supervisor
Antonio Cammi

Co-Supervisors
Laura Savoldi
Stefano Lorenzi
Andrea Di Ronco

Candidate
LORENZO CATTONI – 920251

Academic Year 2019 – 2020

Ringraziamenti

Vorrei esprimere la mia gratitudine al professor Antonio Cammi per avermi trasmesso una profonda passione per questo corso di studi ed aver creduto in me per la realizzazione di questo progetto ambizioso dandomi costante supporto. Ringrazio inoltre la professoressa Laura Savoldi, docente del Politecnico di Torino con cui ho avuto l'opportunità di collaborare, per l' importante contributo alla realizzazione di questo lavoro. Vorrei esprimere inoltre un ringraziamento al professor Stefano Lorenzi ed Andrea Di Ronco per l'indispensabile assistenza tecnica.

Un ringraziamento speciale lo rivolgo ai miei cari amici Alberto, Gabriele, Martino, Christian e Carola che hanno sempre saputo incoraggiarmi.

Un profondo ringraziamento lo rivolgo a Davide Capra, stimato compagno di studi da cui ho imparato molto, ed i compagni Riccardo Chebac e Riccardo Giorgi per essere stati sempre presenti nel percorso universitario.

Ringrazio infine la mia famiglia che è sempre stata al mio fianco dandomi un indispensabile sostegno e credendo sempre in me.

GRAZIE

Abstract

In the last decades topology optimization is playing an increasing important role in the industrial design approach for different applications including structural mechanics, civil engineering, architecture and fluid mechanics especially in connection with aerospace applications. This thesis work was aimed at improving the studies regarding Multiphysics topology optimization of systems governed by fluid flow and heat transfer including cooling devices and nuclear applications. Two different CFD software were used in the investigation of the optimization methods. First, with the well-established COMSOL Multiphysics optimization module, topology optimization gradient based algorithms were studied with 2D benchmarks. Then, a 3D cooling system governed by forced convection was considered. Topology optimization succeeded in defining a new shape for the heat transfer fin with improved cooling capabilities. The COMSOL results represented the starting point for the development of an open source optimization solver in OpenFOAM for flows including heat transfer based on the adjoint approach. This approach led to promising results characterized by lower computational cost but higher residuals which underlined the need of further validation tests. In the final part of the present work, the EVOL geometry of the Molten Salt Fast Reactor (MSFR) was subject to topology optimization aimed at minimizing the temperature gradient and pressure drops inside the reactor. The results showed impressive results regarding the improvement of the system operative conditions.

Sommario

Nell'ultimo decennio l'ottimizzazione topologica sta ricoprendo un ruolo sempre più importante nell'approccio al design industriale per diverse applicazioni riguardanti la meccanica strutturale, ingegneria civile, architettura e meccanica dei fluidi soprattutto in connessione ad applicazioni aerospaziali. Questa lavoro è finalizzato al miglioramento degli studi riguardanti l'ottimizzazione topologica di sistemi multifisici governati da fluidodinamica e scambio termico includendo applicazioni nucleari e sistemi di raffreddamento. I metodi di ottimizzazione topologica vennero studiati attraverso l'uso di due software di fluidodinamica computazionale. Inizialmente, attraverso il modulo di ottimizzazione di COMSOL Multiphysics, gli algoritmi di ottimizzazione basati sul gradiente vennero studiati con benchmark 2D. Successivamente venne considerato un sistema di raffreddamento 3D governato da convezione forzata. L'ottimizzazione si dimostrò un efficacie strumento per la definizione di un aletta per lo scambio termico con capacità di raffreddamento migliori rispetto ad un aletta rettangolare tradizionale. I risultati ottenuti su COMSOL Multiphysics rappresentarono il punto di partenza per lo sviluppo di un solver open-source su OpenFOAM basato sull'approccio degli aggiunti per sistemi fluidodinamici con scambio termico. Questo nuovo approccio condusse a risultati promettenti caratterizzati da un costo computazionale più basso ma residui più alti che inducono la necessità di simulazioni di validazioni successive per una migliore analisi dei risultati. Nella parte finale del presente lavoro, l'analisi di ottimizzazione topologica venne applicata al geometria EVOL del Molten Salt Fast Reactor (MSFR) al fine di minimizzare il gradiente di temperatura e le cadute di pressione all'interno del reattore. I risultati mostrarono enormi miglioramenti per quanto riguarda le condizioni operative del sistema.

Estratto

I problemi di ottimizzazione sono caratterizzati da un set di equazioni primarie e da una funzione di costo J che dipende dalle variabili di stato del sistema. Le equazioni sono governate da un set di variabili di controllo che rappresentano un input aggiuntivo al sistema in grado di modificare le variabili di stato e conseguentemente J. Negli ultimi anni i due approcci di ottimizzazione che stanno riscontrando maggior interesse scientifico ed industriale sono l'ottimizzazione di forma e l'ottimizzazione topologica. Nel primo caso le variabili di stato sono definite dalle dislocazioni su una superficie parametrizzata che portano a cambiamenti della funzione di costo inducendo la definizione di una superficie ottima. Questo metodo, particolarmente performante in applicazioni esterne in meccanica strutturale e fluidodinamica, presenta un costo computazionale elevato vista la necessità di ricalcolare la mesh ad ogni dislocazione. L'approccio topologico, su cui è stato incentrato il presente lavoro, prevede invece la discretizzazione dell'intero dominio attraverso una variabile di controllo γ a cui è associato un materiale fittizio. Interpolando la variabile di controllo compresa tra 0 ed 1 è possibile risolvere le equazioni primarie in caso sia uguale ad 1 ed equazioni associate ad un materiale fittizio nel caso sia uguale a 0. L'analisi topologica determina una struttura ottima definendo per ogni elemento o volume finito del dominio se vi deve essere un materiale (associato a $\gamma = 0$) o un altro ($\gamma = 1$) affinché la funzione di costo risulti minima.
Considerando una discretizzazione agli elementi finiti del dominio di design il problema di ottimizzazione è definito come:

$$\begin{cases} \overset{min}{\gamma} : J = J(u(\gamma), \gamma) = \sum_i \int_{\Omega i} f(u(\gamma_i), \gamma_i)\, dV \\ soggetto\ a : G_0(\gamma) = \sum_i u_i \cdot \gamma_i - V_0 \leq 0 \\ \qquad\qquad : G_i(u(\gamma), \gamma) \leq 0, j = 1, ..., M \\ \qquad\qquad : \gamma_{min} \leq \gamma_i \leq 1 or 1, i = 1, ..., N \end{cases} \tag{1}$$

Ovvero determina la distribuzione di materiale che minimizzi la funzione obiettivo J, soggetta al vincolo di volume $G_0(\gamma)$ ed altri possibili M vincoli dove u è la variabile di stato che soddisfa le equazioni primarie.

Nel presente lavoro l'ottimizzazione topologica di sistemi multifisici venne studiata attraverso due approcci differenti come mostrato in figura 1. Un primo studio sugli algoritmi di ottimizzazione basati sul gradiente e sugli schemi di interpolazione venne condotto sul software di modellazione multifisica COMSOL Multiphysics in cui è già presente un modulo per l'ottimizzazione topologica. Furono quindi presi in considerazione

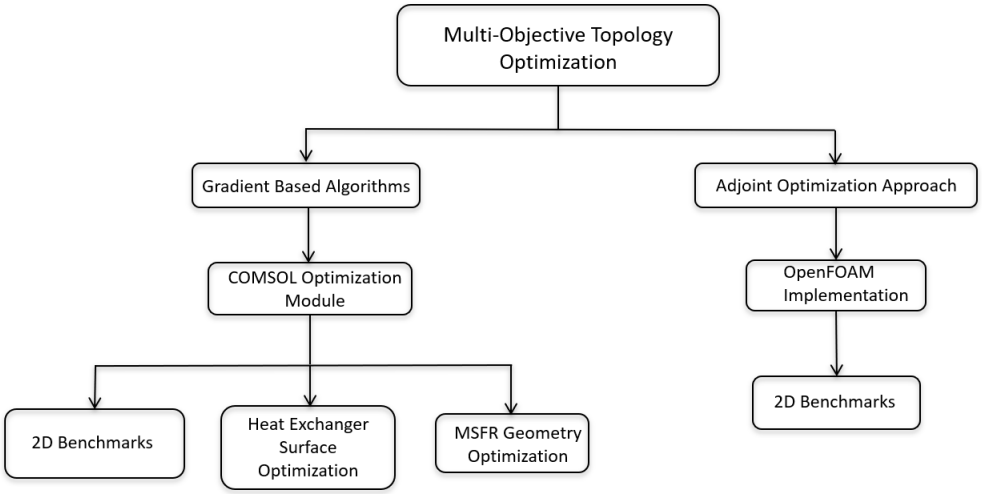

Figure 1: Schema di Flusso del Lavoro di Tesi

benchmark 2D di problemi già presenti in letteratura [1] per poterne confrontare i risultati. Il primo test numerico riguardava un problema governato dalla pura conduzione in cui un dominio quadrato con lati di $100[mm]$ era soggetto a produzione di calore volumetrica pari a $3\left[\frac{W}{m^3}\right]$. Mentre su parte del lato sinistro venne imposta temperatura costante di $293[K]$, tutti gli altri lati presentavano la condizione al contorno di adiabaticità. Il dominio, governato dall'equazione di Fourier in stato stazionario, venne discretizzato con una variabile di controllo γ in grado di interpolare la conduzione termica tra il suo valore massimo di $1\left[\frac{W}{m\,K}\right]$ e quello minimo di $0.001\left[\frac{W}{m\,K}\right]$ come segue:

$$\gamma = \begin{cases} 1 : k = k_{max} = 1\left[\dfrac{W}{mK}\right] \\ 0 : k = k_{min} = 0.001\left[\dfrac{W}{mK}\right] \end{cases} \tag{2}$$

La funzione obiettivo venne definita come la differenza tra il campo di temperatura effettivo ed una temperatura obiettivo. Attraverso l'uso di un risolutore basato sull'algoritmo SNOPT (Sparse Nonlinear OPTimizer), l'ottimizzazione topologica identificò strutture dendritiche in grado di abbassare la temperatura media del sistema in funzione del vincolo di volume imposto. Quest'ultimo venne definito come la frazione di volume associata a $\gamma = 1$, quindi al materiale più conduttivo, sul volume totale. Di seguito il risultato topologico con frazione di volume imposta a 0.5.

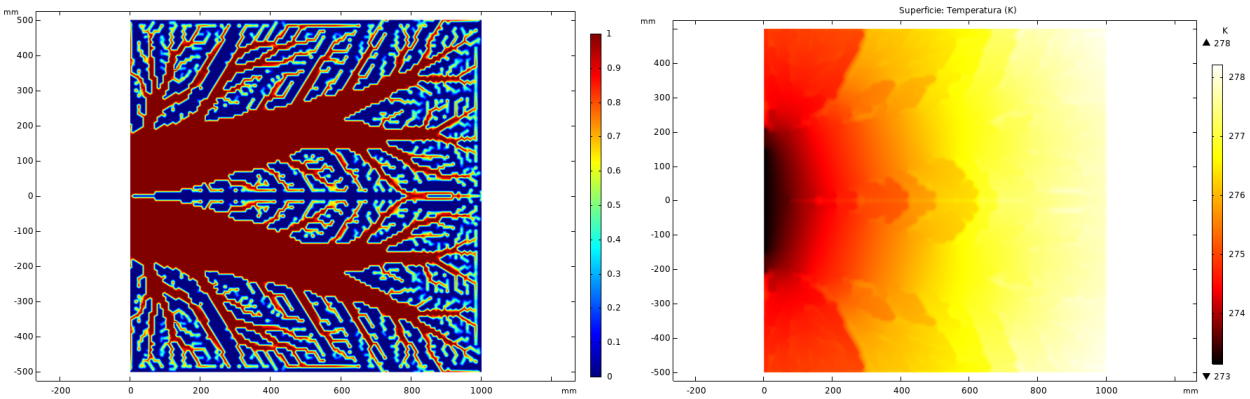

(a) *Topology Optimization* (b) *Temperature*

Figure 2: $V_{target} = 0.5$: ottimizzazione topologica e campo di temperatura

Le simulazioni mostrarono risultati concordi con quelli presenti in letteratura con rilevanti diminuzioni di temperatura media in funzione della frazione di volume.

Nel secondo test numerico venne considerato un problema 2D governato la flusso laminare costituito da due tubi dal diametro di $6[mm]$ connessi ad un volume rettangolare a diverse altezze. Il dominio di ottimizzazione venne discretizzato con una variabile di controllo in grado di interpolare un campo di porosità. Quest'ultimo, definito come l'inverso della permeabilità di un mezzo poroso, identificava, con un termine di Darcy, una forza di volume all'interno delle equazioni di Navier-Stokes in grado di penalizzare il flusso all'interno dei domini solidi. la variabile di controllo γ compresa tra 0 ed 1 definiva, attraverso uno schema di interpolazione di Darcy, il campo di porosità come:

$$\gamma = \begin{cases} 1 : \alpha = 0 \rightarrow dominio\ fluido \\ 0 : \alpha = \alpha_{max} \rightarrow dominio\ solido \end{cases} \tag{3}$$

La funzione obiettivo venne definita come la caduta di pressione totale nel sistema. Il solver di ottimizzazione topologica basato sull'algoritmo MMA (Methods of Moving Asymptotes) riuscì a definire con successo una struttura interna del condotto in grado di eliminare i punti di ricircolo e le conseguenti cadute di pressione come mostrato nella figura 3 in cui le aree rosse corrispondono a regioni di flusso libero senza penalizzazioni di porosità.

L'ottimizzazione topologica condusse ad una riduzione delle cadute di pressione di circa il 54% .

Nell'ultimo benchmark 2D venne analizzato un problema fluidodinamico con scambio termico di un sistema di raffreddamento. Un dominio quadrato di lato $100[mm]$ connesso ad un ingresso e due uscite a lati opposti venne sottoposto ad una produzione di calore volumetrica pari a $100\left[\frac{kW}{m^3}\right]$. Sulle pareti venne imposta la condizione di adiabaticità mentre all'ingresso venne fissata una velocità pari a $0.01\left[\frac{m}{s}\right]$. La funzione obiettivo fu definita come la somma di due contributi, uno termico ed uno fluidodinamico, pesati con coefficienti adimensionali, rispettivamente ω_1 e ω_2. Il primo contributo, proporzionale alla

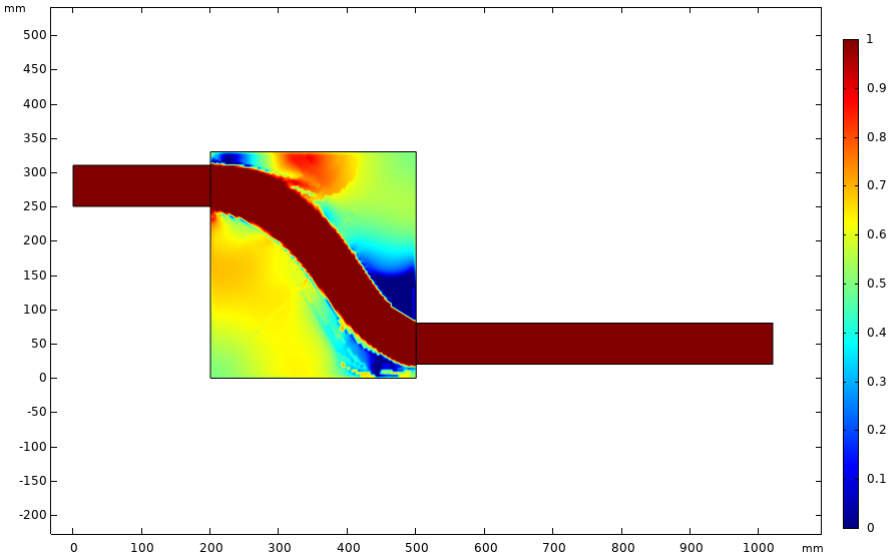

Figure 3: Topology optimization result

temperatura media nel dominio di controllo, era finalizzato a migliorare le capacità di raffreddamento del sistema mentre il secondo era proporzionale all'energia totale dispersa dal flusso. In modo analogo al caso precedente, la variabile di controllo nel sistema interpolava una porosità che definiva una forza di volume nelle equazioni di Navier-Stokes. Attraverso l'algoritmo di ottimizzazione topologica SNOPT si ottennero risultati in funzione dei diversi coefficienti di peso dei due contributi della funzione di costo totale. Abbassando il peso relativo al contributo termico ω_1, l'ottimizzazione si sbilanciava maggiormente verso un miglioramento fluidodinamico. In figura 4 vengono mostrati i risultati con diversi contributi termici ed un vincolo di volume definito come:

$$0 \leq \int_{\Omega} \gamma \, d\Omega \leq 0.003 \tag{4}$$

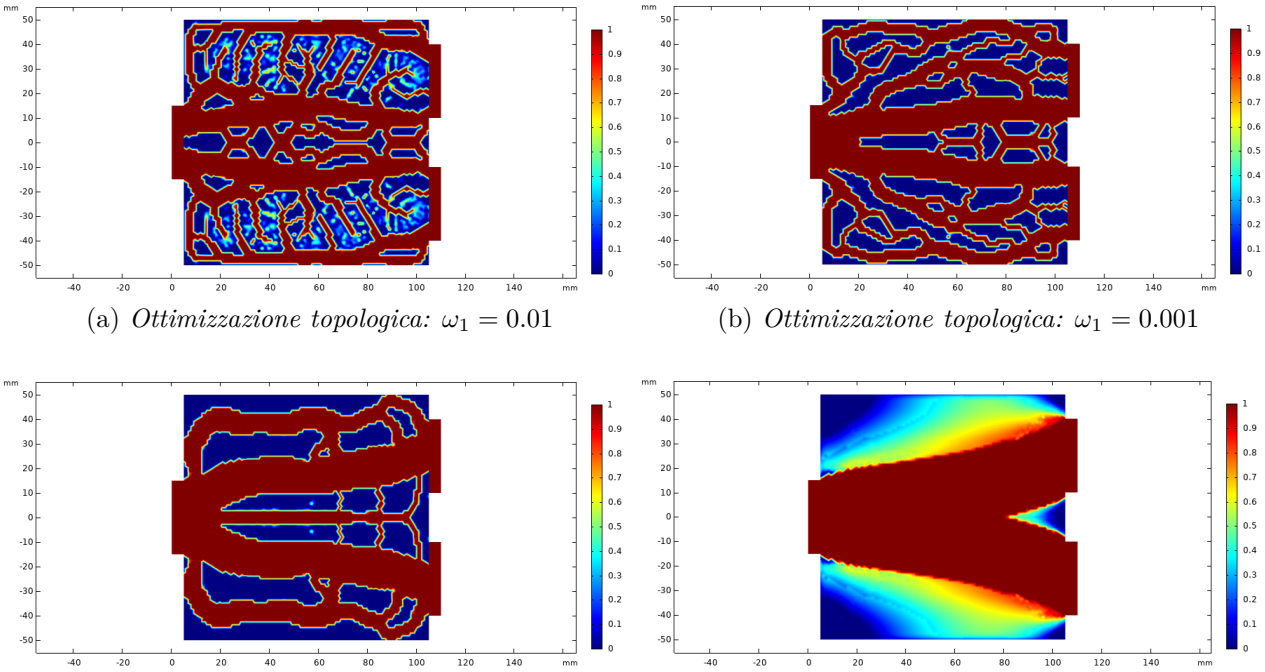

(a) *Ottimizzazione topologica:* $\omega_1 = 0.01$

(b) *Ottimizzazione topologica:* $\omega_1 = 0.001$

(c) *Ottimizzazione topologica:* $\omega_1 = 0.0001$

(d) *Ottimizzazione topologica:* $\omega_1 = 0$

Figure 4: Risultati dell'ottimizzazione topologica.

Aumentando il valore del coefficiente di peso associato al contributo termico, le zone di flusso libero, identificate con il colore rosso ($\gamma = 1$), tendono a occupare regioni del dominio sempre più marginali arrivando ad ottenere una diminuzione dell'escursione termica di $28[K]$ rispetto al caso non ottimizzato aumentando però le cadute di pressione nel sistema. Nel caso di ottimizzazione opposto, in cui la funzione di costo risulta puramente fluidodinamica, l'escursione termica raggiunge un valore di circa $81[K]$ a vantaggio di una diminuzione delle cadute di pressione di circa il 91%.

I risultati ottenuti costituirono un ottimo punto partenza per lo sviluppo dell'ottimizzazione di una superficie per uno scambiatore di calore a convezione forzata. Il modello (figura 5), ispirato ad un sistema di raffreddamento di un processore, era costituito da un parallelepipedo in ottone (solid 1) sottoposto a flusso termico su cui vennero posti una piastra rettangolare (solid 2) e una piccola aletta in alluminio (solid 3) che costituiva il punto di partenza per l'ottimizzazione. La struttura appena descritta venne posta all'interno di un condotto di raffreddamento con sezione rettangolare. La funzione di costo, proporzionale alla temperatura media sulla superficie della piastra rettangolare, era finalizzata alla definizione di una forma ottima per l'aletta di scambio termico. Il fluido di raffreddamento, acqua in questo caso, era sottoposto ad una pressione in ingresso costante. Questo permise di non definire una funzione di costo puramente fluidodinamica in quando ad ogni caduta di pressione sarebbe corrisposta una diminuzione di velocità ed un conseguente peggioramento delle prestazioni di raffreddamento.

Il volume centrale del condotto venne identificato come dominio di design e discretizzato con la variabile di controllo γ. Quest'ultima venne usata per interpolare sia il campo

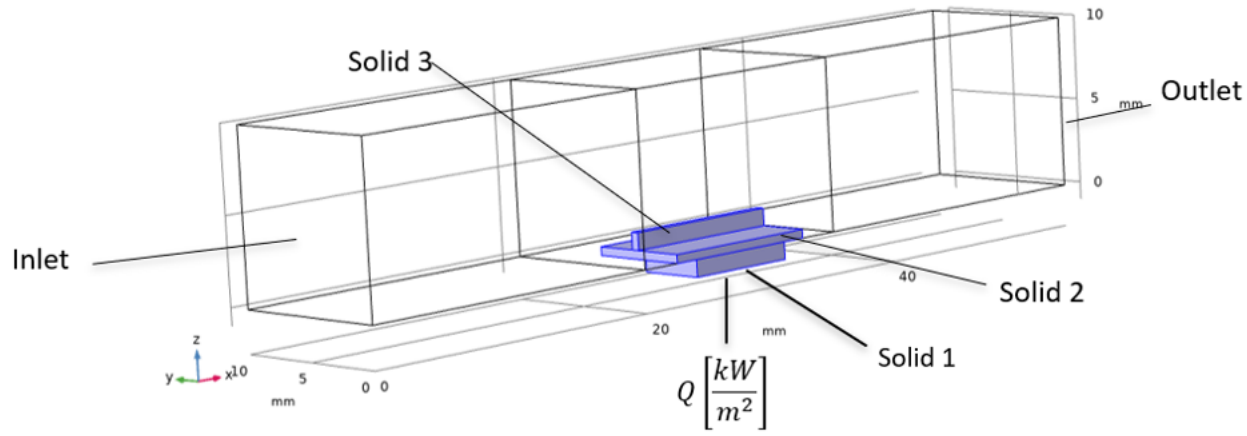

Figure 5: Modello ottimizzazione topologica 3D

di porosità sia la conducibilità termica del dominio solido aggiunto. In questo modo le regioni identificate da valori di variabile di controllo $\gamma = 1$ venivano associate a proprietà termiche del materiale di interesse per l'aletta, in questo caso alluminio. Il solver per l'ottimizzazione topologica SNOPT condusse alla definizione di una forma ottima per l'aletta in grado di abbassare la temperatura media sulla superficie di interesse. Il risultato topologico tuttavia, venne sottoposto ad ulteriori test numerici di validazione in quanto la transizione tra regioni liquide e regioni solide non era sufficientemente netta da garantire un corretto calcolo dello strato limite. La geometria ottenuta (figura 6) venne quindi esportata attraverso un filtro sulla variabile di controllo e sottoposta ad un test numerico con le medesime condizioni operative originali. I risultati mostrarono una notevole diminuzione della temperatura media sulla piastra sia rispetto al caso non ottimizzato, sia rispetto ad un'aletta rettangolare con volume e larghezza pari a quella ottima. Nella tabella 1 vengono mostrati i valori numerici delle temperature medie con diversi carichi termici.

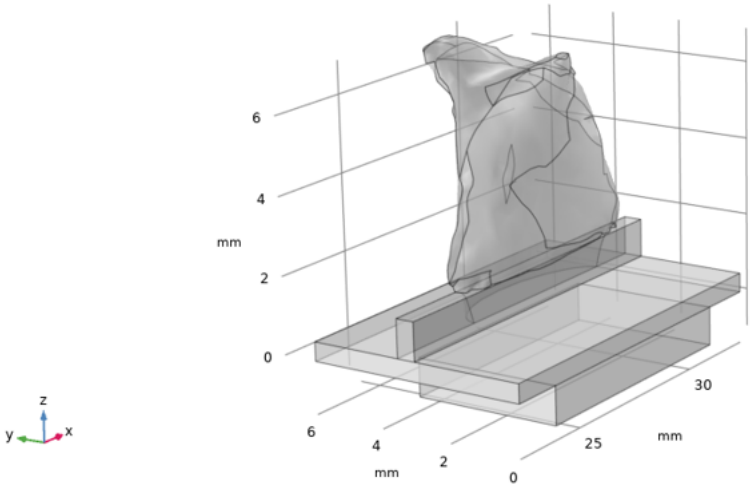

Figure 6: Final fin shape

Results	Non-optimized Fin	Optimized Fin	Rectangular Fin
$T_{avg,50\left[\frac{kW}{m^2}\right]}[K]$	336.84	318.34	321.45
$T_{avg,100\left[\frac{kW}{m^2}\right]}[K]$	375.29	340.45	350.27

Table 1: Confronto risultati numerici dell'ottimizzazione topologica 3D

I problemi di ottimizzazione condotti su COMSOL Multiphysics furono il punto di partenza per lo sviluppo di un solver open-souce per l'ottimizzazione topologica su OpenFOAM. A tal fine venne adottato l'approccio degli aggiunti per l'analisi di sensitività. Questa infatti, in un comune metodo basato sul gradiente, richiede un oneroso costo computazionale nel caso venissero usate numerose variabili di controllo. L'approccio degli aggiunti invece, implementa un'analisi di sensitività indipendente dal numero complessivo di queste ultime aggiungendo un set di equazioni ausiliarie dette appunto equazioni aggiunte. Un approccio Lagrangiano al problema di ottimizzazione fluidodinamico con scambio termico permette di definire una funzione di costo lagrangiana come segue:

$$L = J + \int_{\Omega} (\boldsymbol{u}, q, T_a) R(\boldsymbol{v}, p, T)\, d\Omega \tag{5}$$

Dove J è la funzione obiettivo, $(\boldsymbol{u}, q, T_a)$ è il vettore dei moltiplicatori di Lagrange costituito dalle variabili di stato delle equazioni aggiunte mentre $R(\boldsymbol{v}, p, T)$ è il set di equazioni primarie che governano il problema. Il problema di ottimizzazione Lagrangiano viene quindi definito come:
$Trovare\ (\boldsymbol{y}, \boldsymbol{\lambda}, \gamma)\ tali\ che \nabla L(\boldsymbol{y}, \boldsymbol{\lambda}, \gamma) = 0$
Dove $\boldsymbol{y}$ è il vettore delle variabili di stato, $\boldsymbol{\lambda}$ è il vettore delle variabili aggiunte e γ è la variabile di controllo. Dal calcolo del gradiente della funzione Lagrangiana è possibile ricavare il set di equazioni aggiunte e le corrispondenti condizioni al contorno. L'analisi di sensitività utilizzata per aggiornare i valori della variabile di controllo viene invece ricavata derivando la funzione Lagrangiana rispetto alla variabile di controllo stessa.
L'approccio di ottimizzazione appena descritto venne applicato ai tre benchmark 2D presentati precedentemente. Tale scelta risulta giustificata dalla necessità di un confronto dei risultati ottenuti con OpenFOAM rispetto a quelli ottenuti con COMSOL Multiphysics il cui modulo di ottimizzazione è stato convalidato.
Inizialmente venne preso in considerazione il caso di pura ottimizzazione fluidodinamica utilizzando il solver *adjointShapeOptimizationFoam* già implementato in OpenFOAM che costituì il punto di partenza per lo sviluppo dei solver per le simulazioni successive. Il solver, basato sulla definizione di un campo di porosità nel dominio di controllo attraverso un termine di Darcy nelle equazioni di Navier-Stokes, riuscì a definire una forma ottima del condotto simile alla soluzione di riferimento come mostrato in figura 7.

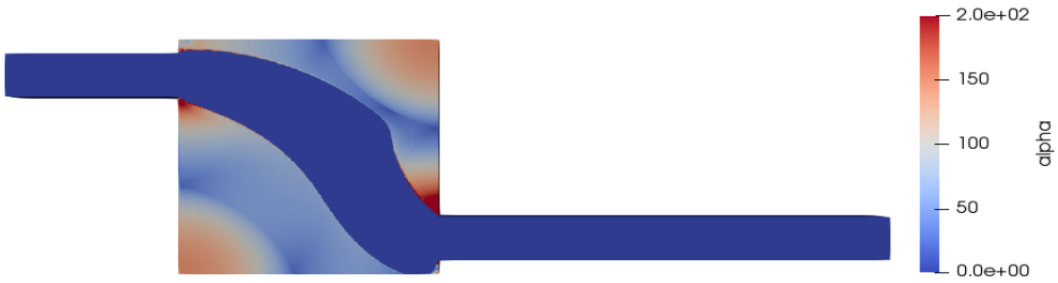

Figure 7: Ottimizzazione topologica

La transizione tra regioni liquide e solide tuttavia non risultava sufficientemente netta da garantire un calcolo corretto dello strato limite. Questo problema venne successivamente risolto inserendo un opportuno schema di interpolazione.

Successivamente venne considerato il problema di ottimizzazione di puro scambio termico conduttivo. In questo caso venne implementato il solver *adjointHeatConduction* basato sull'approccio degli aggiunti all'equazione di Fourier attraverso la discretizzazione del dominio con una variabile di controllo in grado di interpolare il coefficiente di scambio termico conduttivo come in precedenza. I risultati mostrarono pattern topologici simili a quelli ottenuti su COMSOL con diversi valori della frazione di volume definita come il rapporto tra il volume associato alla conducibilità massima sul volume totale. In figura 8 viene mostrata l'ottimizzazione topologica con frazione di volume pari a 0.5.

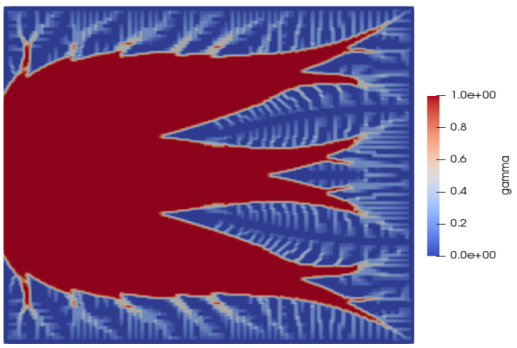

Figure 8: Ottimizzazione topologica

L'ultima simulazione numerica in OpenFOAM fu condotta sul benchmark fluidodinamico con scambio termico. Una parametro di controllo η definiva un campo di porosità attraverso il termine di Darcy. La funzione di costo venne definita come somma di un contributo fluidodinamico, dato dalla caduta di pressione totale, ed uno termico proporzionale alla temperatura media nel dominio, entrambi pesati con coefficienti correttivi. Questi ultimi, come in precedenza, erano in grado di sbilanciare l'ottimizzazione verso un termine della funzione di costo totale rispetto all'altro. I risultati, ottenuti implementando il solver per l'ottimizzazione multifisica *adjointSimpleFoam*, mostrarono miglioramenti

fluidodinamici e delle prestazioni di raffreddamento del sistema in base alla scelta dei coefficienti correttivi nella funzione di costo. In figura 9 vengono mostrati i risultati di ottimizzazione topologica ottenuti con un coefficienti di peso termici ω pari a 0.1 e 0.5.
Alle zone con variabile di controllo η pari a 1 (zone rosse) veniva associato flusso libero

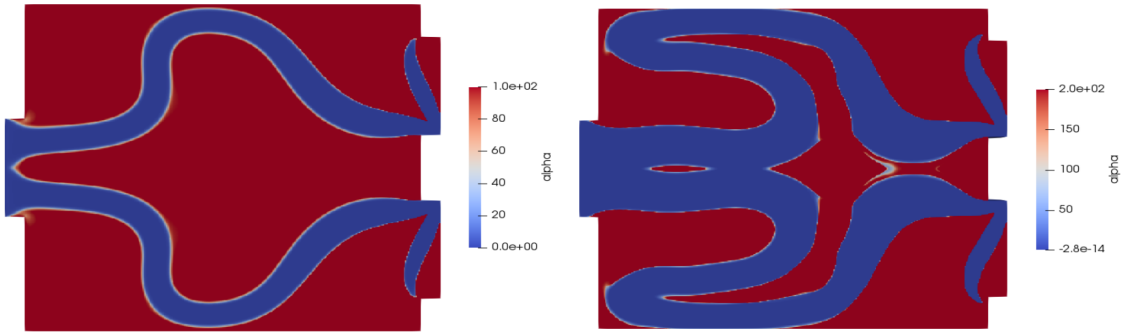

(a) $\omega = 0.1$ (b) $\omega = 0.5$

Figure 9: Risultati topologici dell'ottimizzazione multifisica

mentre quelle con $\eta = 0$ (zone blu) erano associate a regioni solide. Aumentando il coefficiente di peso termico l'ottimizzazione favoriva configurazioni topologiche in grado di ridurre la temperatura media del sistema a discapito delle cadute di pressione. Nella tabella 2 vengono riassunti i risultati numerici riguardanti l'ottimizzazione termica.

	$T_{avg}[K]$	$T_{max}[K]$
No Optimization	299.78	321.84
$\omega = 0.1$	300	294.3
$\omega = 0.5$	297.6	294.1

Table 2: Risultati termicic ottimizzazione multifisica

Un'analisi riguardante le cadute di pressione necessita successivi test di validazione dei risultati ottenuti in quanto i residui del calcolo numerico risultarono troppo alti per questo scopo. Il metodo di ottimizzazione degli aggiunti infatti, venne implementato con l'approccio "one shot" in cui l'analisi di sensitività veniva calcolata su quantità che raggiungevano la sola parziale convergenza aumentando i residui di calcolo. Per questo motivo anche un confronto numerico dettagliato tra i risultati ottenuti dai due software necessita succesivi test di validazione.
I risultati ottenuti con il metodo di ottimizzazione implementato in OpenFOAM rappresenta un ottimo punto di partenza sia per miglioramenti futuri che possano includere ottimizzazioni 3D, sia per problemi più complessi con differenti variabili di controllo.

Nell'ultima parte del presente lavoro di tesi il processo di ottimizzazione topologica venne applicato alla geometria del Molten Salt Fast Reactor (MSFR) presentata dal

progetto EVOL. Il MSFR rappresenta uno dei più promettenti concept per i reattori di quarta generazione. La sua peculiarità risiede nell'utilizzo di combustibile immerso in una matrice di sale in forma liquida che agisce da refrigerante. Il reattore veloce omogeneo permette di ottenere condizioni operative con pressioni più basse e coefficienti di retroazione di temperatura e di vuoto molto negativi. Non esiste tuttavia una geometria definitiva per il nocciolo del reattore. Molti studi fanno riferimento ad una geometria cilindrica proposta dal progetto EVOL finalizzata a minimizzare le perdite neutroniche. Le simulazioni termofluidodinamiche condotte in questo lavoro evidenziarono però che questa configurazione induce la formazione di grosse zone di recircolo del combustibile. Questo non potendosi raffreddare attraverso lo scambiatore di calore con il sistema secondario, si surriscaldava portando a gradienti termici insostenibili per i materiali strutturali e per i riflettori. Venne quindi condotta un'analisi di ottimizzazione topologica attraverso COMSOL Multiphysics al fine di ridurre le temperature massime nel sistema. Il modello di partenza, mostrato in figura 10, era costituito da un nocciolo cilindrico, una gamba calda ed una gamba fredda che costituivano il dominio di design, posti in serie ad uno scambiatore di calore ed una pompa modellizzata con una forza volumetrica.

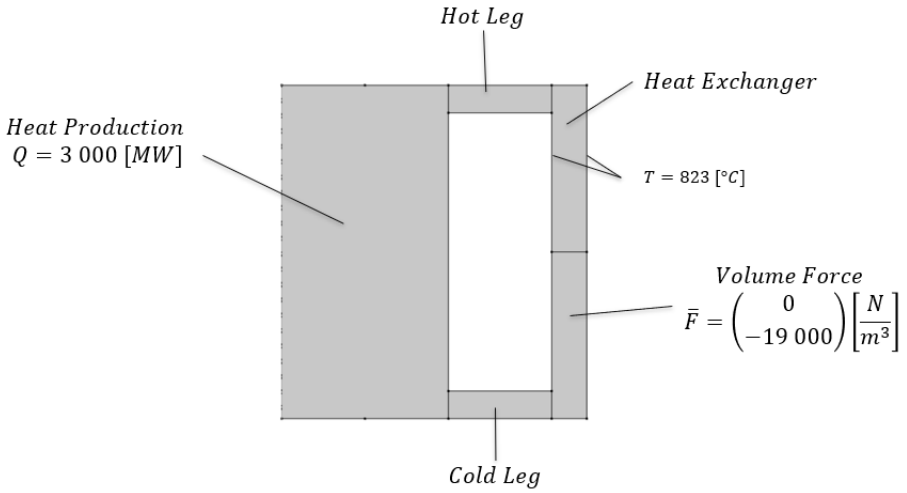

Figure 10: MSFR initial geometry and boundary conditions

Al fine di eliminare le zone di recircolo, la funzione di costo venne definita come la caduta di pressione tra l'uscita dalla pompa e l'ingresso nello scambiatore di calore. Una variabile di controllo γ interpolava un campo di porosità tramite i termine di Darcy nelle equazioni del momento del sale fuso. Il risultato topologico dell'ottimizzazione (figura 11) venne filtrato ed esportato per essere sottoposto ad un test di validazione.

Il test di validazione condusse ai risultati mostrati in figura 12. La completa eliminazione delle zone di recircolo portò ad una diminuzione della temperatura massima del sistema di 580 [K] mentre la temperatura media nel nocciolo passò da 1137 [K] a 991 [K]. Ciò nonostante, la temperatura media nella gamba calda aumentò da 1050 [K] a 1082.2 [K] rendendo il ciclo di potenza associato ancora più termodinamicamente prestante.

I risultati ottenuti rappresentano un importante risultato per lo sviluppo di una geometria definitiva del MSFR nonché un ottimo punto di partenza per studi successivi. Questi dovranno considerare anche aspetti riguardanti l'economia neutronica del reattore

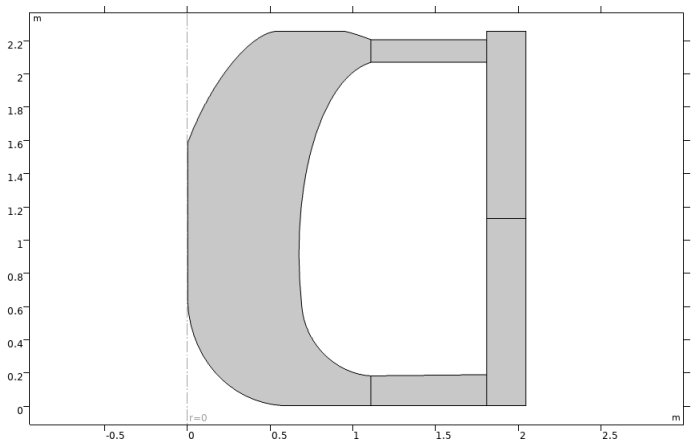

Figure 11: MSFR refined geometry

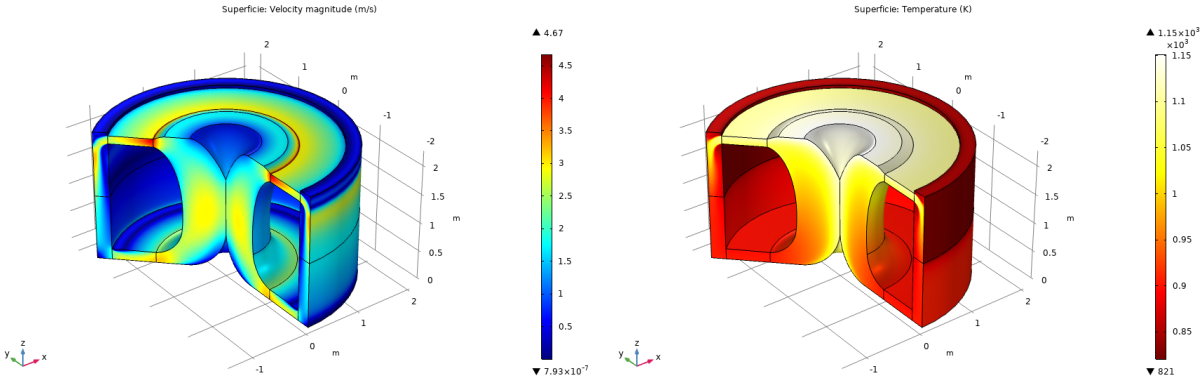

(a) *Campo di velocità ottimizzato* (b) *Campo di temperatura ottimizzato*

Figure 12: Risultati test di validazione MSFR ottimizzato

all'interno di un'ottimizzazione topologica multifisica.

Contents

List of Figures

List of Tables

List of Symbols

η	Adjoint control variable [−]
η_{II}	Second thermodynamic principle energy yield[−]
η_I	Fist thermodynamic principle energy yield[−]
η_{rev}	Carnot cycle yield[−]
γ	Control variable [−]
μ	Dynamic viscosity $[Pa \cdot s]$
ν	Kinematic viscosity $\left[\frac{m^2}{s}\right]$
ω	Weighting factor [−]
ρ_{fl}	Water density $\left[\frac{kg}{m^3}\right]$
C	Heat capacity $\left[\frac{J}{kg\,K}\right]$
L	Characteristic lenght [m]
p	Pressure [Pa]
Q	Volumetric heat source $\left[\frac{W}{m^3}\right]$
T	Temperature $[K]$
T^*	Objective temperature $[K]$
T_{avg}	Average temperature $[K]$
T_{in}	Inlet temperature $[K]$
v	Velocity $\left(\frac{m}{s}\right)$
Vol	Design domain volume $[m^3]$

Introduction

Design optimization is an old field of research which was subjected to deep mathematical theories and inspired numerous industrial and engineering applications. In the last decades, the rise of computational power led to the development of several advanced programming methods in order to achieve the optimum shape of engineering structures in numerous scientific fields under different constrains such as stress, displacement and kinematic stability. The increase in the cost of raw materials and the increasing efforts to reduce the energy consumption made the optimization a key aspect for the components production from the early stages of design, so that they fulfil their purpose for a minimum amount of constitutive material. Furthermore, design optimization represents an important tool for the performance improvements of existing devices in different applications such as automotive and aerospace industry, as well as in civil engineering, material science, biomechanics and with the design of cooling devices.

The generic optimization problem is characterized by a function $J(\boldsymbol{x}) : \Omega \to \mathbb{R}^n$ called objective function. $\boldsymbol{x}$ is the vector of the state variables which represent the degrees of freedom of the problem and Ω is the feasible space defined by the constraints, equalities or inequalities, that $\boldsymbol{x}$ must satisfy. The problem is aimed at determining $\boldsymbol{x}_0 \in \Omega$ such that $J(\boldsymbol{x}_0) < J(\boldsymbol{x}) \; \forall \boldsymbol{x} \in \Omega$. If the objective function is analytically defined it is possible to determine the best performing optimization algorithms depending on the function properties.
The optimization algorithms can be divided in deterministic or stochastic. The former are aimed at determining the local extreme of the cost function imposing the zero gradient condition or defining positive the Hessian matrix. The quality and velocity of these methods depend on the starting point of the optimization and the gradient calculation procedure. Furthermore, if the objective function is defined by n degrees of freedom, the numerical evaluation of the gradient requires $n + 1$ samplings of the cost function with direct consequences on the algorithm velocity.
On the other hand, the stochastic algorithms represent an alternative procedure since they do not include the cost function gradient calculation (zero order methods) but introduce specific random parameters variation in the problem. These methods are independent from the specific problem and are inspired from natural problem solving. The most important peculiarity of the stochastic methods is the presence of a random factor which leads to a different optimum research in each run. Hence, the performance evaluation is carried out with statistical calculations. The stochastic methods succeed in finding the global extreme of the cost function despite a lower velocity with respect to the deterministic approaches.

Among the different stochastic optimization methods, the genetic algorithm is one of the best performing. This evolutionary approach was inspired by the theory of natural selection and genetic evolution principles. An initial population of solutions, randomly created by the algorithm, is tested with a fitness function. The solutions with higher fitness values are selected and combined each other in order to produce new solutions carrying the good advantageous characteristics of the older generation. This procedure is iteratively repeated until the stopping criterion is reached. The genetic algorithms find numerous applications in project design optimization of industrial components (figure 1.4), limited resource utilization plan including air route definition and water resource planning and management [10], systems control, automatic learning and also data mining. In general, the evolutionary methods represent an efficient approach when the feasible space of optimum research is not well known.
Because of their intrinsic random nature it is not always possible to define if the methods are able to converge to acceptable results and the physical reasons of the solutions. Moreover, the numerical errors of the problems include statistical uncertainties. For this reasons, the stochastic approaches are more used in biology or economic contexts and in the present work only the deterministic methods were used in the numerical optimization tests.

In deterministic optimization problems, the set of algebraic or differential governing equations and the objective function J, depending on the state system, are both controlled by a set of design variable which behave as additional input of the system. The purpose of the optimization problem is defining the design variables that leads to a maximum (or minimum) of J. The two most important optimization approaches, that nowadays are gaining influence in scientific researches, are the shape optimization and topology optimization.
The difference between the two methods is the choice of the control variable. In shape optimization the displacements over a parametrized surface are usually selected. The deformation of the surface on which the sensitivity is applied leads to a variation of the objective function and the definition of an optimal shape. Nevertheless this method is characterized by an expansive computational cost derived from the need of compute the mesh at each shape modification to fit the new design. The shape optimization approach find applications for external implementation specially in structural and fluid mechanics for example in connection with aerospace applications.
From the 80's the topology optimization approach was developed. This method was initially formulated in structural mechanics (figure 1.1) by the definition of a fictious material in the design domain. The optimization problem was solved evaluating the fictitious material density in order to identify the areas where structural material should be added or deleted to increase the overall stiffness with the least possible material. In recent years the density approach was exported also in fluid-dynamics applications but differently from shape optimization, topology method finds more usage in internal applications. Each cell is identified by a design variable associated to a porosity field that defines which portions of the system should be solid and which instead fluid in order to minimize (or maximize) the objective function. The final porosity field defines the optimal topology of the problem.

In this case the geometry is defined by the mesh of the entire volume, while in shape optimization it was defined through a parametrized surface (figure 1.2).

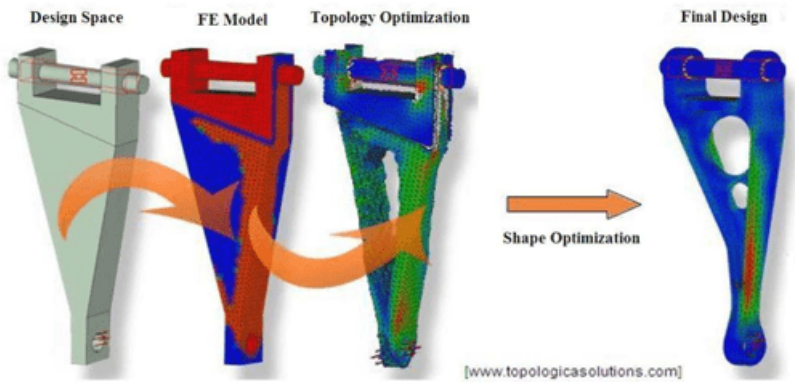

Figure 1.1: Shape optimization applied on bearings for enhanced load-carrying capacity [2]

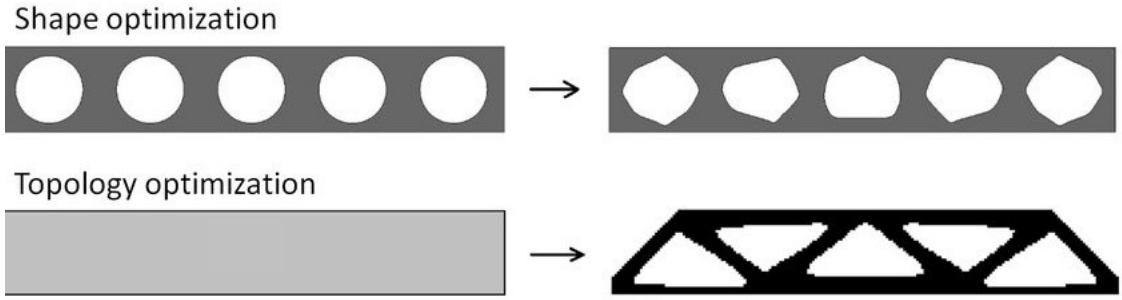

Figure 1.2: Comparison between shape and topology optimization on structural component [3]

The computational effort for the topology approach results improved. Nevertheless, density models do not always produce a sharp porosity transition. This leads the formation of regions with intermediate porosities devoid of physical interpretation. In the numerical test reported in this thesis work, this drawback was dealt with an accurate study of the porosity interpolation schemes.

Design optimization represents an established operating procedure for the initial design concepts, especially in structural mechanics applications, so that, in the last decades, most commercial software including COMSOL, Ansys and MATLAB developed an optimization interface. Furthermore, topology optimization applications are enhanced by the additive manufacturing (AM), a recently introduced fabrication method which allows the 3D building of as-designed structures in a layer-by-layer manner regardless of their complexities [11]. This unconventional fabrication method led to a wide usage of topology optimization in industrial application, specially in aerospace and automotive industries where the weight reduction and stiffness improvement of components are of primary importance. For example, the Airbus Group Innovations of Filton, Bristol, succeeded in demonstrating that AM processes have the advantage of integrating business and ecological sustainability with respect to conventional casting process. In particular an Airbus A320 nacelle hinge bracket (figure 1.3) optimization was investigated. The results

showed a design characterized by an impressive weight reduction which led to decrease of the CO_2 emission by nearly 40% over the whole lifecycle of the nacelle hinges.

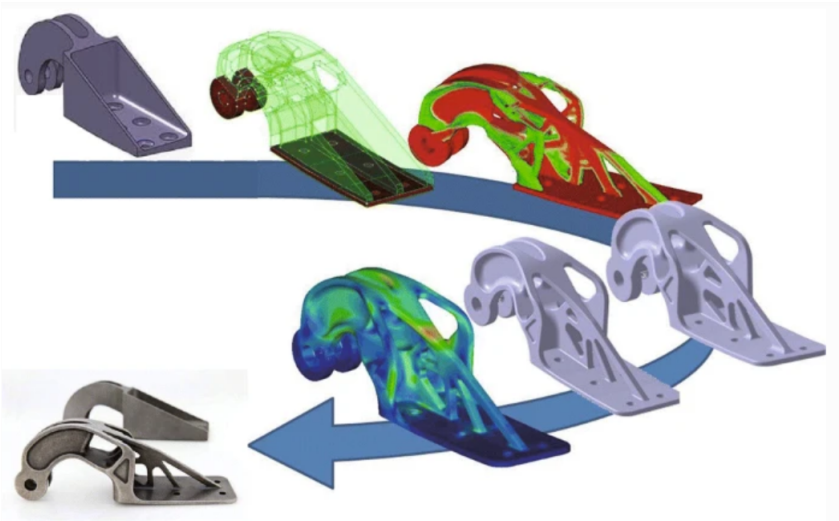

Figure 1.3: Airbus A320 Nacelle Hinge Bracket redesigned for additive manufacturing through topology optimization [4]

Regarding fluid flow, CFD driven optimization find numerous applications in different technology frameworks. In aerospace industry the aerodynamic jet design or blended wing body optimizations for minimum total drag are becoming standard project procedures. Moreover, design optimization is also used to increase the turbines power generation efficiency [5]. In figure 1.4, CFD-driven design optimization approach is applied to the valve of a cross-flow turbine. The valve represents one of the most critical parts of the system regarding power production efficiency since it determines the fluid flow velocity and pressure magnitudes in the turbine. The optimization procedure, carried out with different algorithms, succeeded in providing improved cross-flow turbine performances.

Optimizaion of coupled fluid flow and heat transfer problems, on the contrary, is not widely widespread in industrial applications. Only in recent years optimization of heat transfer systems witnesses an increasing interest in the scientific community with the publication of numerous articles ([12], [13], [14], [15], [16], [17]).
The purpose of the first part of this thesis work was to enhance the studies regarding fluid flow and heat transfer optimizations. Starting from numerical simulations of benchmarks already present in literature([1], [18]), a tridimensional Multiphysics and multi-objective optimization problem was studied with the purpose of defining an optimal shape for an heat exchanger with the topology approach. The forementioned optimizations were performed with COMSOL Multiphysics, a commercial software based on Finite Elements Method (FEM).

The efficiency of the gradient based optimization algorithms is limited by the number of control variable in the system. The evaluation of the sensitivity analysis, performed through the derivation of the cost function with respect to the control variables, can

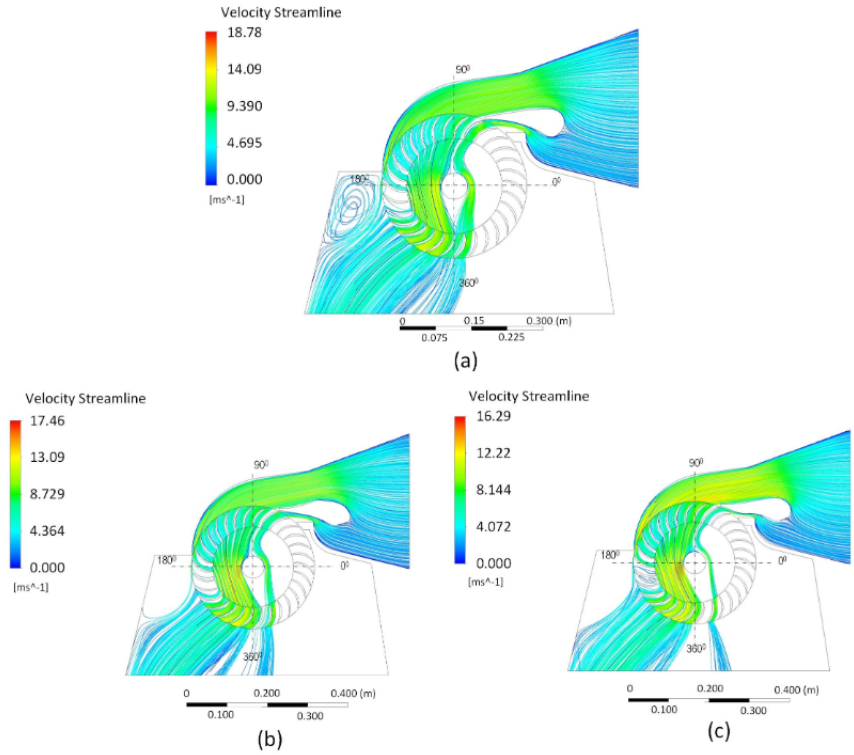

Figure 1.4: Velocity streamlines from steady analyses: (a) original model; (b) GA-optimized model; and(c) MMAO-optimized model. [5]

represent an onerous computational cost. The adjoint optimization approach instead, is an optimization method characterized by a sensitivity analysis independent from the number of control variables through the introduction of an auxiliary linear system. This makes the adjoint approach a promising tool for complex Multiphysics and multi-objective optimizations problems. In figure 1.5 the flowchart of computations of the standard gradient based optimization proceduce used in COMSOL is compared with the adjoint procedure scheme. The second part the thesis work is then focused in the development of an adjoint topology optimization solver for Multiphysics problems in open source code using OpenFOAM.

In the last part of the thesis, the optimization of the Molten Salt Fast Reactor (MSFR) core was taken into account. The MSFR represents one of the most promising and innovative concepts for the forth nuclear reactor generation. The employment of nuclear fuel in liquid form with salt acting also as coolant leads to numerous advantages including low operative pressure of the system and high boiling temperature. Furthermore, MSFR is characterized by large temperature and void coefficients, high capacity factor and high burnup that make this concept competitive among the new nuclear reactor generation regarding sustainability, safety, reliability and proliferation resistance. Nevertheless, a definitive core shape has not yet been established. Numerous works referred to a square cylinder geometry which was selected as official core configuration for neutronic benchmarks of the EVOL project. The cylindrical shape however, leads to the formation of huge recirculation areas that induce pressure drops and high pressure gradient. The

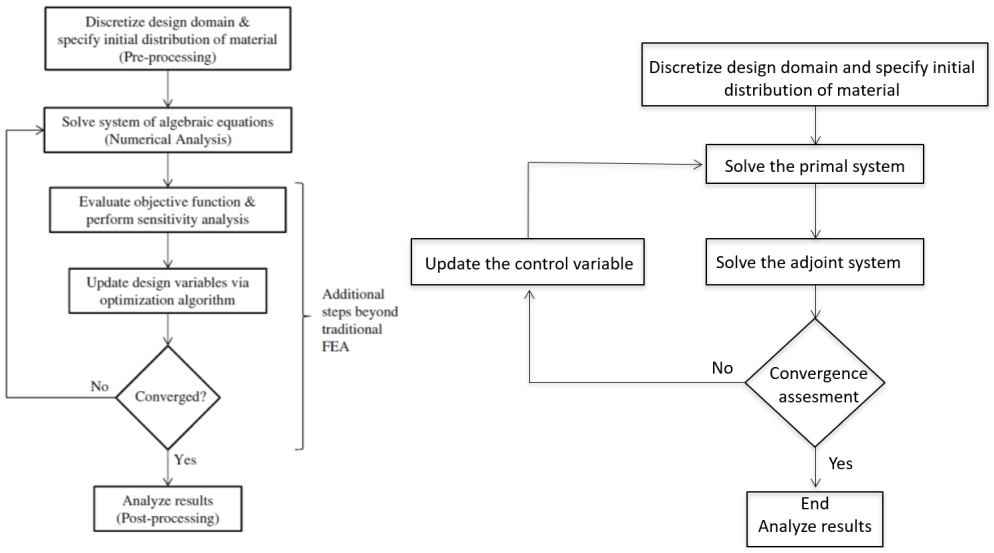

(a) *COMSOL Optimization Flowchart* (b) *OpenFOAM adjoint based optimization flowchart*

Figure 1.5: COMSOL and OpenFOAM optimization procedures

temperature reached in the reactor are not compatible with the operative conditions of the structural component. This section of the work was focused on the MSFR core optimization with the COMSOL Multiphysics optimization module.
In the last chapter, the conslusios are drawn including the comparison between the COMSOL Multiphysics and OpenFOAM optimization.

Topology Optimization: COMSOL

The following optimization studies were conduced with a finite element analysis through the use of COMSOL Multiphysics, a solver and multiphysics simulation software. It provides an Integrated Development Environment and unified workflow for different applications such as electrical, mechanical and fluid. In the COMSOL Optimization module [19] there are two classes of problems. The Design problem, aimed at finding the control variables that lead to the best performance of a model evaluated with an objective function, and the inverse problem. The latter, to which it belongs the parameter estimation in Multiphysics models and the curve fitting, provides a tool for the parameters evaluation that yield to a optimal matching between the simulated and the measured results. In this work the attention was completely focused on the Design problem solutions.
The COMSOL Optimization module allows to consider any model input as control variable and any model output as an objective function in order to evaluate the optimal solution to engineering problems. The purpose of the optimization is to find the control variables which minimize (or maximize) the objective under the given constrains. Therefore, in order to set up an optimization problem it is required to set up a finite number of independent control variables that the objective function depends on ($\boldsymbol{x} = [x_1, x_2, \cdots, x_n]$), a scalar objective function of the control variables $f(\boldsymbol{x})$ and constrain condition which must be satisfied by the control variables.

2.1 Optimization Algorithms

Considering two control variables x_1 and x_2 (the input parameters) the control plot given by the numerical value of the objective function that the control variables return is showed in the design space 2.1.

The presence of constraints in the formulation of the problem leads to feasible design space region with upper and lower bounds and infeasible design space. The optimum solution is represented by the peak on the top of the control plot that is the maximum of the objective function.
The gradient based approach for the optimization problems provides the use of the derivative of the cost function with respect to the design variable in order to evaluate the sensitivity analysis. A maximum or a minimum in the design space represents a location with zero gradient. From the second derivative instead, it is possible to evaluate if the zero radient point is a maximum or a minimum.

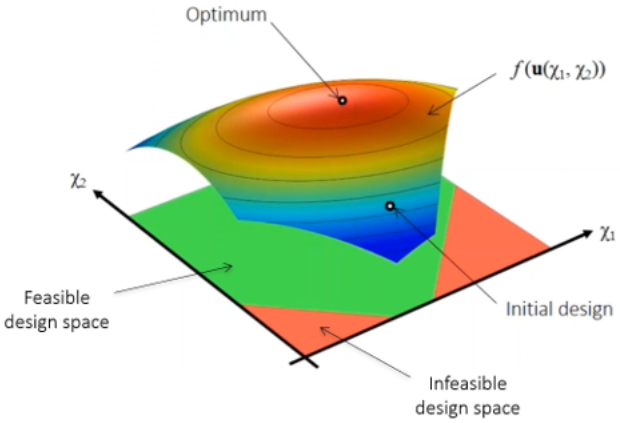

Figure 2.1: Design space of two control variables

In case the cost function is not differentiable or the gradient fluctuates, COMSOL Multiphysics provides Gradient-Free methods in which the optimum is evaluated through a triangulation algorithm: the solution is computed in three different points and the algorithms tends to move in the direction of the maximum (or minimum).
An important issue for optimization problem is the presence of multiple minima (or maxima) in the design space. In this case, since the algorithm can converge to a local minima rather than a global one, the solution depends on the starting point.

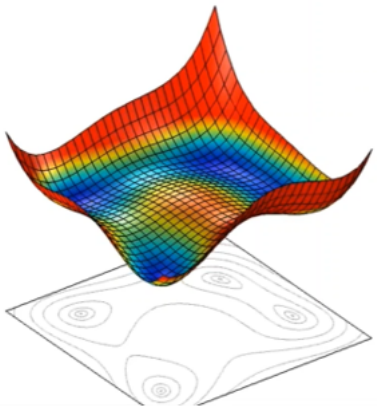

Figure 2.2: Design space with local minima

In the module there are three gradient based solvers.
The first is based on the SNOPT (Sparse Nonlinear OPTimizer) algorithm, developed by Philip E. Gill of the University of California San Diego, and Walter Murray and Michael A. Saunders of Stanford University. It implements a sparse sequential quadratic programming (SQP) algorithm with limited-memory quasi-Newton approximations to the Hessian of the Lagrangian. It is mainly used for nonlinear problems and can be applied for any cost function with no limitation on the constrains.
The second is the MMA (Method of Moving Asymptotes). It was developed by Krister

Svanberg of KTH Royal Institute of Technology and can manage problems with large number of control variables, as in case of Topology optimization.
The last solver is the Levenberg-Marquardt. It converges faster than the previous algorithms, however, since it require the objective function to be of least-squares type and it does not support constrains, this solver is not used in the following optimizations.

The gradient-free algorithms available are Nelder-Mead, BOBYQA, COBYLA and a coordinate search method.

2.2 Optimization Theory

As discussed before, the optimization problem is aimed at defining the control variables that minimize or maximize the objective function subjected to constrains that collectively define the feasible set of allowable values for the control variable. The problem can be formulated as:

$$\begin{cases} \overset{min}{\xi} Q(\xi) \\ \xi \in C \end{cases} \tag{2.1}$$

Where ξ are the control variables, Q is the scalar-valued objective function and C is the feasible set. With the hypothesis of sufficient continuity the feasible set can be expressed as a set of inequality constraints:

$$C = \{\xi : lb \leq G(\xi) \leq ub\} \tag{2.2}$$

Where G is a vector valued function.
Considering Multiphysics problems modelled with PDE, it is worthwhile to parametrize the problem with the control variable and optimize a cost function which depends on the PDE solution. Hence, the objective function results to be a function of the PDE solution and ultimately of the control variables. The discretization of the system can be represented by a set of equations $L(u(\xi), \xi) = 0$, where u is the solution of the PDE and ξ is the control variable. The PDE is added as an equality constraint to the general optimization problem to obtain the complete PDE-constrained optimization problem.

$$\begin{cases} \overset{min}{\xi} Q(\xi) \\ L(u(\xi), \xi) = 0 \\ \xi : lb \leq \xi \leq ub \end{cases} \tag{2.3}$$

In COMSOL Optimization Module the objective function can be defined as the sum of three contributions:

$$Q(u, \xi) = Q_{global}(u, \xi) + Q_{probe}(u, \xi) + \sum_{k=0}^{n} Q_{int,k}(u, \xi) \tag{2.4}$$

Where n is the dimensional space of the Multiphysics problem. The contributions are defined as:

- Q_{global} is the global contribution of the objective function Q and it is given as a general global expression.
- Q_{probe} is a probe contribution to the objective function Q. its definition is confined to a point in a given geometrical entity.
- $Q_{int,k}$ is an integral contribution to the objective function Q. its definition is restricted to a set of geometric entities of the same dimension.

In genral, the total contribution of each term of the objective funtion is defined as the sum of each single contribution of the same optimization interface even if defined in different nodes. This leads to the possibility of weight each contribution with a weighting coefficient in order to define a customized optimization scaling the different contribution of the objective function.
Regarding the specification of constraints, the Optimization interface differentiates the bounds between those applied on the control variable, those defined with pointwise or integral inequalities and global inequality constraints.

2.3 Topology Optimization

In literature several approaches to topology optimization are present including homogenization, density model, level set, topological derivatives and evolutionary approaches. The density model, one of the the oldest methods and the most used nowadays, is based on the discretization of the design domain with a control variable associated to a fictitious material on nodes or elements. Through an interpolation of the control variable ranging from 0 to 1 it is possible to solve the physical governing equation in case it is equal to 1, and an equation associated with the fictious material in case the control variable is equal to 0 [20].
Furthermore, a filter able to introduce a minimum legth scale is often applied on the design variable as a contrain in order to avoid the ill posedness of the problem.
In a finite element analysis, the design control variable previously discussed is defined as γ. The optimal structure layout is obtained by topology optimization determining for each element of the design domain if there should be a material, associated to ($\gamma = 1$) or another with ($\gamma = 0$). The topology optimization problem is formulated as:

$$\begin{cases} \overset{min}{\gamma} : F = F(u(\gamma), \gamma) = \displaystyle\int_\Omega f(u(\gamma), \gamma)\, dV \\ subjected\ to : G_0(\gamma) = \displaystyle\int_\Omega \gamma(x)\, dV - V_0 \leq 0 \\ \qquad\qquad\qquad : G_i(u(\gamma), \gamma) \leq 0, i = 1, ..., M \end{cases} \tag{2.5}$$

The problem reads: Find the material distribution that minimizes the objective function F, subject to a volume constraint $G_0(\gamma)$ and other possible M constraints, $G_i(u(\gamma), \gamma)$. Where u is the state variable field which satisfies the state equations. The density variable $\gamma(x)$, which is the control variable of the optimization problem, defines the material distribution. The design domain Ω is characterized by point with $\gamma(x) = 1$ indicating, as discussed in next sections, liquid material, and points with $\gamma(x) = 0$ indicating solid material.
Considering a finite element discretization of the design domain Ω, the control variable is defined by N elements or nodal design variables. The optimization problem reads:

$$\begin{cases} \overset{min}{\gamma} : F = F(u(\gamma), \gamma) = \sum_i \int_{\Omega i} f(u(\gamma_i), \gamma_i)\, dV \\ subjected\ to : G_0(\gamma) = \sum_i u_i \cdot \gamma_i - V_0 \leq 0 \\ \qquad\qquad\qquad : G_i(u(\gamma), \gamma) \leq 0, j = 1, ..., M \\ \qquad\qquad\qquad : \gamma_i = 0\ or\ 1, i = 1, ..., N \end{cases} \tag{2.6}$$

Where γ is the design variable vector of length N.
In this formulation of the optimization problem, the control variable can only have discrete values (0 or 1). Nevertheless, since the presence of a large number of variables in topology optimization makes the problem difficult to solve, the discrete variables are replaced with continuous ones. Since the intermediate values of the design variable can't be associated to a physical interpretation, the optimization problem is modified using a penalty method. Defining γ the control variable used for volume computation, the penalysed material volume γ_p is used for the material interpolation with the introduction of a penalization to get a 0-1 solution.In the optimization Module different interpolation schemes are present:

- SIMP $\gamma_p = \gamma_{min} + (1 - \gamma_{min})\gamma^p$
- RAMP $\gamma_p = \gamma_{min} + \frac{\gamma(1-\gamma_{min})}{1+q(1-\gamma)}$
- Darcy $\gamma_p = \frac{q(1-\gamma)}{q+\gamma}$

Where p is the penalization parameter.
The SIMP (Solid Isotropic Material with Penalization) and RAMP (Rational Approximation of Material Properties) interpolation schemes are suitable in solid mechanics applications, while Darcy method is more performing with fluid mechanics.
Through the use of a continuous design variable it is possible to use gradient-base algorithms since it is possible the evaluation of the derivative of the objective function with

respect to the control variables. The continuous problem reads:

$$\begin{cases} \overset{min}{\gamma} : F = F(u(\gamma), \gamma) = \sum_i \int_{\Omega i} f(u(\gamma_i), \gamma_i)\, dV \\ subjected\ to : G_0(\gamma) = \sum_i u_i \cdot \gamma_i - V_0 \leq 0 \\ \qquad\qquad : G_i(u(\gamma), \gamma) \leq 0, j = 1, ..., M \\ \qquad\qquad : \gamma_{min} \leq \gamma_i \leq 1 or 1, i = 1, ..., N \end{cases} \tag{2.7}$$

In case of 3D simulations, the density filter is an effective tool to avoid the ill-posedness of the optimization problem. Furthermore, this filter introduces a minimum length-scale R_{min} on a domain control variable γ. In the following optimizations an efficient density filtering is obtained with a Helmholtz-type PDE filter.

$$\gamma_f = R_{min}^2 \bigtriangledown^2 \gamma_f + \gamma_c \tag{2.8}$$

γ_f is the filtered material volume factor. The continous filtered variable is discretized with linear polynomials.
The filtered design variable can present a band with intermediate densities. Even if it leads to an optimization easier to solve, the intermediate control variables introduce unphysical intermediate properties affecting the final optimal design. The intermediate band can be reduced introducing a projection of the filtered design variable field toward the limit values 0 and 1. The projection used is based on the hyperbolic tangent function:

$$\gamma = \frac{tanh(\beta(\gamma_f - \gamma_\beta)) + tanh(\beta\gamma_\beta)}{tanh(\beta(\gamma_\beta)) + tanh(\beta\gamma_\beta)} \tag{2.9}$$

γ is the output material volume factor while γ_β and β are the projection point and slope, respectively.

In figure 2.3 the flow of computations of COMSOL Topology Optimization with density model is shown. The initial homogeneous distribution of material is defined through a constant distribution of the design variable gamma. The finite element analysis is performed solving the system of algebraic equation and the state variables are obtained. The initial objective function and the constrains are evaluated and the sensitivity analysis is performed. Than the design variables are updated through a gradient based algorithm. The exposed loop is iterated until a convergence criterion is satisfied. The optimal solution can be finally analyzed.

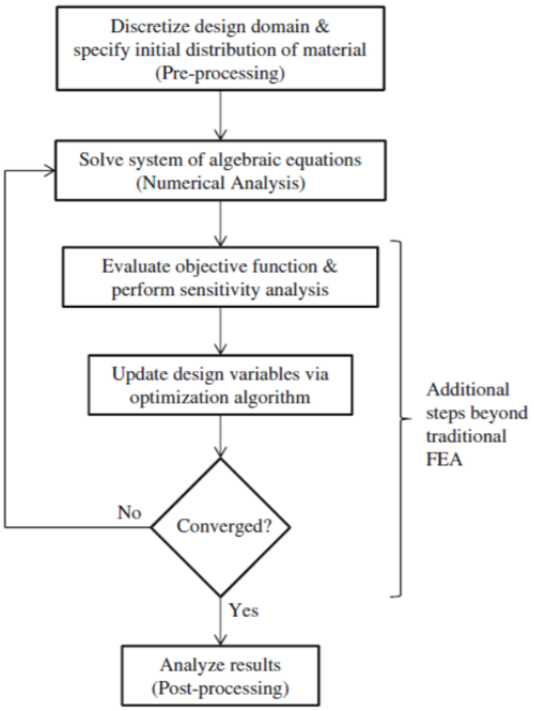

Figure 2.3: Flowchart of computations of COMSOL topology optimization

Numerical Tests: COMSOL

In this chapter the numerical results of the simulations carried out with the optimization module introduced in the previous chapter are reported. In the first part three 2D benchmarks already present in literature [1] are presented: two single physics problems governed by pure heat conduction and laminar flow and a Multiphysics problem of fluid flow including heat transfer. This first part was meant to achieve a compete knowledge of the optimization software and the solutions represented a promising starting point for the developement of an open source code optimization solver in chapter 4. Than a tridimensional Multiphysics problem was investigated carrying out the optimization of a fin for the heat transfer between a heat sink and a cooling system in forced convection regime.

3.1 2D Optimizations

In the following paragraphs 2D numerical simulations of optimization problems are presented. Starting from single physics problems of pure heat conduction and laminar flow, following with Multiphysics problem optimization. The decision of starting with single physics problems is justified by the intent of characterize the optimization parameters and interpolation schemes needed for the single physics aspect and a better understanding of the optimization solvers.

3.1.1 Single Physics: heat conduction

In the following section the numerical results for pure heat conduction optimization problem are presented. These simulations represent a good starting point for topology optimization investigation due the semplicity of the governing equation. In this first numerical test the objective is the definition of the optimal conduction path to remove from a square uniformly heated.

Problem description

The numerical optimization problem, figure 5.6, was constituted by a 2D square with 100 [mm] edges subjected to uniform heat generation of 3 $\left[\frac{W}{m^3}\right]$ in a pure heat conduction domain. The temperature in the central portion of the left edge was set equal to 293 [K] and represented the heat sink while adiabatic boundary conditions were imposed to the

other edges.

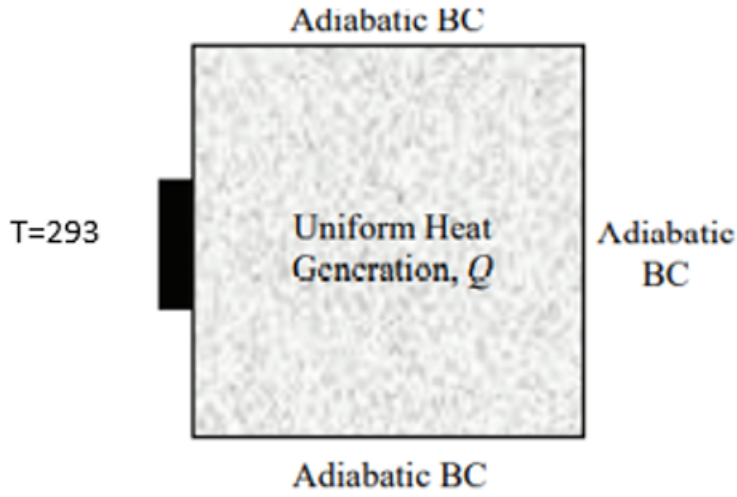

Figure 3.1: design domain and boundary conditions for pure heat conduction [1]

Each element was associated to a value of the design variable γ that was related to the thermal conductivity through ad interpolation scheme. The design variable ranges between 0 and 1 and represent materials with respectively low and high thermal conduction coefficients values.

Governing equation
The governing equation for steady state pure heat conduction is the Fourier's law:

$$- \bigtriangledown(k(\gamma)\nabla T) = Q \tag{3.1}$$

Where $k(\gamma)$ was the thermal conductivity of the material depending on the design variable, T was the temperature state variable and Q was the volumetric heat generation in the domain.

Objective funtion
The objective function J of this optimization problem was defined as the dissipation of heat transport potential capacity:

$$J = \int_{\Omega} (k\nabla T)^2 \, dV \tag{3.2}$$

This expression for the objective function had the physical meaning of the overall heat transfer capability. Since its dissipation is the dissipation rate of the heat transfer capacity, this objective function was equivalent to minimize the mean temperature of the design domain Ω subjected to a constant heat generation.

Interpolation scheme

For the interpolation of the thermal conductivity the SIMP approach was used.

$$\gamma_p = \gamma_{min} + (1 - \gamma_{min})\gamma^{p_{simp}} \tag{3.3}$$

Where γ is the control design variable, γ_p is the penalized variable, p_{simp} is the penalization coefficient and γ_{min} is defined as 0.001.
With the preceding interpolation scheme the thermal conductivity was defined as:

$$k(\gamma) = k_{max}\gamma_p \tag{3.4}$$

Where k_{max} was the thermal conductivity of the more conductive material and was set equal to 1 $[\frac{W}{mK}]$. Therefore, the thermal conductivity ranges from 0.001 for the less conductive material to 1 depending from the design variable as shown below:

$$\gamma = \begin{cases} 1 : k = k_{max} = 1 \left[\dfrac{W}{mK}\right] \\ 0 : k = k_{min} = 0.001 \left[\dfrac{W}{mK}\right] \end{cases} \tag{3.5}$$

In figure 3.2 the SIMP interpolation curves of the thermal conductivity are shown.

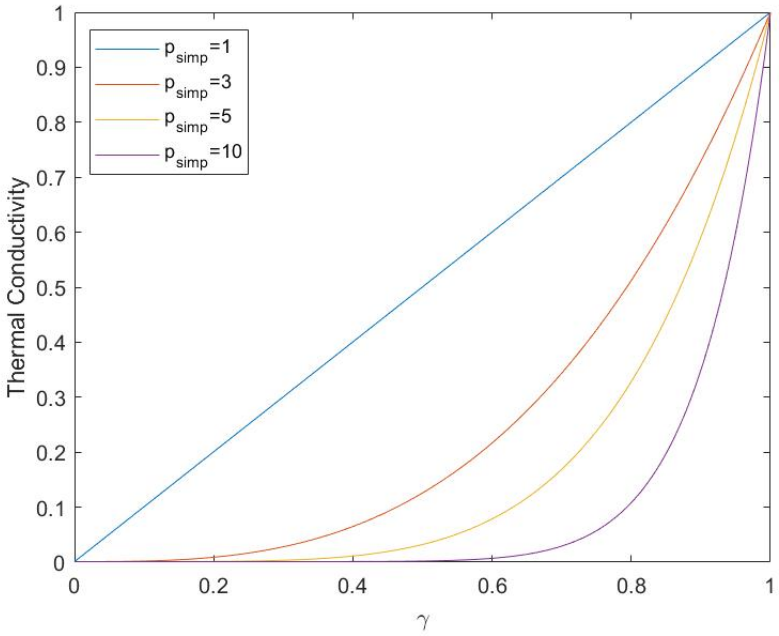

Figure 3.2: SIMP intermpolation of thermal conductivity

The final expression of the optimization problem was defined as:

$$\begin{cases} Find : \gamma \\ Minimize : J = \omega \int_{Omega} k(\nabla T)^2 \, d\Omega \\ Subjectto : -\nabla[k(\gamma)\nabla T] = Q \\ \qquad\qquad \int \gamma \, d\Omega_d - V_{max} \leq 0 \\ \qquad\qquad 0 \leq \gamma \leq 1 \\ Given : K(\gamma) = (0.001 + 0.999\gamma^{p_{simp}})k_{max} \end{cases} \tag{3.6}$$

The limit volume of the solid material, imposed through the upper bound limit on the allowable solid material V_{max} is mandatory for this kind of optimization since, as easily expected, the solver algorithm would tend to set all the possible volume as most conductive material.
The mesh, halved for the symmetry of the problem, was unstructured triangular type with 12 480 elements.

Numerical Results
In this section the optimal solutions obtained with SNOPT solver with different volumetric fraction of the conductive material are shown.

- $V_{target} = \frac{\int_{\Omega_d} \gamma \, d\Omega d}{V_{max}} = 0.3$

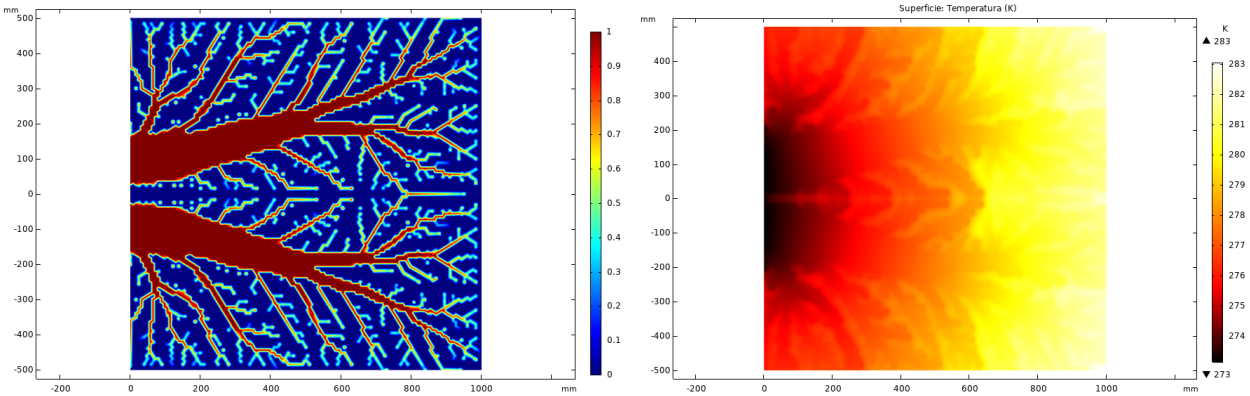

(a) *Topology Optimization* (b) *Temperature*

Figure 3.3: $V_{target} = 0.3$: topology optimization and temperature field

- $V_{target} = 0.4$

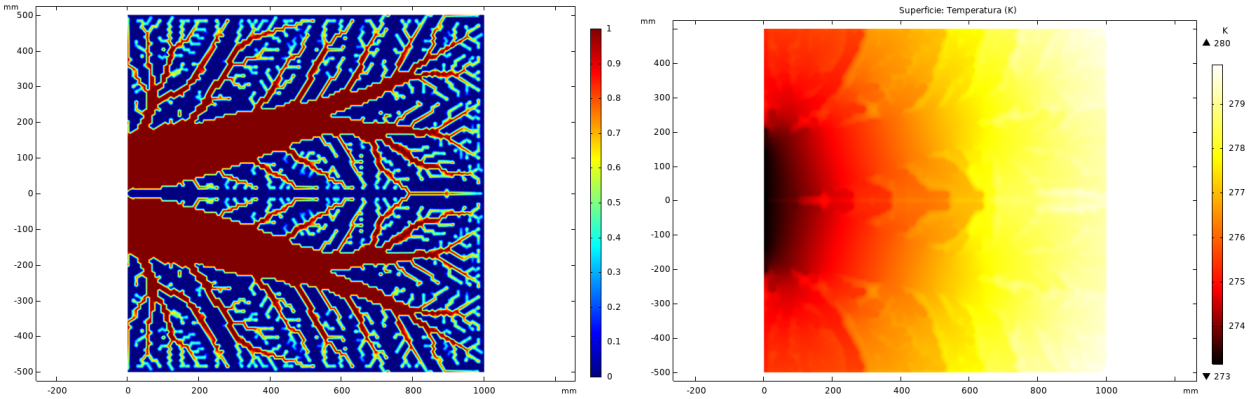

(a) *Topology Optimization* (b) *Temperature*

Figure 3.4: $V_{target} = 0.4$: topology optimization and temperature field

- $V_{target} = 0.5$

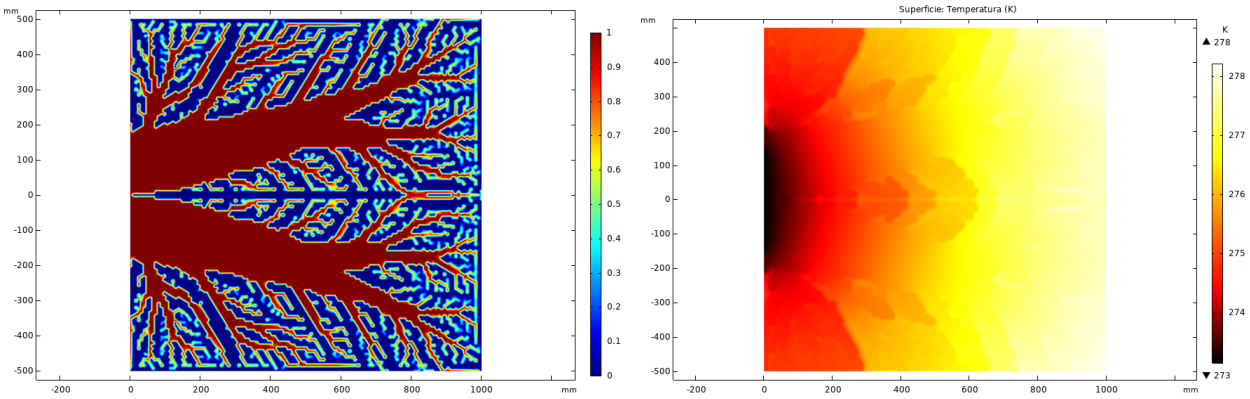

(a) *Topology Optimization* (b) *Temperature*

Figure 3.5: $V_{target} = 0.5$: topology optimization and temperature field

In the optimal solutions obtained, the dendritic distributions of the conductive material were consistent with those already present in literature. Increasing the volume fraction of the conductive material, the total thermal excursion of the domain decreased from 10 [K] for the fist case with $V_{target} = 0.3$ to 5 [K] in the last case with $V_{target} = 0.5$. Consequently, also the average temperature of the domain presented a decreasing pattern. In the first case the mean temperature was equal to 278.23 [K] while in the third case was 276.28 [K].

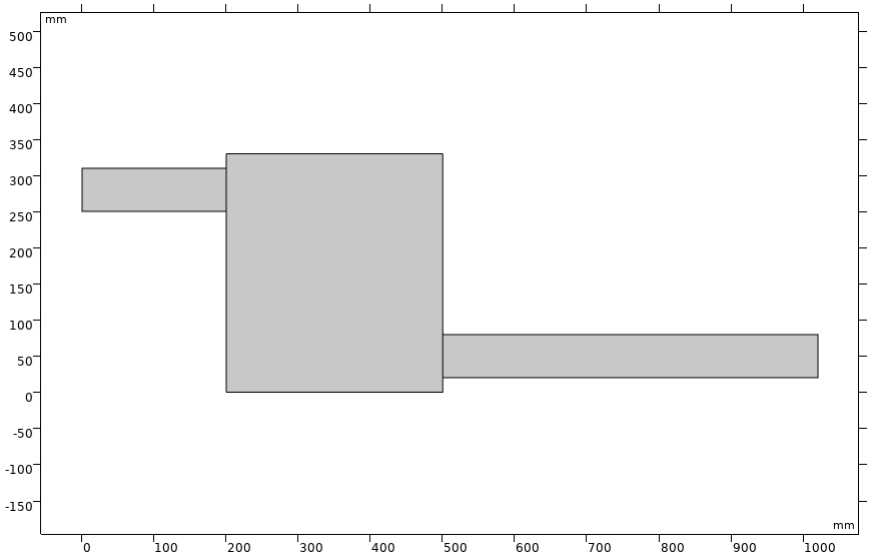

Figure 3.6: Laminar Flow: initial geometry

3.1.2 Single Physics: Laminar Flow

In this section the optimization of a domain only governed by pure laminar flow is presented. Topology optimization of Navier-Stokes equations is subject of interest for different applications and branches for example ventilation systems and pipes design. In this model the objective was to find the optimal distribution of a porous material in a box connecting two pipes set at different height minimizing the total pressure drop of the system. The expected solution is a S-bend shape geometry of the final duct.

Problem description
The problem, as shown in figure 5.1 was constituted by two pipes, 0.2 [m] and 0.52 [m] long with 0.06 [m] diameter, connected to a rectangular box 0.33 [m] heigh and 0.3 [m] width. The centerlines of the two parallel pipes are at 0.23 [m] of distance. The inlet velocity was imposed at 0.0266 $[\frac{m}{s}]$ and zero pressure boundary condition was imposed for the outlet.

Governing equations
The fluid dynamics was modeled with 2D Navier-Stokes equations and continuity equation under the assumptions of stationary laminar flow and incompressible fluid:

$$\begin{cases} \rho_{fl} \cdot (\boldsymbol{u} \cdot \nabla)\boldsymbol{u} = -\nabla p + \mu(\nabla^2 \boldsymbol{u}) + \boldsymbol{F} \\ \rho_{fl}(\nabla \cdot \boldsymbol{u}) = 0 \end{cases} \tag{3.7}$$

In the Navier-Stokes equation the Brinkman friction term $\boldsymbol{F}$ was present to introduce a penalization for the fluid velocities in the solid material of the design domain. This term, represented by a volumetric force, was present only in the design domain, in this case the

central rectangular box, and was a function of the design control variable:

$$\boldsymbol{F} = \alpha(\gamma) \cdot \boldsymbol{u} \tag{3.8}$$

Where α is the inverse permeability of porous medium and was defined with the interpolation scheme as a function of the design variable $\gamma : \Omega \rightarrow [0, 1]$.
In this case the Darcy interpolation scheme for the design variable was used:

$$\gamma_p = \frac{q(1-\gamma)}{q+\gamma} \tag{3.9}$$

Where γ_p was the penalized design variable and q wass the penalization factor. in figure 3.7 the Darcy interpolation scheme with different values of the penalization factor q is shown.

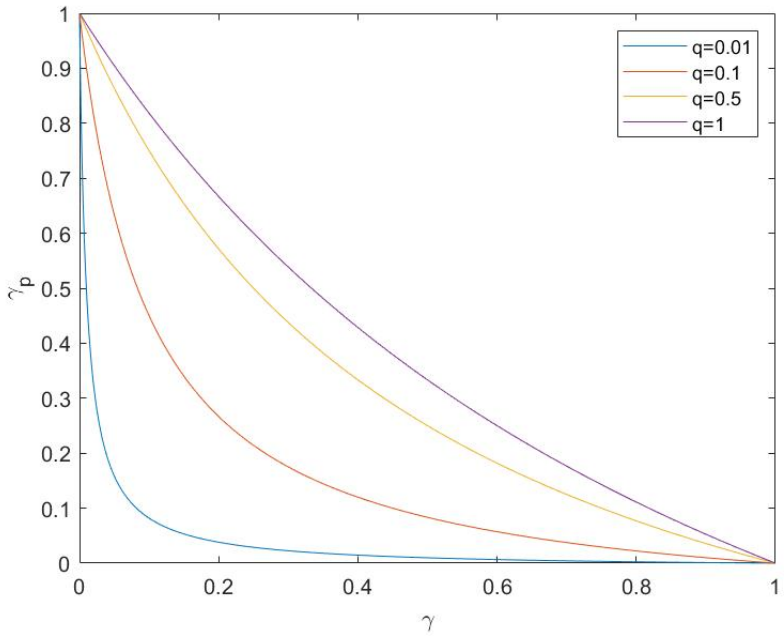

Figure 3.7: Darcy interpolation scheme

The inverse of permeability was so defined as:

$$\alpha = \alpha_{max} \cdot \gamma_p \tag{3.10}$$

Where α_{max} was related to the dimensionless Darcy number, Da, according to:

$$Da = \frac{\mu}{\alpha_{max} \cdot L^2} \tag{3.11}$$

where μ is the dynamic viscosity $[Pa \cdot s]$. Therefore the porosity in the design domain varies from zero to α_{max} according to:

$$\gamma = \begin{cases} 1 : \alpha = 0 \rightarrow \textit{liquid domain} \\ 0 : \alpha = \alpha_{max} \rightarrow \textit{solid domain} \end{cases} \tag{3.12}$$

Objective function

The objective function chosen for this single physics benchmark was defined as the difference between the average pressure at the inlet and the outlet of the duct.

$$J = p_{avg,inlet} - p_{avg,outlet} \tag{3.13}$$

The final expression of the optimization problem was defined as:

$$\begin{cases} Find : \gamma \\ Minimize : J = p_{avg,inlet} - p_{avg,outlet} \\ Subjectto : \rho_{fl} \cdot (\boldsymbol{u} \cdot \nabla)\boldsymbol{u} = -\nabla p + \mu(\nabla^2 \boldsymbol{u}) + \boldsymbol{F} \\ \qquad\qquad \rho_{fl}(\nabla \cdot \boldsymbol{u}) = 0 \\ \qquad\qquad 0 \leq \gamma \leq 1 \\ Given : \alpha = \alpha_{max} \cdot q \cdot \dfrac{(1-\gamma)}{q+\gamma} \end{cases} \tag{3.14}$$

In this case a volume constrain on the porosity field was not mandatory. A value of solid volume fraction different from the optimal one was penalized inducing an higher value of inlet pressure.

Numerical results

in the figure below the distribution of porous material obtained with MMA solver is shown. The red areas, characterized by a value of control variable equal to 1, represent the open channel with free fluid flow while the other areas represent the solid domain.

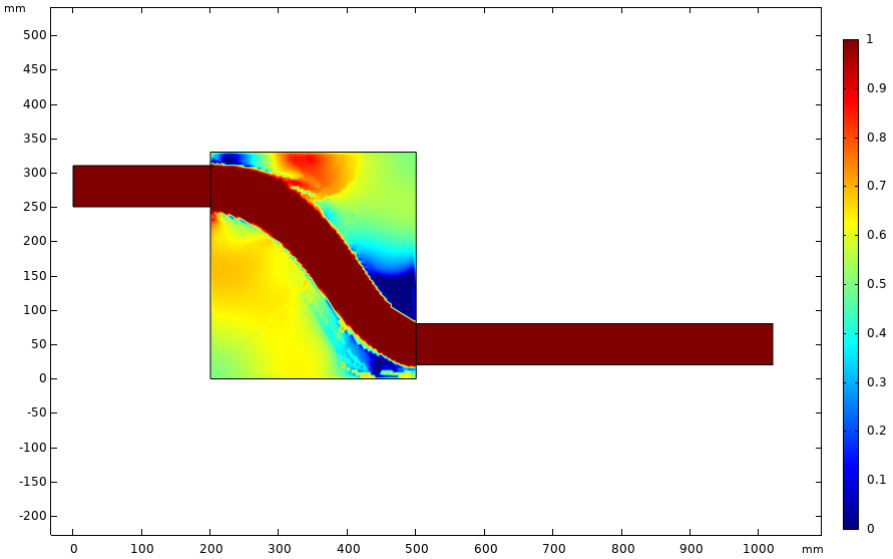

Figure 3.8: Topology optimization result

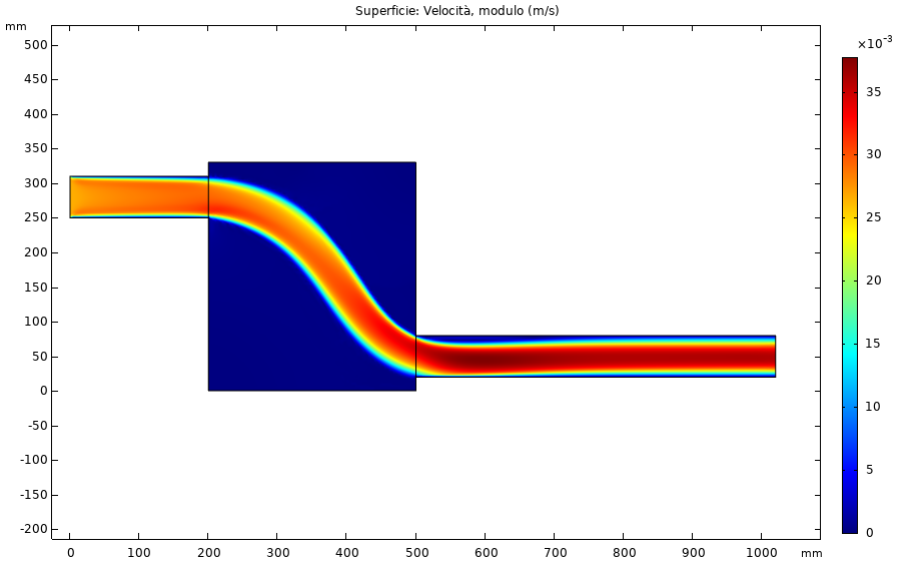

Figure 3.9: Velocity field in optimized geometry

The expected S-bend shape for the duct was obtained and the pressure drop in the system decreased from the value of 0.729 [Pa] before the optimization to 0.335 [Pa].

3.1.3 Multiphysics Optimization

In this section more complex physics are examined in the optimization problem. The optimization of a 2D three-terminal heat sink cooling performances were investigated through topology optimization process.
In the following numerical tests the objective function was defined as the sum of two contribution: a thermal contribution aimed at the minimization of the mean temperature in the device and a fluidic one aimed in reducing the total pressure drop in the system. Varying weighting factors that multiply each contribution of the objective function, was possible to obtain different results scaled more toward an optimization despite the other one.
COMSOL's Optimization Module with SNOPT and GCMMA as optimization algorithms were used. In the following sections the 2D Multiphysics model and the optimization set up are presented.

Model description

The 2D three-terminal structure, figure 5.10, was composed by four subdomains. The central square domain with 100 [mm] edges, subjected to uniform heat generation Q=100 $[\frac{kW}{m^3}]$, represented the primary design domain. The distance between the two fluid outlet terminals on the right side was 20 [mm]. The inlet temperature was fixed at 293 [K] and parabolic normal fluid flow with average value of 0.01 $[\frac{m}{s}]$ was assumed at the single inlet of the device. Convective flux, zero pressure and normal flow boundary conditions were assumed at both the outlets. No-slip and adiabatic boundary conditions were enforced on all the external walls of the device.

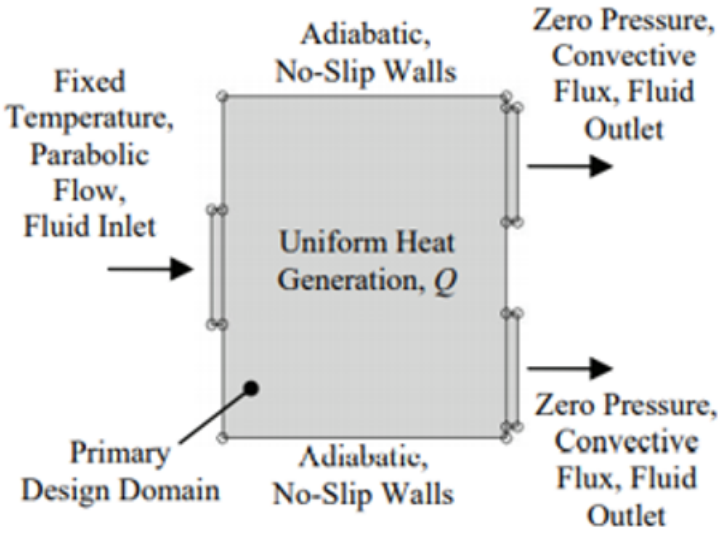

Figure 3.10: topology optimization design domain and boundary conditions for fluid flow and heat transfer [1]

Governing equations
The fluid dynamics was modeled under the assumptions of stationary laminar flow and incompressible fluid with 2D Navier-Stokes equations and continuity equation:

$$\begin{cases} \rho(\boldsymbol{u} \cdot \nabla)\boldsymbol{u} = -\nabla p + \mu(\nabla^2 \boldsymbol{u}) + \boldsymbol{F} \\ \rho(\nabla \cdot \boldsymbol{u}) = 0 \end{cases} \tag{3.15}$$

As in the previous case, in the Navier-Stokes equation the Brinkman friction term was introduced as penalization term for the fluid velocities in the solid material of the design domain. The volume force was defined as function of control variable as before and the same Darcy interpolation scheme was adopted.

The heat transfer in the fluid was modelled with the steady state convection-diffusion equation:

$$\rho C(\boldsymbol{u} \cdot \nabla T) = \nabla \cdot (k \nabla T) + Q \tag{3.16}$$

Where C is the heat capacity, k is the thermal conductivity of the fluid and Q is the uniform heat generation.

Objective function
In this optimization, a dual objective function was adopted for the optimization of both heat transfer and fluid flow. The global objective function is defined as:

$$A = \omega_1 B + \omega_2 C \tag{3.17}$$

where B and C were defined as follows:

$$B = \int_{\Omega} (T - T_{in})^2 \, d\Omega \tag{3.18}$$

$$C = \int_{\Omega} \left[\frac{1}{2} \eta \sum_{i,j} \left(\frac{\partial u_i}{\partial x_j} + \frac{\partial u_j}{\partial x_i} \right) + \sum_i \alpha(\gamma) u_i^2 \right]^2 d\Omega \tag{3.19}$$

The thermal objective function B is related to the difference between the mean temperature of the design domain and an objective temperature, in this case the inlet temperature of the fluid flow. The second objective function is proportional to the total flow power dissipated in the fluidic system.
ω_1 and ω_2 are weighting factors of the two objective function used to calibrate the convergence of the optimization toward the minimization of the fluidic power dissipation or the mean temperature. In the following section these two parameters were changed manually to investigate the different topology solutions with different dominance of one objective function term to the other one.

Numerical results

Before proceeding with the optimization, the simulation of the initial problem was performed. This allowed to evaluate the benchmark initial condition and the margin of improvement introduced by the optimizations. The results are shown below:

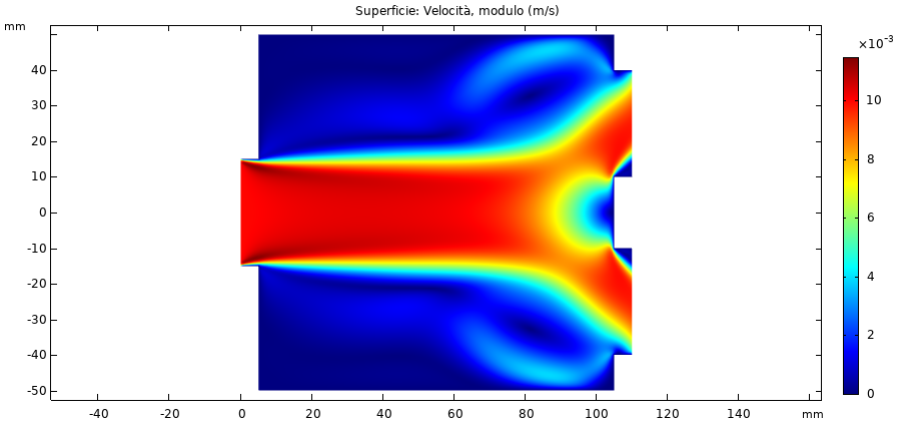

Figure 3.11: Velocity field with no optimization

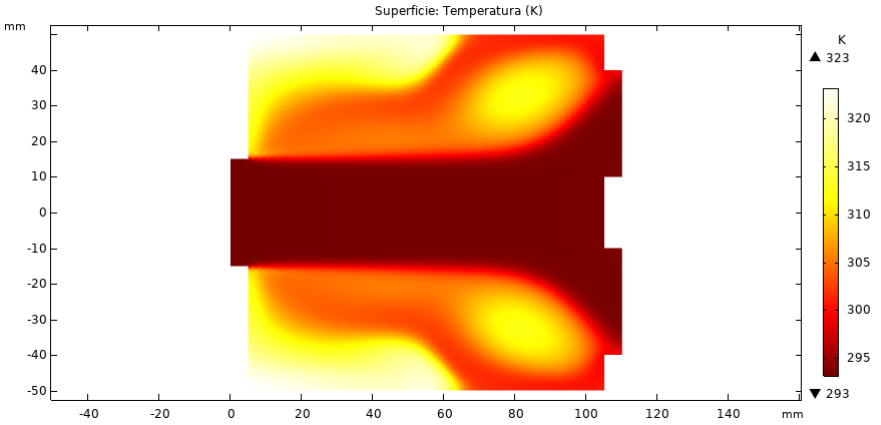

Figure 3.12: Temperature field with no optimization

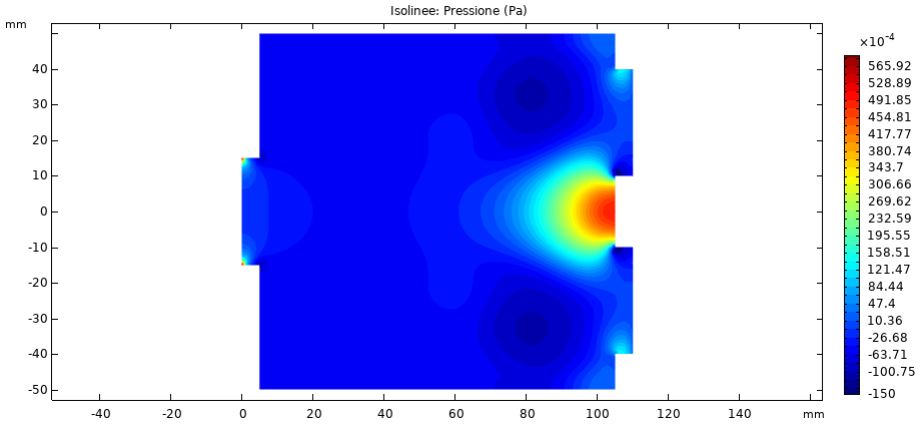

Figure 3.13: Pressure field with no optimization

The results obtained from this first simulation outlined a pressure drop in the domain equal to 0.0051259 [Pa] and the maximum temperature reached was equal to 323 [K] which induced a thermal excursion of about 30 [K] .

In the following optimization tests, the initial values of the design variables are reported since multiphysics topology optimization problems present a large dependence on the starting point of the optimization algorithm. The initial value reported led to the global minima of the objective function. Other values of starting point could lead to local minima.

Test 1

In the first numerical optimization, the weighting factor ω_1 associated to the thermal objective function was set equal to 0.01. This induced an optimization dominated by the thermal objective function to the detriment of the fluidic one. The SNOPT solver algorithm was used for the multiphysics optimizations specially for the low error of convergence even if it toke an higher number of iterations despite the MMA algorithm. For this optimization a very low value of error was required for the consistency of the results due the low values of state variables, in particular the pressure.

The volume constrain imposed in the simulations was set as follows:

$$0 \leq \int_{\Omega} \gamma \, d\Omega \leq 0.003 \tag{3.20}$$

The initial value of the design domain was $\gamma_0 = 0.3$.

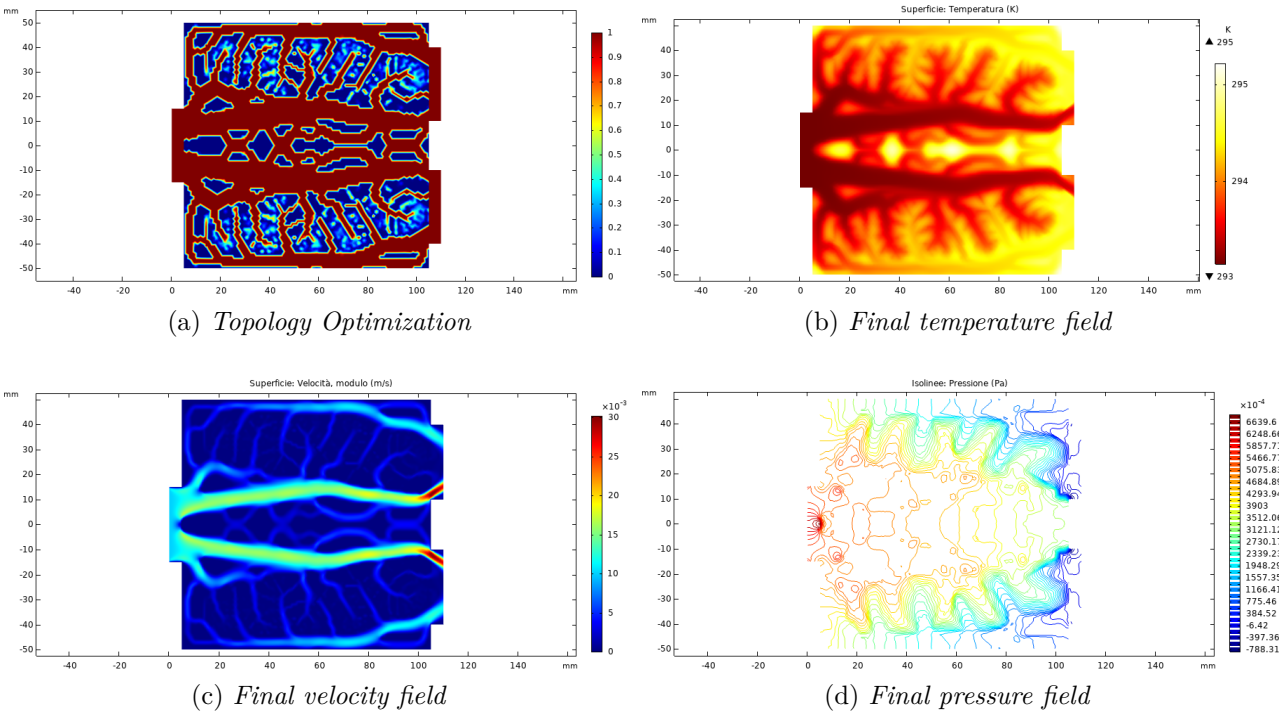

(a) *Topology Optimization* (b) *Final temperature field*

(c) *Final velocity field* (d) *Final pressure field*

Figure 3.14: Numerical results with $\omega_1 = 0.01$

In figure 3.14 the topology optimization of the design domain is shown. The red parts, corresponding to $\gamma = 1$, are associated to liquid water regions dominated by fluid flow. The blue parts with $\gamma = 0$ instead, represents the solid regions in which the fluid flow is inhibited by the volume force. The topology result shows how the algorithm tends to maximize the length of the liquid path in the domain in order to export the maximum value of heat in the heated region.
With this first Multiphysics optimization, aimed in a maximum thermal optimization of the domain, the temperature excursion dropped from 30 [K] to 2 [K]. This important thermal result was obtained neglecting the optimization of the total flow power dissipated in the fluidic system. Indeed the total pressure drop of the system was equal to 0.5691 [Pa] against the initial value of 0.0051259 [Pa].
The initial and final values of the total objective function were $A_i = 0.0089794$ and $A_f = 1.0339 \cdot 10^{-4}$.

Test 2

In the second numerical optimization the weighting factor associated to the thermal objective function was decreased to $\omega_1 = 0.001$, ten times smaller than the previous one. Whith this new value of weighting factor, the fluid flow optimization started to affect the

overall optimization. In this case the starting value of the design variable was $\gamma_0 = 0.7$.

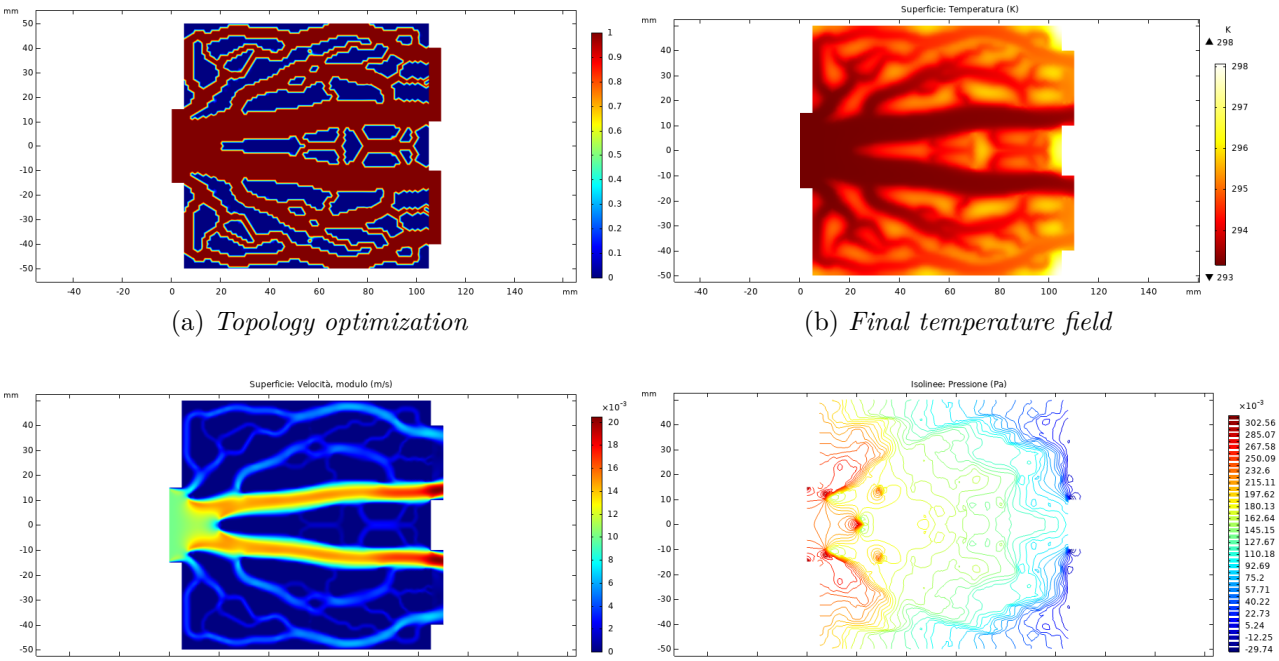

(a) *Topology optimization* (b) *Final temperature field*

(c) *Final velocity field* (d) *Final pressure field*

Figure 3.15: Numerical results with $\omega_1 = 0.001$

As shown in the results(figure 3.15), the thermal excursion raised up to 5 [K], 3 [K] higher than to the previous case but, as expected, the total pressure drop decreased to 0.25036 [Pa].
The total objective function before the optimization was $A_i = 8.9953 \cdot 10^{-4}$, while after the optimization its value was equal to $A_f = 3.5818 \cdot 10^{-5}$.

Test 3

In the last multi-objective function optimization, the weighting factor was decreased to $\omega_1 = 0.0001$, that is 100 times smaller with respect to the first case. This parameter selection leads to an optimization more oriented toward the fluidic optimization than before, even if globally more unbalanced toward the thermal optimization.
The starting point of the design variable was increased up to 1 in this simulation. The numerical results are shown below.

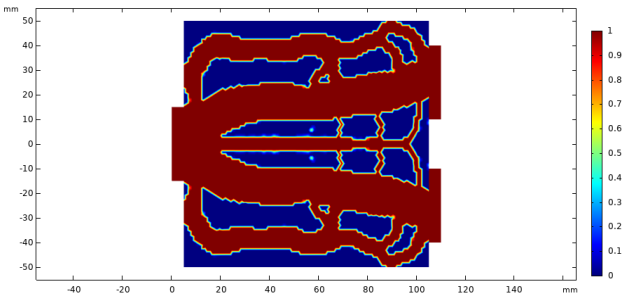

(a) *Topology optimization*

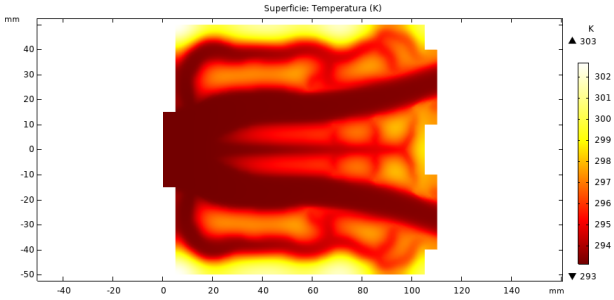

(b) *Final temperature field*

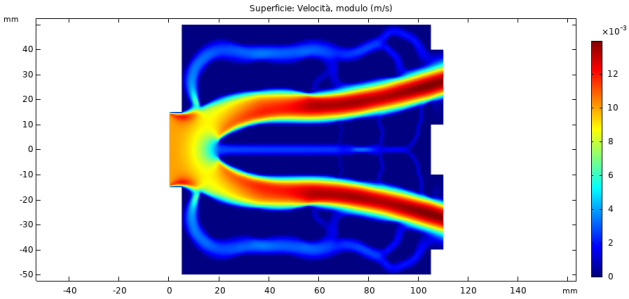

(c) *Final velocity field*

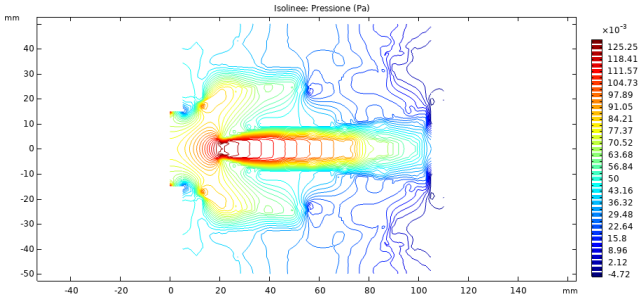

(d) *Final pressure field*

Figure 3.16: Numerical results with $\omega_1 = 0.0001$

The highest temperature difference reached in the system was equal to 10 [K] and the total pressure drop was 0.07659 [Pa]. The initial and final values of the total objective function were: $A_i = 9.1542 \cdot 10^{-5}$ and $A_f = 1.3606 \cdot 10^{-5}$. The results showed a decrease of the cost function of about 85%.

Test 4: single physics objective function test
In this last optimization of 2D Multiphysics problem, the coefficient regarding the weighting of the thermal contribution of the objective function was set equal to zero. Hence, the following numerical results are associated to a pure fluidic optimization of the system aimed at minimizing the total flow power dissipated in the system.
In this case, the MMA optimization algorithm was used.

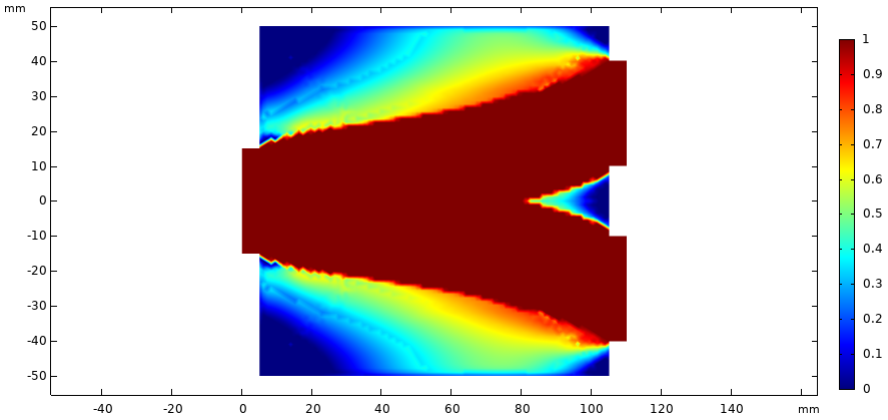

(a) *Topology optimization*

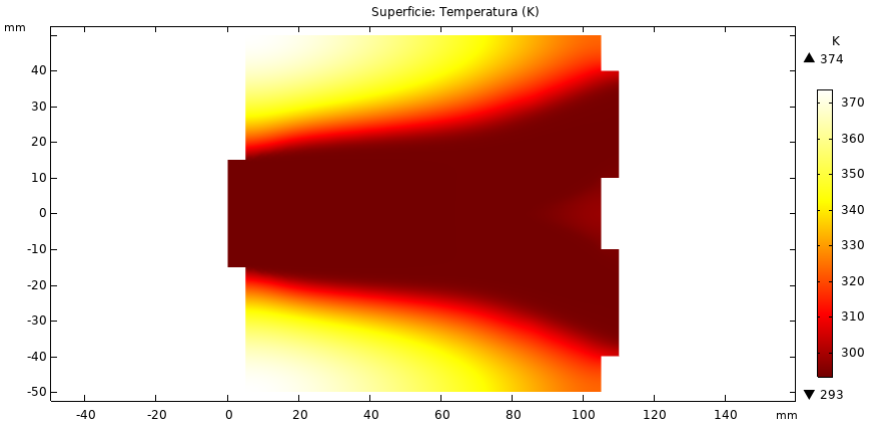

(b) *Final temperature field*

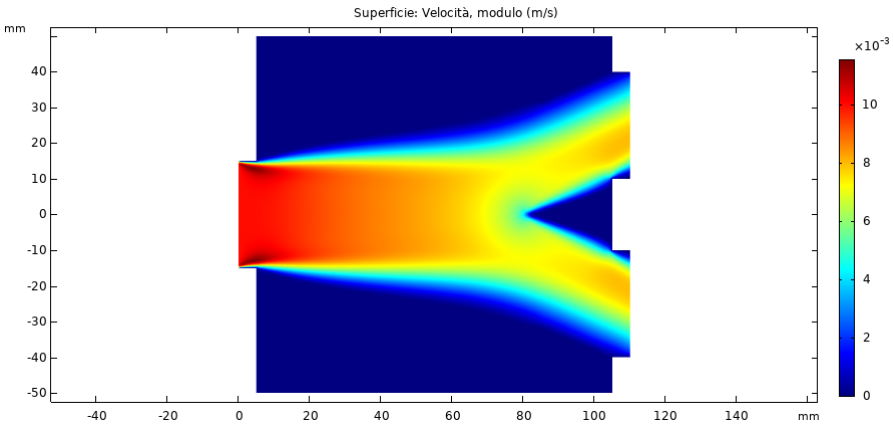

(c) *Final velocity field*

Figure 3.17: Numerical results with pure fluid flow optimization

The preceding optimization led to a maximum temperature difference of 81 degrees. Nevertheless, the total pressure drop decreased to a value of $4.4969 \cdot 10^{-4}$[Pa].

3.1.4 Benchmarks conclusions

In the proceedings sections, the COMSOL topology optimization via gradient based algorithms was applied to a series of 2D benchmarks. First, single physics optimizations were investigated. The density model was applied to the design domain to account the interpolation of a fictious porosity material and the thermal conductivity. The method was then extended to multiple physical processes including convection-diffusion and Navier-Stokes flow. The results obtained in these benchmarks proved to be coherent with those obtained in previous studies so that they represented a good starting point for the developement of this thesis work. In particular, these results turned out to be important for both the next optimization problem of 3D ducted cooling system in forced convection regime and the development of an adjoint based algorithm for topology optimization in OpenFoam.

3.2 3D Optimization

In this section, the optimization of a tridimensional Multiphysics problem is presented. The knowledge gained in the previous simulation is used to set up an optimization of the interface between a heated solid material and a cooling fluid, water in this case. In particular, the following numerical simulation wass aimed at defining an optimal topological design of a fin used for an heat sink cooling. Then, the topology optimization result was filtered and exported as a geometry and used for a validation test aimed at analyzing and quantifying the improvement of the heat transfer capability of the structure in comparison with a standard rectangular fin. This kind of simulation can eventually find an industrial application in particular device including chip cooling.

Model description

The model, showed in the figure fig.3.18, was constituted by an heat sink in the lower part (solid 1) and a rectangular plate with a fin above it (respectively solid 2 and solid 3). Solid 3 represented the starting point for the fin optimization. The solid components were mounted inside a duct with rectangular cross section and cooled by water in forced convection regime. This structure was used to define and analyze the cooling capacity of the system.
At the inlet a pressure boundary condition (p_{inlet}) was imposed. With this condition there was no need to impose a minimization of flow power dissipated in the fluidic system in the objective function. A topology design inducing a large pressure drop results in a lower value of fluid velocity and consequently a degraded cooling capacity. In the following simulation the pressure at the inlet was set equal to 0.005[Pa].
The fluid inlet temperature was imposed at 293 [K].
The lower part of the heat sink was subjected to a heat flux Q equal to 50[$\frac{kW}{m^2}$]. The external faces of the channel were thermally insulated with the exception of right one in which a symmetry boundary condition was imposed.

As mentioned before, the solid components were divided into 3 objects: solid 1, solid 2 and solid 3. The former characterizes the heat sink while the other two, in aluminum, defines respectively the fin base and the fin initial structure. The material characteristics

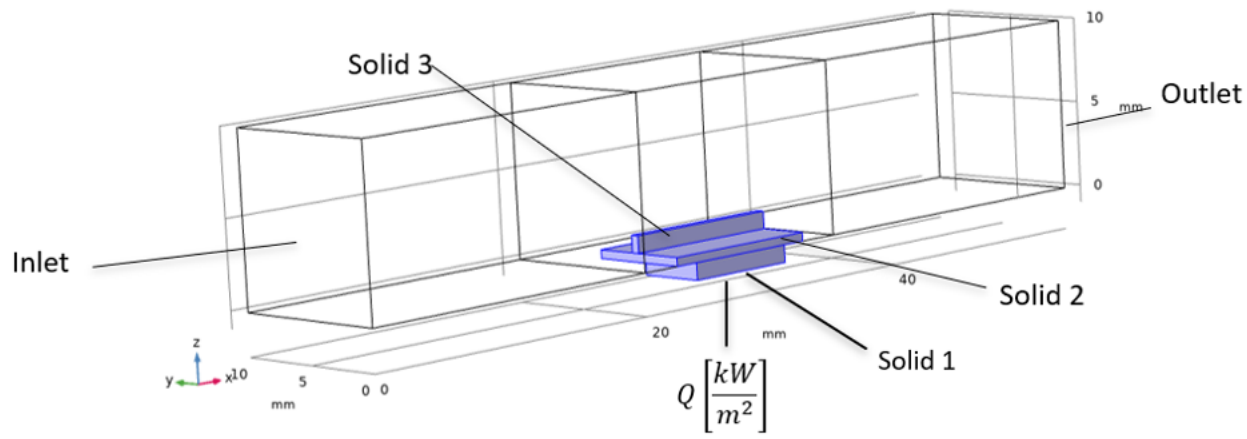

Figure 3.18: Design domain for 3D topology optimization

are described below:

Physical properties	solid 1	solid 2	solid 3
Thermal conductivity k $\left[\frac{W}{mK}\right]$	80	250	250
Density ρ $\left[\frac{kg}{m^3}\right]$	7874	2750	2750
Heat capacity C $\left[\frac{J}{kgK}\right]$	378	896	896

Table 3.1: Physical properties of solid componens

The decision of considering a little fin as the starting point for the heat exchanger optimization relies on the fact that the gradient based optimization algorithms need initial point near to the global solution to avoid the convergence in a local solution.
The fluid domain was divided into three sections. Only the central one was selected as design domain. For this reason the mesh,constituted by 218562 tetrastichal elements, was finer in the central part as shown in figure 3.19

Governing equations
The fluid dynamics was modeled with the Navier-Stokes equations and continuity equation under the assumption of stationary laminar flow and incompressible fluid:

$$\begin{cases} \rho_{fl} \cdot (\boldsymbol{u} \cdot \nabla)\boldsymbol{u} = -\nabla p + \mu(\nabla^2 \boldsymbol{u}) + \boldsymbol{F} \\ \rho_{fl}(\nabla \cdot \boldsymbol{u}) = 0 \end{cases} \tag{3.21}$$

Where $\boldsymbol{F}$ represented again the Brinkman friction term penalizing the fluid velocity inside the solid domain and, as in the previous Multiphysics optimization problem, it was defined as:

$$\boldsymbol{F} = \alpha(\gamma) \cdot \boldsymbol{u} \tag{3.22}$$

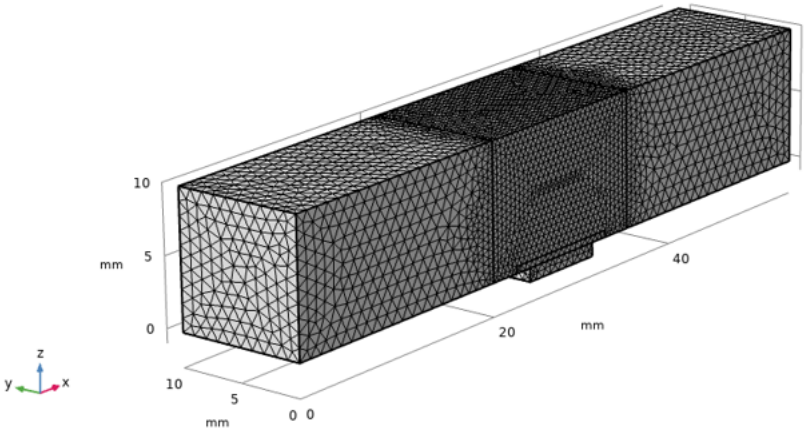

Figure 3.19: Mesh for 3D topology optimization

Again α was the inverse permeability of porous medium defined as:

$$\alpha = \alpha_{max} \cdot \gamma_p \tag{3.23}$$

Where γ_p was the penalized design variable interpolated through the Darcy scheme and q was the penalization factor.

The heat transfer in the fluid outside the design domain is modelled according to equation eq:3.24. Within the design space insted, the modelling of heat transfer is described by the equation eq:3.25 which includes an interpolation of the thermal conductivity based on γ.

$$\rho_{fl} C_{fl} \boldsymbol{u} \cdot \nabla T_{fl} - \nabla \cdot (k_{fl} \nabla T_{fl}) = 0 \tag{3.24}$$

$$\rho_{fl} C_{fl} \boldsymbol{u} \cdot \nabla T_{fl} - \nabla \cdot (k_{fl} I_k(\gamma) \nabla T_{fl}) = 0 \tag{3.25}$$

In solid domains, heat transfer was governed by pure heat conduction through the Fourier's law:

$$-\nabla(k(\gamma)\nabla T) = Q \tag{3.26}$$

The interpolation function of the thermal conductivity is presented below:

$$I_k(\gamma) = \frac{\gamma(C_k(1+b)-1)+1}{C_k(1+b\gamma)} \tag{3.27}$$

$$C_k = \frac{k_{fl}}{k_s} \tag{3.28}$$

Where $k_{fl} = 0.65[\frac{W}{mK}]$ and $k_s = 250[\frac{W}{mK}]$ are respectively the thermal conductivity of water and the solid material considered to optimize the fin, in this case aluminium. The

parameter b determines the convexity of the interpolation function. The plot of the interpolation function with different values of b is shown in figure fig.3.20. In this case b was set equal to 10.

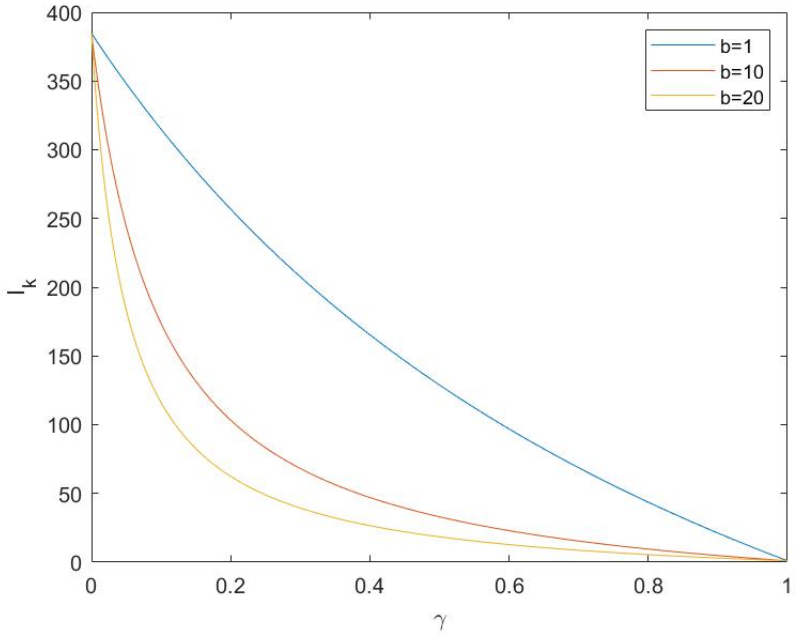

Figure 3.20: I_k interpolation

Hence, the design variable was used to interpolate both a volume force in the domain creating solid regions and the thermal conductivity of this solid fraction. This allowed to associate to the implemented solid region the thermal properties of the metal of interest, in this case the same thermal conductivity of the aluminum fin subjected to optimization.

Optimization problem
The objective function, proportional to the temperature difference with the inlet temperature of water, was valuated on the surface between the solid 2 and the fluid flow:

$$J = \omega \int_S (T - T_{in})^2 \, ds \tag{3.29}$$

The cost function is proportional to the mean temperature on the surface of the heat transfer between solid and cooling fluid. A minimization of this function leads to an improvement of the cooling capability of the fin.

A volume constrain was imposed considering the fraction of liquid over the total volume in the design domain as follows:

$$\int_\Omega \frac{\gamma}{Vol} \, d\Omega = 0.92 \tag{3.30}$$

Where Ω in the design domain and Vol is its total volume of the aforementioned domain.

A density filter was used for tridimensional fluid-thermal topology optimizations to avoid ill posedness of the problem and to introduce a minimum length scale into the design. The Helmholtz-type PDE filter was used for a computationally efficient density filtering. As mentioned in the previous chapter, the density filtering introduces a band with intermediate densities between the solid and the fluid region. Since this band has no physical meaning in the problem and can induce the simulation to wrong results, a smoothed Heaviside projection was used. The design variable field resulted projected toward 0 and 1 obtaining a design with sharper transition from fluid to solid.

3.2.1 Base case numerical results

First, a numerical test of the case without the optimization is performed. The temperature,velocity and pressure field are showed respectively in figures fig.3.21,fig.3.22 and fig.3.23

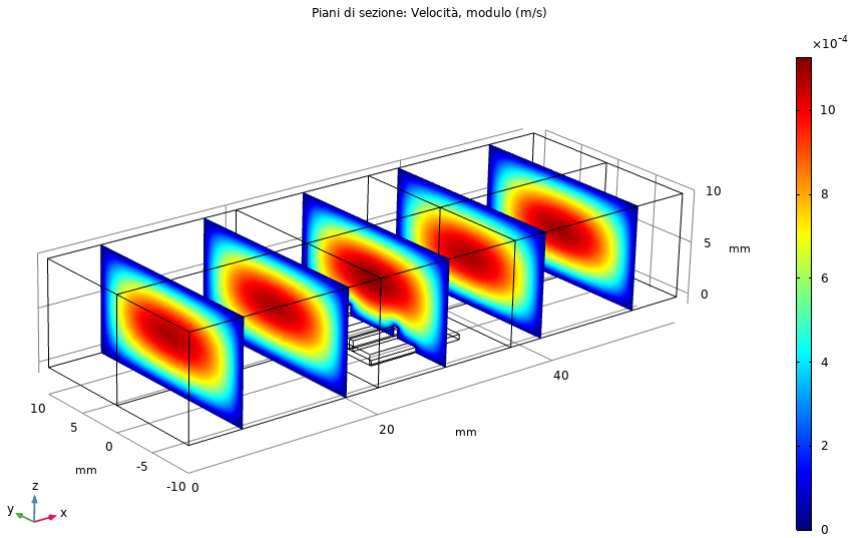

Figure 3.21: Initial velocity field

The average temperature on the surface between the solid plate and the cooling fluid was $T_{AVG} = 336.84[K]$ and the initial value of the cost function was $J = 0.0011533[\frac{m^2}{K^2}]$. These values were used to quantify the improvement introduced by the optimization.

3.2.2 Optimization numerical results

The optimization was performed using the SNOPT algorithm imposing a tolerance to the optimum equal to 10^{-9} and required 30 iterations of the COMSOL Topology optimization loop. The temperature,velocity and pressure fields obtained are shown in figures

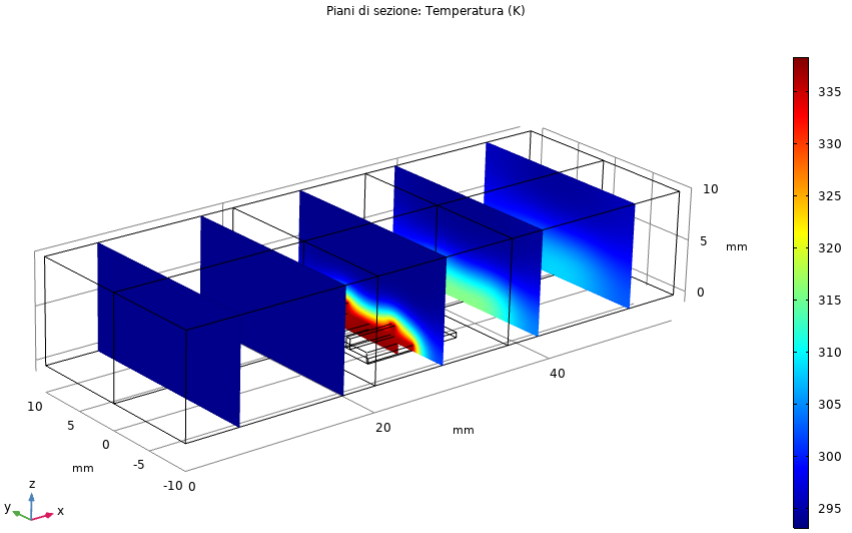

Figure 3.22: Initial temperature field

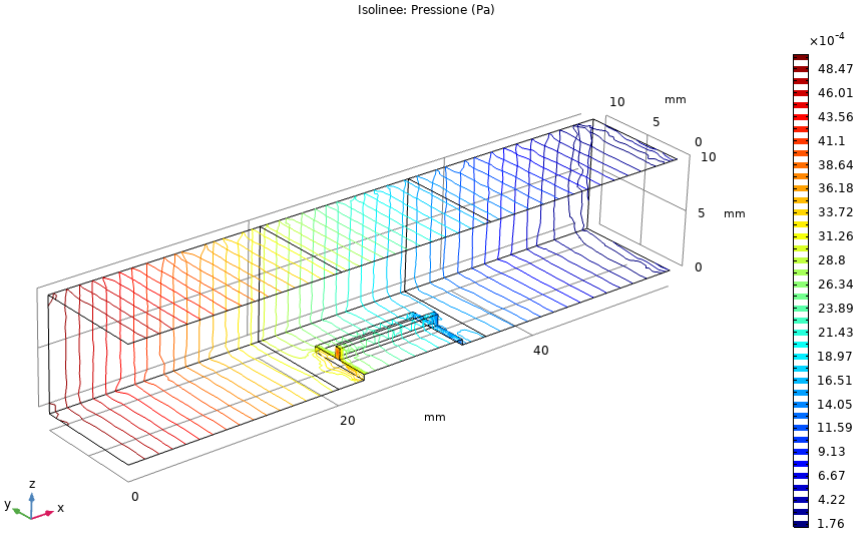

Figure 3.23: Initial pressure field

fig.3.24,fig.3.25 and fig.3.26

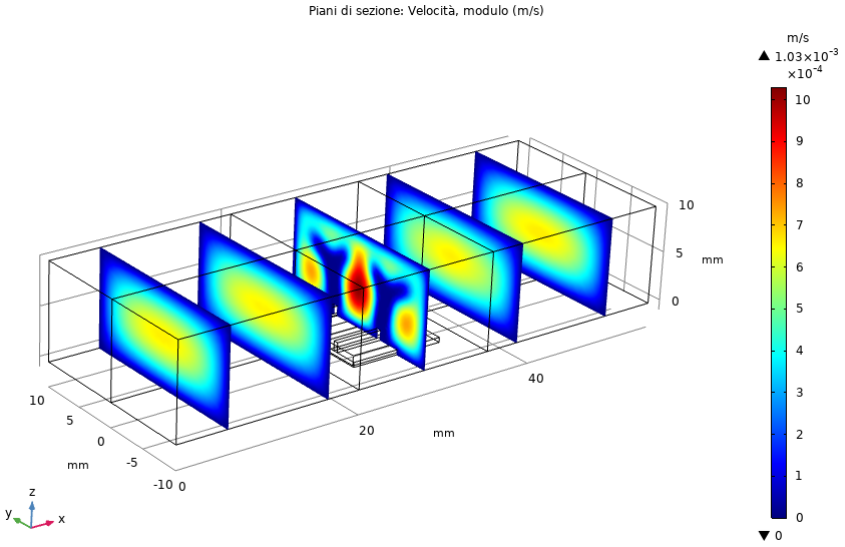

Figure 3.24: Optimized velocity field

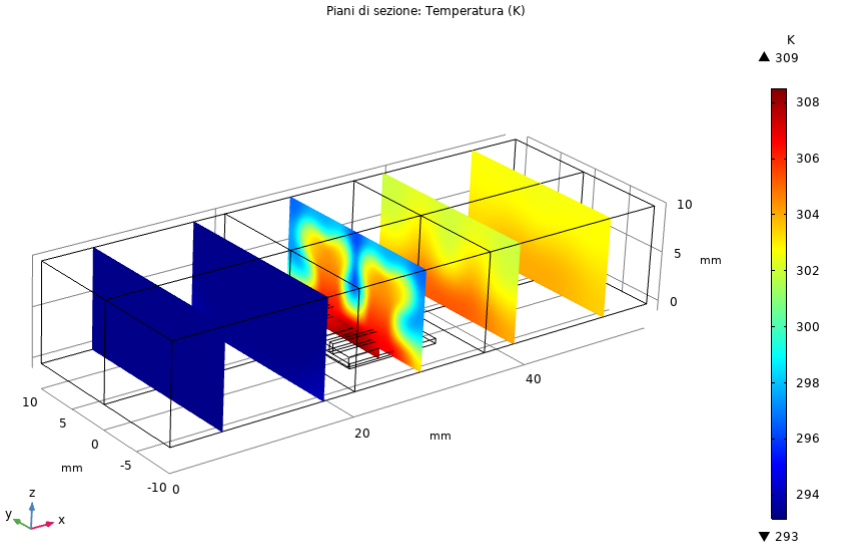

Figure 3.25: Optimized temperature field

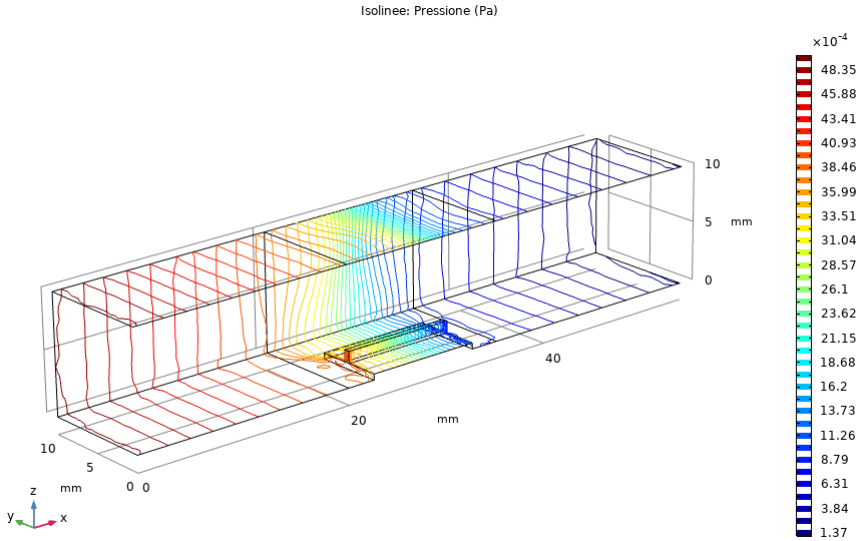

Figure 3.26: Optimized pressure field

The topology optimization is shown in figures fig.3.27 where a lower limit filter of 0.3 on the design variable is applied.

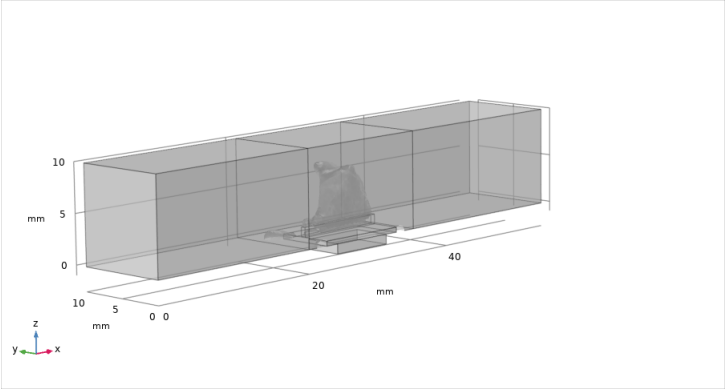

(a) *Topology optimization: axonometry*

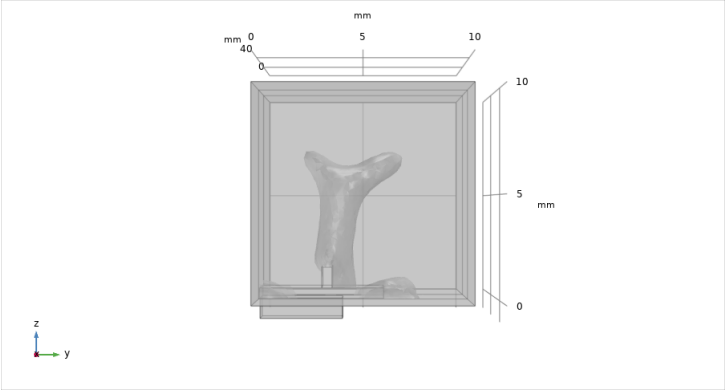

(b) *Topology optimization: (z,y) plane*

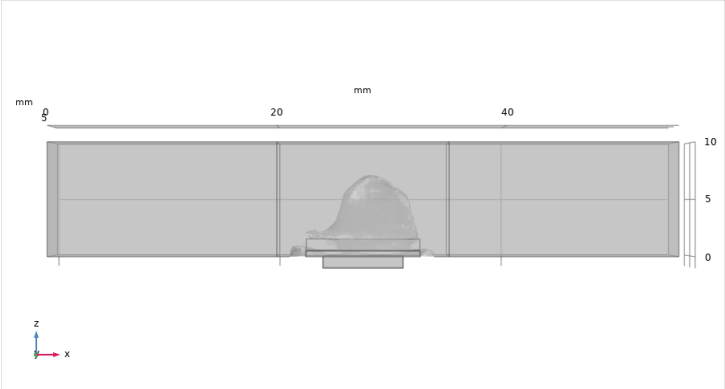

(c) *Topology optimization: (z,x) plane*

Figure 3.27: Topology optimization result

The geometry obtained with the optimization process led to a value of the cost function equal to $1.1793 \cdot 10^{-4}$ $[\frac{m^2}{K^2}]$ and an average temperature of the heated plate of 307.01 [K]. The decrease of the cost function of about 89% obtained led to a decrease of 29.83 [K] in the heated surface temperature, showing a promising optimization results.

3.2.3 Validation test

The optimized geometry just presented must be submitted to a validation test. Since in the topology optimization results the transition from fluid to solid was not enough sharp to induce a correct boundary layer evaluation, the topology outcome was exported for further tests. First, using the COMSOL Optimization Module tools, an initial mesh was built from the result filtered with lower limit filter equal to $(1 - \gamma) = 0.85$. Than the mesh was adapted to the geometry and the spurious entities were deleted obtaining the result shown in figure fig.3.28.

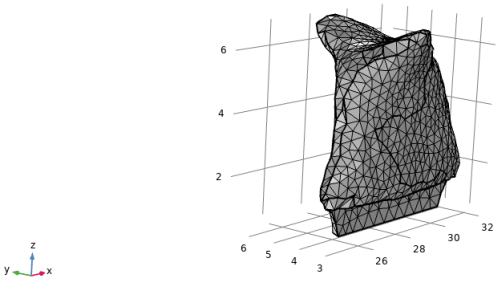

(a) *Mesh of opology optimization: axonometry*

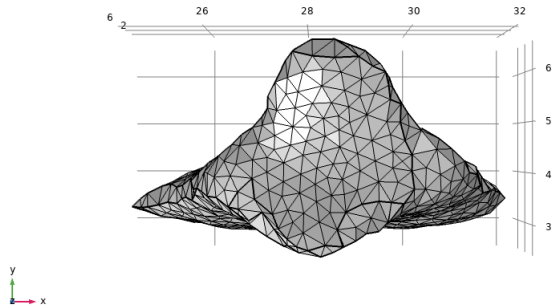

(b) *Mesh of opology optimization: (z,y) plane*

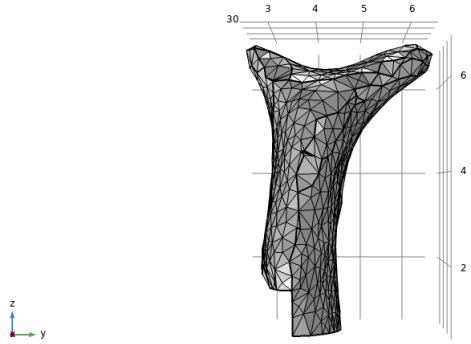

(c) *Mesh of opology optimization: (z,x) plane*

Figure 3.28: Mesh of opology optimization result

From the mesh, a new geometric entity was created. The complete solid structure obtained adding the solid 1,2 and 3 was collocated in the same cooling duct as before where the same boundary condition and operative conditions were imposed.

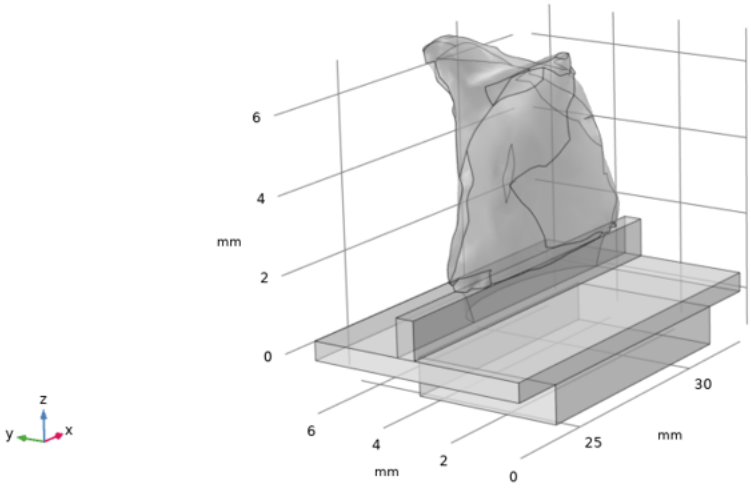

Figure 3.29: Final fin shape

In figures fig.3.30, fig.3.31 and fig.3.32 the final results of the optimized geometry are presented.

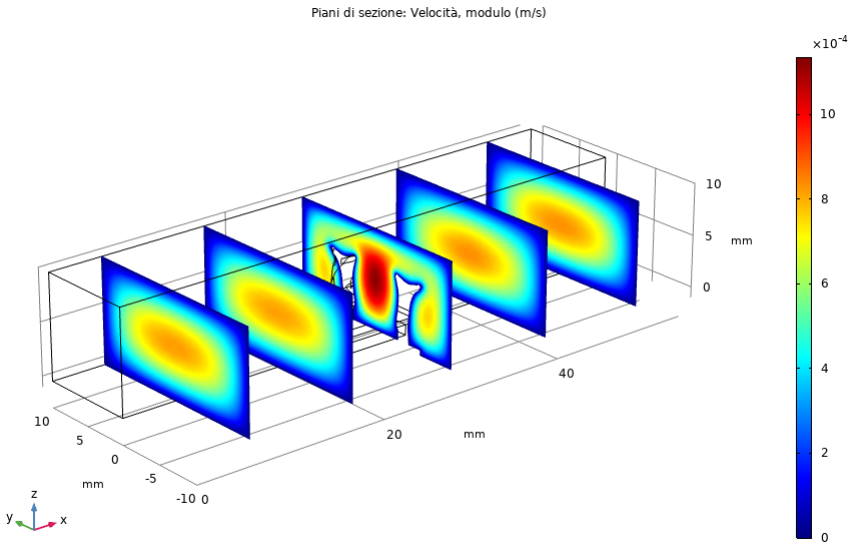

Figure 3.30: Final velocity field

As expected, the validation test led to different results in comparison with the previous one. In particular, this numerical evaluation presented degraded cooling performances. This is due to the absence of regions with intermediate values of the design variable that induce the presence of unphysical porous media with thermal properties improved respect water. In the previous results, this fictious material, even if it was not widely extended,

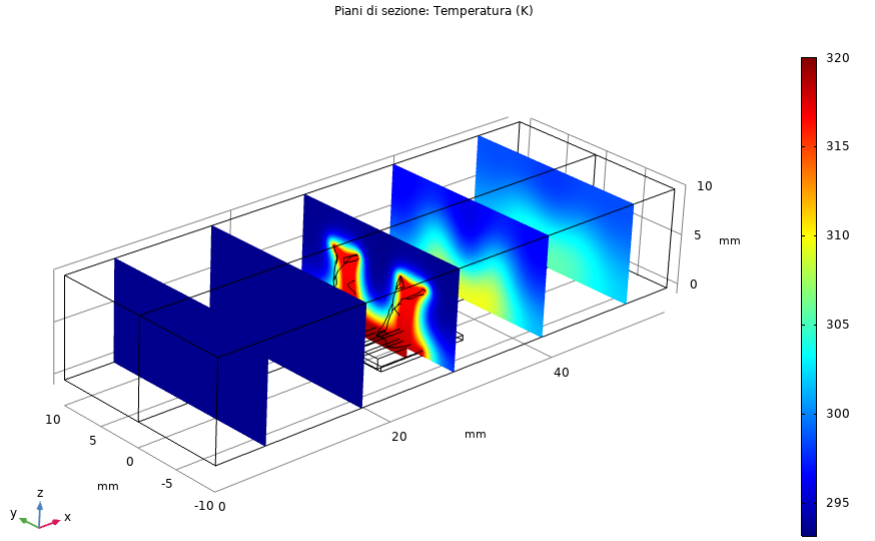

Figure 3.31: Final temperature field

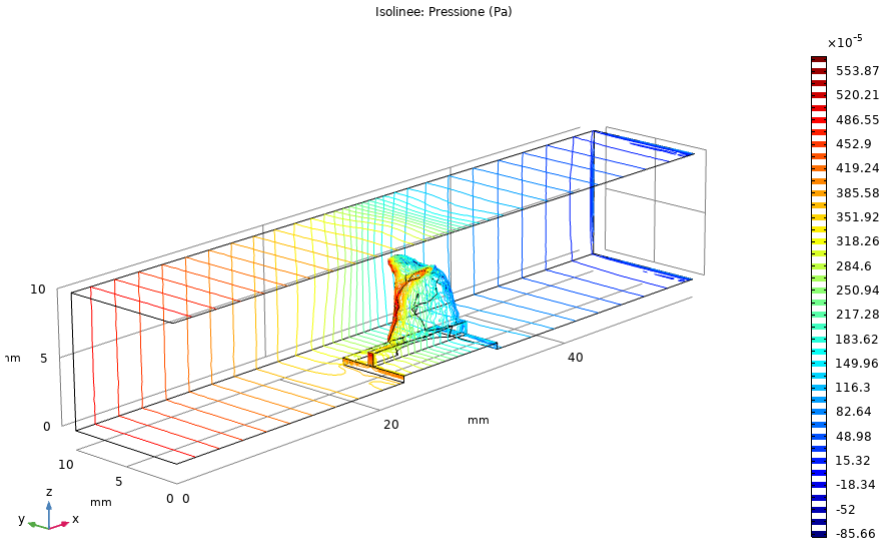

Figure 3.32: Final pressure field

led to a distortion of every vectorial and scalar field which induced improved heat transfer capability of the system.
In the validation test the average temperature on the heated surface was $T_{avg} = 318.34[K]$, 11.33 [K] higher that the optimization test but 18.5 [K] lower that the not-optimized case.

3.2.4 Comparison test

In conclusion, a comparison between the optimized fin and a standard rectangular one was performed. In order to make the two tests comparable, the fins presented the same total volume of $5.1136 \cdot 10^{-8}[m^3]$ and the same width(fig.3.33). The rectangular fin numerical results are shown below.

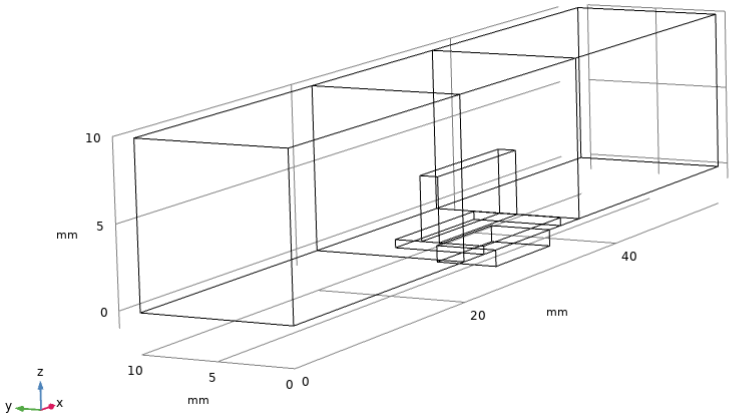

Figure 3.33: Geometry with rectangular fin

The comparison of the cooling performances of the three geometries exposed with different heat fluxes are showed in table 3.2

Results	Non-optimized Fin	Optimized Fin	Rectangular Fin
$T_{avg,50\left[\frac{kW}{m^2}\right]}[K]$	336.84	318.34	321.45
$T_{avg,100\left[\frac{kW}{m^2}\right]}[K]$	375.29	340.45	350.27

Table 3.2: 3D Optimization Results Comparison

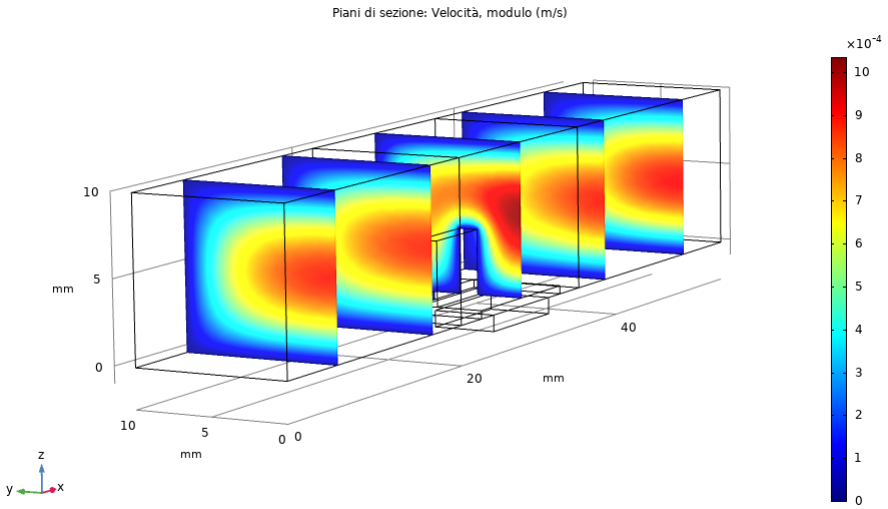

Figure 3.34: Velocity field with rectangular fin

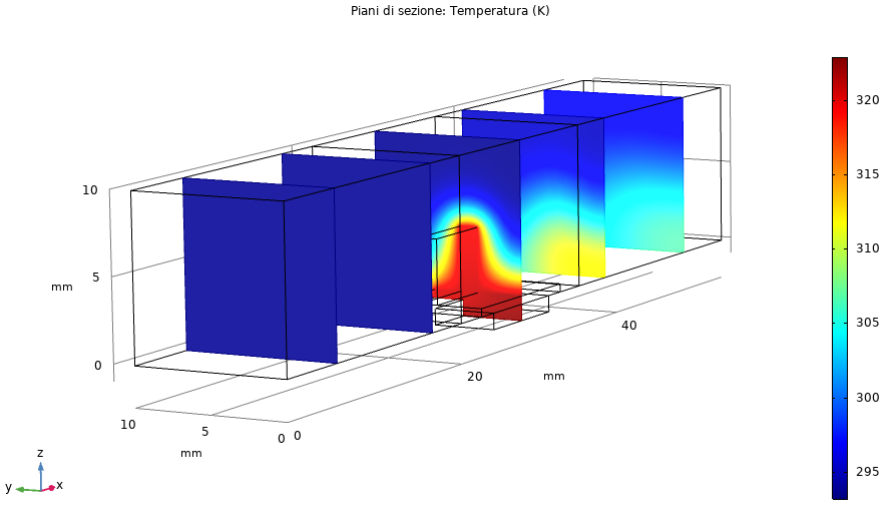

Figure 3.35: temperature field with rectangular domain

3.2.5 Conclusions

In this section of the thesis work, a tridimensional Multiphysics optimization has been performed. The knowledge achieved from benchmarks optimizations in the previous chapter resulted to be important for the interpolation of both porosity field and thermal conductivity.
The cooling performances optimization of an heat exchanger with fixed heat flux have been investigated. The solver increased the surface of the fin keeping a low total volume, as expected, obtaining a peculiar final shape. Than, the topology optimization result was filtered and exported to proceed with a more accurate validation test. The optimized fin was finally compared with a rectangular fin with the same volume. The results (table 3.2) showed that the optimized geometry actually led to increased cooling performances with respect to the other cases and this difference was more prominent with the increase of the applied thermal flux.
The COMSOL Optimization module resulted to be a very efficient tool also for the Multiphysics improvement of tridimensional geometries giving an initial conceptual design for further studies.

Adjoint Based Optimization: Openfoam

This chapter of the thesis work was aimed at developing a CFD open source code in OpenFoam for adjoint based topology optimization for fluid dynamics problems including heat transfer. The purpose of the following section was to lay a good starting point for further complex Multiphysics optimizations in nuclear application with the adjoint sensitivity analysis. This optimization methods represent a promising and efficient mathematical tool to face up to numerous nuclear engineering challenges regarding heat transfer systems and can be extended to other field such as neutronic. The results obtained with COMSOL Optimization module represented the starting point for following studies with an open source code. The three 2D simulations presented in the previous chapter were used as benchmarks also in the Openfoam optimization in order to make a comparison between the two software. First, a single physics optimization problem governed by laminar flow was considered using the adjoint shape optimization solver implemented in Openfoam. Then, a pure heat conduction problem was studied with an adjoint optimization solver based on Fourier's law. Finally the Multiphysics problem was faced with an adjoint optimization solver based on SimpleFoam and BuoyantBoussinesqSimpleFoam solvers.
As in the COMSOL module, Openfoam optimization is focused in minimizing an objective function dependent from the solution of the physical problem considered. In topology optimization a porosity field is introduced in the design domain as control variable acting on the solution of fluid dynamic problem and on the cost function. The porosity field defines regions characterized by solid domain and region with fluid domain in order to minimize the cost function and obtaining an optimal porosity distribution.
The use of an adjoint based method rises from the necessity of release the evaluation of the cost function gradient from the number of control variables. The majority of optimization methods base their algorithms on the information contained in the gradient of the objective function. This implies an onerous computational cost increasing proportionally to the number of control variables. The adjoint method represents an alternative procedure since the gradient is valuated from the governing equations of the system and the adjoint equations related to the first. Hence, the adjoint method constitutes a promising method for topology optimization problem characterized by a large number of design variable and its application can find numerous applications in complex systems.
In the following sections a Multiphysics problem governed by forced convection laminar flow and advection-diffusion heat transfer is presented. Then the adjoint equations are obtained showing the mathematical procedure through a Lagrangian approach.

4.1 Introduction

As exposed in the previous chapter, an optimization problem is aimed at finding the control and design variables that yield the minimization of a cost function J depending on a state system governed by algebraic and differential equations. The cost function can be an explicit expression of the control variable alone but in most cases is a function of the solution variables which are in turn implicitly functions of the design variable. Hence, the control parameters behave as input in the state system controlling the equations ad allowing the minimization of J. Any variation of the control variables leads to a variation of the function J. The purpose of the optimization problem is to find the control variable field that lead to a minimization of J. The sensitivity analysis, that is the sensitivity of a specific quantity with respect to variations in certain parameters included in the model, is the operative procedure for the control parameter evaluation. Gradient-based algorithms proceed in the sensitivity analysis through the evaluation of the cost function gradient with respect to the design parameters. The result of gradient evaluation defines how the objective function varies to changes in the design variable. The steepest descend algorithms is a common gradient based method for the design parameter update. According to this method, the design variable γ is valuated moving in the direction of negative gradient of the cost function:

$$\gamma_{n+1} = \gamma_n - \lambda \nabla J_\gamma = \gamma_n - \lambda \frac{\partial J(\gamma_n)}{\partial \gamma_n} \tag{4.1}$$

Where n is the current iteration and λ is the step size.
The gradient of the cost function respect the control variable can be expressed by finite difference method using forward differencing:

$$\frac{\partial J}{\partial \gamma} \approx \lim_{h \to 0} \frac{J(\gamma + h) - J(\gamma)}{h} \tag{4.2}$$

This represent an onerous algorithms since each calculation of $J(\gamma_n)$ require the state system to be solved that means one solver call and the complete gradient evaluation needs $n + 1$ solver calls. The computation cost represent an efficiency limit unless the number of design parameters is very few. Adjoint method overcomes this drawback because computation is made independent of the number of design variables introducing an auxiliary linear problem. The sensitivity analysis is computed with one call of the primal solver (represented by the governing equations of the problem) and one call of the adjoint solver (including the auxiliary equations) with no dependence from the number of design parameters n.
Despite this sensitivity analysis is limited to simple applications due complexity of the mathematical formulation of the adjoint equations and boundary condition, the adjoint method have witnessed a recent resurgence in interest among the engineering community ranging from aerospace to automotive applications and represent the best alternative for possible complex optimization problems typical of nuclear applications. The adjoint

based optimization includes both external and internal flows. As forementioned in the introduction chapter, these applications represent the two principal application of this method. While the external flow application is used for surface optimization problems, the internal flow optimization is used in topology optimization. In the following section, only the latter was taken into account.
The main peculiarity of adjoint optimization is the presence of a set of adjoint equations directly defined from the set of primal governing equations. The adjoint equations can be derived with two different approaches: the continuous and the discrete approach. In the former method, the analytical form of the primal equation is first linearized, then the adjoint equations are derived analytically and finally discretized. With the discreate approach instead, the discrete adjoint equations are composed from the algebraic system derived from primal equation discretization. In the following sections the continuous approach was adopted due its independence from discretization and consequent simpler implementation in C++ framework.

The present chapter is aimed in developing an Openfoam Multiphysics optimization solver able to deal with incompressible fluid flow problems including heat transfer. The 2D benchmarks of the previous chapter are presented and solved with the adjoint approach. The purpose of this work is the setup of an open source algorithm for Multiphysics optimizations using the validated results of COMSOL module as starting point.

4.2 Primal Equations of Thermal-Fluid Flow Problems

The following sections considers internal forced convection fluid flow with heat transfer problems. The fluid flow is governed by incompressible Navier-Stokes equations and continuity equation while the heat transfer is modelled with transport diffusion equation for the temperature:

$$\begin{aligned}(R_1, R_2, R_3)^T = (\boldsymbol{v}\cdot\nabla)\boldsymbol{v} + \nabla p - \nabla\cdot(2\nu D(\boldsymbol{v})) + \alpha(\gamma)\boldsymbol{v} = 0 \\ R_4 = -\nabla\cdot\boldsymbol{v} = 0 \\ R_5 = \boldsymbol{v}\cdot\nabla T - \nabla\cdot(K\nabla T) = 0\end{aligned} \tag{4.3}$$

The porosity field is introduced in the momentum equation through the Darcy term $\alpha(\gamma)\boldsymbol{v}$. Here, α is the inverse permeability or the friction coefficient which is linked to the local design variable $\gamma : \Omega \to [0,1]$ through an increasing monotone and continuously differentiable interpolation function of γ such that:

$$\alpha(\gamma) = \begin{cases}\alpha(1) = \alpha_{max}\ solid\,material \\ \alpha(0) = 0\ liquid\,material\end{cases} \quad \gamma : \Omega \to [0,1] \tag{4.4}$$

In the momentum equations, the velocity field results penalized in the solid parts where $\alpha(\gamma)$ tends to large values dominating the other terms of the equations. On the

contrary, when the Darcy term is zero, in the design domain region related to fluid, the momentum equations become the standard Navier-Stokes equations Porosity values are identified in every cell of the selected design domain.

As discussed in the previous chapter, α_{max} is related to the Darcy number according to:

$$Da = \frac{\boldsymbol{v}}{\alpha_{max} L^2} \tag{4.5}$$

where $\boldsymbol{v}$ is the inlet velocity, L is the characteristic length and $Da \approx 10^{-5}$ for nonpermeable domain.

This optimization problem is focused on definition of the optimal path of a cooling fluid inside a heated domain without the definition of the solid thermal properties. Hence only the porosity field was interpolated with the design variable γ neglecting the interpolation of the thermal conductivity of the materials.

4.3 Adjoint Equations

In this section the adjoint equations and corresponding boundary conditions are derived and the sensitivity of the cost function with respect to the control variable is calculated [21], [22]. Introducing the Lagrangian approach, the objective function was reformulated with the Lagrangian function L as:

$$L = J + \int_{\Omega} (\boldsymbol{u}, q, T_a) R(\boldsymbol{v}, p, T)\, d\Omega \tag{4.6}$$

The vector of Lagrangian multipliers is defined by the adjoint vector $(\boldsymbol{u}, q, T_a)$ where $\boldsymbol{u}$, q and T_a are respectively the ajoint velocity, the adjoint pressure and the adjoint temperature. $R = (R_1, R_2, R_3, R_4, R_5)^T$ is the state equations for incompressible steady state Navier-Stokes equations coupled with heat transfer and Ω refers to the flow domain.

The sensitivity analysis of the Lagrangian function with respect to the design variable is studied considering the total variation of L. The adjoint velocity, pressure and temperature are chosen in such a way that the variation with respect to the primal variables $(\boldsymbol{v}, p, T)$ vanishes. The Lagrangian form of the constrained optimization problem reads:

$Find\,(\boldsymbol{y}, \boldsymbol{\lambda}, \gamma)\, such\, that\, \nabla L(\boldsymbol{y}, \boldsymbol{\lambda}, \gamma) = 0$

That corresponds to:

$$\begin{cases} \partial_{\boldsymbol{y}} L[\delta \boldsymbol{y}] = 0 \quad \forall \boldsymbol{y} \\ \partial_{\boldsymbol{\lambda}} L[\delta \boldsymbol{\lambda}] = 0 \;\; \forall \boldsymbol{\lambda} \\ \partial_{\gamma} L[\delta \gamma] = 0 \;\; \forall \gamma \end{cases}$$

Where $\boldsymbol{y}$ is the vectore of state variables, $\boldsymbol{\lambda}$ is the vector of adjoint variables, *gamma* is the control variable and the *Gâteaux* formalism of the Lagrangian function is adopted:

$$\partial_{\boldsymbol{y}} L[\delta \boldsymbol{y}] = \lim_{h \to 0} \frac{L(\boldsymbol{y} + h\delta \boldsymbol{y}, \boldsymbol{\lambda}, \gamma) - L(\boldsymbol{y}, \boldsymbol{\lambda}, \gamma)}{h}$$
$$\partial_{\boldsymbol{\lambda}} L[\delta \boldsymbol{\lambda}] = \lim_{h \to 0} \frac{L(\boldsymbol{y}, \boldsymbol{\lambda} + h\delta \boldsymbol{\lambda}, \gamma) - L(\boldsymbol{y}, \boldsymbol{\lambda}, \gamma)}{h}$$
$$\partial_{\gamma} L[\delta \gamma] = \lim_{h \to 0} \frac{L(\boldsymbol{y}, \boldsymbol{\lambda}, \gamma + h\delta \gamma) - L(\boldsymbol{y}, \boldsymbol{\lambda}, \gamma)}{h}$$

Furthermore, $\partial_{\boldsymbol{y}} L[\delta \boldsymbol{y}]$ is the weak form of the adjoint equations, $\partial_{\boldsymbol{\lambda}} L[\delta \boldsymbol{\lambda}]$ is the weak form of the primal governing equations and $\partial_{\gamma} L[\delta \gamma]$ is the optimality condition.

Now the adjoint equation are derived starting from the definition of their weak form as the derivative of L with respect to the state variable and set it equal to zero:

$$\partial_{\boldsymbol{y}} L[\delta \boldsymbol{y}] = \partial_{\boldsymbol{v}} L[\delta \boldsymbol{v}] + \partial_{p} L[\delta p] + \partial_{T} L[\delta T]$$

The three terms are calculated separately. The first was is developed as follows

$$\begin{aligned}
&\partial_{\boldsymbol{v}} L[\delta \boldsymbol{v}] = \partial_{\boldsymbol{v}} J[\delta \boldsymbol{v}] + \int_{\Omega} (\boldsymbol{u}, 1, T_a)\, d\Omega \\
&= \partial_{\boldsymbol{v}} J[\delta \boldsymbol{v}] + \int_{\Omega} (\boldsymbol{u}, 1, T_a) \begin{bmatrix} (\delta \boldsymbol{v}) \cdot \nabla) \boldsymbol{v} + (\boldsymbol{v} \cdot) \delta \boldsymbol{v} - \nabla \cdot (2\nu D(\delta \boldsymbol{v})) + \alpha(\gamma) \delta \boldsymbol{v} \\ \nabla \cdot \delta \boldsymbol{v} \\ \delta \boldsymbol{v} \cdot \nabla T \end{bmatrix} \\
&= \partial_{\boldsymbol{v}} J[\delta \boldsymbol{v}] + \int_{\Omega} \boldsymbol{u} \cdot ((\delta \boldsymbol{v} \cdot \nabla) \boldsymbol{v} + (\boldsymbol{v} \cdot \nabla) \delta \boldsymbol{v} - \nabla \cdot (2\nu D(\delta \boldsymbol{v})) + \alpha(\gamma) \delta \boldsymbol{v}) \\
&+ \int_{\Omega} -q \nabla \cdot \delta \boldsymbol{v} + T_a \delta \boldsymbol{v} \cdot \nabla T
\end{aligned}$$

The second terms is defined as:

$$\begin{aligned}
&\partial_{p} L[\delta p] = \partial_{p} J[\delta p] + \int_{\Omega} (\boldsymbol{u}, q, T_a) \partial_{p} \boldsymbol{R}[\delta p] \\
&\partial_{p} J[\delta p] + \int_{\Omega} (\boldsymbol{u}, q, T_a) \begin{bmatrix} \nabla \delta p \\ 0 \\ 0 \end{bmatrix} \\
&\partial_{p} J[\delta p] + \int_{\Omega} \boldsymbol{u} \cdot \nabla \delta p
\end{aligned}$$

Finally the last term is defined as:

$$
\begin{aligned}
\partial_T L[\delta T] &= \partial_T J[\delta T] + \int_\Omega (\boldsymbol{u}, q, T_a)\partial_T \boldsymbol{R}[\delta T] \\
&= \partial_T J[\delta T] + \int_\Omega (\boldsymbol{u}, q, T_a) \begin{bmatrix} 0 \\ 0 \\ \boldsymbol{v}\cdot\nabla\delta T - \nabla\cdot(K\nabla\delta T) \end{bmatrix} \\
&= \partial_T J[\delta T] + \int_\Omega T_a \boldsymbol{v}\cdot\nabla\delta T - T_a\nabla\cdot(K\nabla\delta T)
\end{aligned}
$$

The derivative of L with respect to the state varibale can now be written as:

$$
\begin{aligned}
&\partial_{\boldsymbol{y}} L[\delta \boldsymbol{y}] = \partial_v L[\delta \boldsymbol{v}] + \partial_p L[\delta p] + \partial_T L[\delta T] \\
&= \partial_v J[\delta \boldsymbol{v}] + \partial_p J + \partial_T J[\delta T] \\
&+ \partial_v J[\delta \boldsymbol{v}] + \int_\Omega \boldsymbol{u}\cdot((\delta\boldsymbol{v}\cdot\nabla)\boldsymbol{v} + (\boldsymbol{v}\cdot\nabla)\delta\boldsymbol{v} - \nabla\cdot(2\nu D(\delta\boldsymbol{v})) + \alpha(\gamma)\delta\boldsymbol{v}) \\
&+ \int_\Omega -q\nabla\cdot\delta\boldsymbol{v} + T_a\delta\boldsymbol{v}\cdot\nabla T \\
&+ \int_\Omega \boldsymbol{u}\cdot\nabla\delta p \\
&+ \int_\Omega T_a\boldsymbol{v}\cdot\nabla\delta T - T_a\nabla\cdot(K\nabla\delta T)
\end{aligned}
\tag{4.7}
$$

The cost funtion is composed by the contributions from the boundary Γ and from the design domain Ω:

$$
J = \int_\Gamma J_\Gamma \, d\Gamma + \int_\Omega J_\Omega \, d\Omega \tag{4.8}
$$

Proceeding with the integration by part of the equation 4.7 the equation can be written as:

$$
\begin{aligned}
&\int_\Omega (-(\nabla\boldsymbol{u})\boldsymbol{v} - (\boldsymbol{v}\cdot\nabla)\boldsymbol{u} - \nabla\cdot(2\nu D(\boldsymbol{u})) + \alpha(\gamma)\boldsymbol{u} + \nabla q + T_a\nabla T + \frac{\partial J_\Omega}{\partial \boldsymbol{v}})\cdot\delta\boldsymbol{v} \\
&+ \int_\Omega (-\nabla\cdot\boldsymbol{u} + \frac{\partial J_\Omega}{\partial p})\delta p \\
&+ \int_\Omega (-\boldsymbol{v}\cdot\nabla T_a - \nabla\cdot(K\nabla T_a) + \frac{\partial J_\Omega}{\partial T})\delta T \\
&+ \int_\Gamma ((\boldsymbol{u}\cdot\boldsymbol{v})\boldsymbol{n} + \boldsymbol{u}(\boldsymbol{v}\cdot\boldsymbol{n}) + 2\nu\boldsymbol{n}\cdot D(\boldsymbol{u}) - q\boldsymbol{n} + \frac{\partial J_\Gamma}{\partial \boldsymbol{v}})\cdot\delta\boldsymbol{v} - \int_\Gamma 2\nu\boldsymbol{n}\cdot D(\delta\boldsymbol{v})\boldsymbol{u} \\
&+ \int_\Gamma (\boldsymbol{u}\cdot\boldsymbol{n} + \frac{\partial J_\Gamma}{\partial p})\delta p \\
&+ \int_\Gamma (T_a\boldsymbol{v}\cdot\boldsymbol{n} + K\boldsymbol{n}\cdot\nabla T_a + \frac{\partial J_\Gamma}{\partial T})\delta T + \int_\Gamma K\boldsymbol{n}\cdot\nabla\delta T T_a = 0 \;\; \forall\, \delta\boldsymbol{v}, \delta p, \delta T
\end{aligned}
\tag{4.9}
$$

The previous equation must be satisfied for every $\delta\gamma$ then for any $\delta\boldsymbol{v}, \delta p, \delta T$, hence each integral must vanish individually. Posing equal to zero the integrals over the domain Ω leads to the definition of the adjoint equations, while the integrals on the boundary Γ give rise to the boundary conditions of the adjoint equation. Therefore, both the new set of equation and its boundary condition depends on the cost function:

$$\begin{cases} -(\nabla \boldsymbol{u})\boldsymbol{v} - (\boldsymbol{v}\cdot\nabla)\boldsymbol{u} - \nabla\cdot(2\nu D(\boldsymbol{u})) + \alpha(\gamma)\boldsymbol{u} + \nabla q + T_a\nabla T + \dfrac{\partial J_\Omega}{\partial \boldsymbol{v}} = 0 \\ \nabla\cdot\boldsymbol{u} + \dfrac{\partial J_\Omega}{\partial p} = 0 \\ -\boldsymbol{v}\cdot\nabla T_a - \nabla\cdot(K\nabla T_a) + \dfrac{\partial J_\Omega}{\partial T} = 0 \end{cases} \tag{4.10}$$

The adjoint variable should not be interpreted as velocity, pressure and temperature in physical sense. The names are rather used to highlight that a similar solution procedure can be adopted and presents similar properties. For example, both the primal and adjoint velocity are solenoidal.
An important approximation, known as *frozen turbulence* was used in the derivation of equation 4.9 neglecting the variation of ν. This approximation holds for laminar regimes but not in case of turbulences.

4.3.1 Adjoint Boundary Conditions

The boundary conditions for the adjoint variable are obtained from the boundary integrals of equation 4.9:

$$\begin{cases} \displaystyle\int_\Gamma ((\boldsymbol{u}\cdot\boldsymbol{v})\boldsymbol{n} + \boldsymbol{u}(\boldsymbol{v}\cdot\boldsymbol{n}) + 2\nu\boldsymbol{n}\cdot D(\boldsymbol{u}) - q\boldsymbol{n} + \frac{\partial J_\Gamma}{\partial \boldsymbol{v}})\cdot\delta\boldsymbol{v} - \int_\Gamma 2\nu\boldsymbol{n}\cdot D(\delta\boldsymbol{v})\boldsymbol{u} = 0 \\ \displaystyle\int_\Gamma (\boldsymbol{u}\cdot\boldsymbol{n} + \frac{\partial J_\Gamma}{\partial p})\delta p = 0 \\ \displaystyle\int_\Gamma (T_a\boldsymbol{v}\cdot\boldsymbol{n} + K\boldsymbol{n}\cdot\nabla T_a + \frac{\partial J_\Gamma}{\partial T})\delta T + \int_\Gamma K\boldsymbol{n}\cdot\nabla\delta T T_a = 0 \end{cases} \tag{4.11}$$

Following (metti ruberto) and considering $u_n = \boldsymbol{u}\cdot\boldsymbol{n}$, $v_n = \boldsymbol{v}\cdot\boldsymbol{n}$ and $\nabla\nu = 0$ for laminar fluxes the equation 4.11 can be written as:

$$\begin{cases} \displaystyle\int_\Gamma ((\boldsymbol{u}\cdot\boldsymbol{v})\boldsymbol{n} + \boldsymbol{u}(\boldsymbol{v}\cdot\boldsymbol{n}) + \nu(\boldsymbol{n}\cdot\nabla)\boldsymbol{u} - q\boldsymbol{n} + \frac{\partial J_\Gamma}{\partial \boldsymbol{v}})\cdot\delta\boldsymbol{v} - \int_\Gamma \nu(\boldsymbol{n}\cdot\nabla)\delta\boldsymbol{v}\cdot\boldsymbol{u} = 0 \\ \displaystyle\int_\Gamma (\boldsymbol{u}\cdot\boldsymbol{n} + \frac{\partial J_\Gamma}{\partial p})\delta p = 0 \\ \displaystyle\int_\Gamma (T_a\boldsymbol{v}\cdot\boldsymbol{n} + K\boldsymbol{n}\cdot\nabla T_a + \frac{\partial J_\Gamma}{\partial T})\delta T + \int_\Gamma K\boldsymbol{n}\cdot\nabla\delta T T_a = 0 \end{cases} \tag{4.12}$$

The specific boundary conditions of each simulations will be derived defining the cost function of each case.

4.4 Gradient of the cost function

In this section the gradient of the cost function is valuated to define the sensitivity that will be employed into an iterative gradient based method to obtain the optimality condition $\partial_\gamma L[\delta\gamma] = 0$. The sensitivity of the cost function with respect to the design variable is valuated from the gateaux derivative of the Lagrangian $\partial L_\gamma[\delta\gamma]$. Since the derivative of the Lagrangian is linearly dependent from $\delta\gamma$, the gateaux formulation can be written as follows:

$$\partial_\gamma L[\delta\gamma] = \int_\Omega J'(\gamma)\delta\gamma \tag{4.13}$$

Hence, the sensitivity can be written as:

$$\begin{aligned} J'(\gamma)\delta\gamma] = \partial_\gamma L[\delta\gamma] &= \int_\Omega (\boldsymbol{u}, q, T_a)\partial_\gamma \boldsymbol{R} \\ &= \int_\Omega (\boldsymbol{u}, q, T_a) \begin{bmatrix} \boldsymbol{v}h(\gamma)\delta\gamma \\ 0 \\ 0 \end{bmatrix} \\ &= \int_\Omega \boldsymbol{u} \cdot \boldsymbol{v}h(\gamma)\delta\gamma \end{aligned} \tag{4.14}$$

Where $h(\gamma)$ is the derivative of $\alpha(\gamma)$. Since in the following numerical tests the cost function J does not depend directly from the design variable γ, the contribution $\partial_\gamma J$ was removed.
Finally, the discrete formulation of the sensitivity in a finite volume approximation is written as:

$$\begin{aligned} J'_h(\gamma_h)[\delta\gamma_h] &= \sum_i ((\boldsymbol{u}_i \cdot \boldsymbol{v}_i h(\gamma_i) V_i \delta\gamma_i \\ &= \nabla J_h \cdot \delta\gamma_h \end{aligned} \tag{4.15}$$

Where V_i is the volume of the i-th cell.

4.5 Conclusions

In this chapter the adjoint optimization formalism was presented. Then, starting from the primal equations of a general Multiphysics problem, the adjoint optimization problem was formulated. The cost function was defined in a general form as composed by a domain contribution coupled with a boundary contribution in order to give the procedure and the final results the most generic formulation. In the following chapter, the obtained adjoint equation, boundary condition and sensitivity analysis were adapted to each benchmark.

Numerical Tests: Openfoam

In this chapter the three benchmarks presented in the COMSOL module were solved with the adjoint formalism using OpenFOAM as computational fluid dynamic software.
The choice of transpose the optimization solver from a commercial code to an open source one rises from the possibility of extend the potentials of the solver so that it can be applied in more and more complex Multiphysics problems. For each numerical test a different optimization solver was used regarding different primal equations and cost function. First the fluid flow problem was taken into account and the solver adjointShapeOptimizationFoam.C already implemented in OpenFOAM library was used for the optimization process. Then, the single physics problem of heat conduction was considered. Following the procedure exposed in the previous chapter, an adjoint optimization solver regarding heat conduction was developed. Finally the Multiphysics benchmark was studied. Starting from the already implemented code, a Multiphysics optimization solver was implemented following the results of the previous chapter. The results of the benchmarks simulation was compare with the COMSOL ones.

5.1 Laminar Flow Optimization

The OpenFOAM optimization of the numerical problem exposed in section 3.1.2 is now presented. After the definition of cost function and governing equations the final set of adjoint equation and adjoint boundary condition are shown. Then the solver algorithm and the numerical result are presented.

5.1.1 Problem Description

In the following numerical test the same geometry and boundary condition of the problem presented in section 3.1.2 of COMSOL optimizations were adopted. The design domain and primal boundary condition are summarized below:

The cost function J_f was defined as the difference between the inlet and outlet pressure:

$$J_f = p_{avg,inlet} - p_{outlet} \tag{5.1}$$

The set of governning equation was given by the Navier-Stokes equation for incompressible fluids and the continuity eqaution. The Darcy term was added in the momentum

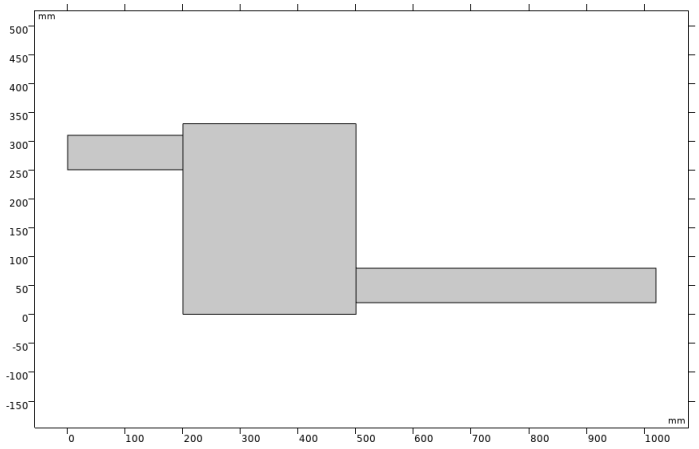

Figure 5.1: Laminar Flow: initial geometry

	Wall	Inlet	Outlet
v	No-slip	$0.0266\left[\frac{m}{s}\right]$	Zero gradient
p	Zero gradient	Zero gradient	$0[Pa]$

Table 5.1: Fluid flow optimization: boundary conditions

equations:

$$\begin{cases} \rho_{fl} \cdot (\boldsymbol{u} \cdot \nabla)\boldsymbol{u} = -\nabla p + \mu(\nabla^2 \boldsymbol{u}) + \alpha \boldsymbol{u} \\ \rho_{fl}(\nabla \cdot \boldsymbol{u}) = 0 \end{cases} \tag{5.2}$$

In the adjoint solver used for this optimization the design variable was the porosity field α which was not interpolated by a control variable.

5.1.2 Adjoint Equations

Introducing the Lagrangian multipliers, the Lagrangian relaxation of the problem was:

$Minimize\ L = J + \int_\Omega (\boldsymbol{u}, q)\boldsymbol{R} d\Omega$

The Lagrangian multipliers were the adjoint velocity $\boldsymbol{u}$ and pressure q. The sensitivity analysis is studied with the total variation of L and the adjoint variables are chosen to vanish the variation with respect to the primal variables $(\boldsymbol{v}, p)$ according to:

$$\delta L = \delta_\alpha L + \delta_{\boldsymbol{v}} L + \delta_p L, \tag{5.3}$$

$$\delta_v L + \delta_p L = 0 \tag{5.4}$$

The equations 5.3 and 5.4 led to the following formulation of the sensitivity analysis of the cost function with respect to the porosity field α in the cell i:

$$\frac{\partial L}{\partial \alpha_i} = \boldsymbol{u}_i \cdot \boldsymbol{v}_i V_i \tag{5.5}$$

Where V_i is the volume of the cell i. Following the mathematical procedure showd in the previous chapter, the final adjoint equation for the fluid flow optimization were:

$$\begin{cases} -2D(\boldsymbol{u})\boldsymbol{v} = -\nabla q + \nabla \cdot (2\nu D(\boldsymbol{u})) - \alpha \boldsymbol{u} \\ \nabla \cdot \boldsymbol{u} = 0 \end{cases} \tag{5.6}$$

In this case the cost funtion do not contain any contribution from the fluid flow domain Ω but only from the inlet boundary. For this reason, considering the results of the equation 4.9, the formulation of the cost funtion affects only the adjoint boundary conditions since the contribution on the domain Ω vanishes.

5.1.3 Adjoint Boundary Conditions

The adjoint boudary condition were derived from the procedure exposed in the previous chapter and were as follows:

Wall and inlet boundary conditions :|

$$\boldsymbol{u}_t = 0 \tag{5.7}$$

$$u_n = -\frac{\partial J_\Omega}{\partial p} \tag{5.8}$$

$$\boldsymbol{n}\nabla q = 0 \tag{5.9}$$

Outlet boundary conditions :

$$q = \boldsymbol{u} \cdot \boldsymbol{v} + u_n v_n + \nu(\boldsymbol{n} \cdot \nabla)u_n + \frac{\partial J_\Gamma}{\partial v_n} \tag{5.10}$$

$$0 = v_n \boldsymbol{u}_y + \nu(\boldsymbol{n} \cdot \nabla)\boldsymbol{u}_t + \frac{\partial J_\Gamma}{\partial \boldsymbol{v}_t} \tag{5.11}$$

where $\frac{\partial j_\Gamma}{\partial v_n}$ and $\frac{\partial J_\Gamma}{\partial \boldsymbol{v}_t}$ are the tangential and normal component of $\frac{\partial J_\Gamma}{\partial \boldsymbol{v}}$ respectively.

5.1.4 Sensitivity Analysis

The sensitivity of the cost function with respect to the control variable was written as:

$$\begin{aligned} J'(\alpha)[\delta\alpha] = \partial_\alpha L[\delta\alpha] &= \partial_\alpha J + \int_\Omega (\boldsymbol{u}, q)\partial_\alpha \boldsymbol{R} \\ &= \int_\Omega (\boldsymbol{u}, q) \begin{bmatrix} \boldsymbol{v}\delta\alpha \\ 0 \\ 0 \end{bmatrix} \\ &= \int_\Omega (\boldsymbol{u} \cdot \boldsymbol{v})\delta\alpha \end{aligned} \tag{5.12}$$

Considering the finite volume approximation, the discrete gradient of the cost function was:

$$\begin{aligned} J'_h(\alpha_h)[\delta\alpha_h] &= \sum_i (\boldsymbol{u} - i \cdot \boldsymbol{v}_i) h(\alpha_i) V_i \delta\alpha_i \\ &= \nabla J_h \cdot \delta\alpha_h \end{aligned} \tag{5.13}$$

The expression cost function variation due the variation of the control variable $\delta\alpha$ is used in a gradient base optimization algorithm, in this case the steepest descend algorithm. In linear systems, the steepest descend method defines a search direction as:

$$\boldsymbol{p}_k = -\nabla f(\boldsymbol{x}_k) \tag{5.14}$$

Where $\boldsymbol{x}_k$ is the current location at the iteration k and f is the function to be minimized continuous in some neighbourhood around $\boldsymbol{x}_k \in \mathbb{R}^n$. The steepest descend algorithm was applied to the porosity field according to:

$$\alpha_{n+1} = \alpha_n - \boldsymbol{u}_i \cdot \boldsymbol{v}_i V_i \delta \tag{5.15}$$

where δ is the step lenght, V_i is the volume of the cell while α_n and α_{n+1} are the old value of the porosity and the updated one. In the solver *adjointShapeOptimizationFoam*, the steepest descend algorithm is implementated also with underrelaxation factor η to improve stability as follows:

$$\alpha_{n+1} = \alpha_n(1-\eta) + \eta min(max((\alpha_n - \boldsymbol{u}_i \cdot \boldsymbol{v}_i V_i \delta), 0), \alpha_{max}) \tag{5.16}$$

The functions *min* and *max* are aimed in limiting the porosity values so that it never becomes negative or greater that α_{max}.

5.1.5 Fluid Flow Optimization Algorithm

The fluid flow problems require an algorithm able to deal with velocity and pressure coupling. The primal and adjoint systems are solved with a SIMPLE-type algorithm [6], an algorithm based in the reformulation of Navier-Stokes equations with a momentum predictor and an equation for pressure correction which includes also the continuity constrain. The iterative solution uptade of the SIMPLE approach is summarized below:

1. Set the boundary conditions.
2. Calculate the velocity and pressure gradients.
3. Compute the intermediate velocity field through the discretized momentum equation.
4. Evaluate the uncorrect mass fluxes at faces.
5. Evaluate the cell values of pressure correction with the pressure correction equation.
6. Correct the pressure field: $p^{k+1} = p^k + \eta_p \cdot p'$ where η_p is the under-relaxation factor for pressure.

7. Correct the mass fluxes.

8. Correct the cell velocities: $\boldsymbol{v}^{k+1} = v^* - \frac{Vol\nabla p'}{\boldsymbol{a}_p^v}$ where $\nabla p'$ is the gradient of pressure corrections, $\boldsymbol{a}_p^v$ is the vector of central coefficients for the discretized linear system of the velocity equation and Vol is the volume of the cell.

In the optimization algorithm, the sensitivity is valuated from the primal and adjoint systems implementing the *one shot* approach in which the quantities are only partially converged. In the figure 5.2 the graphycal solution procedure is shown.

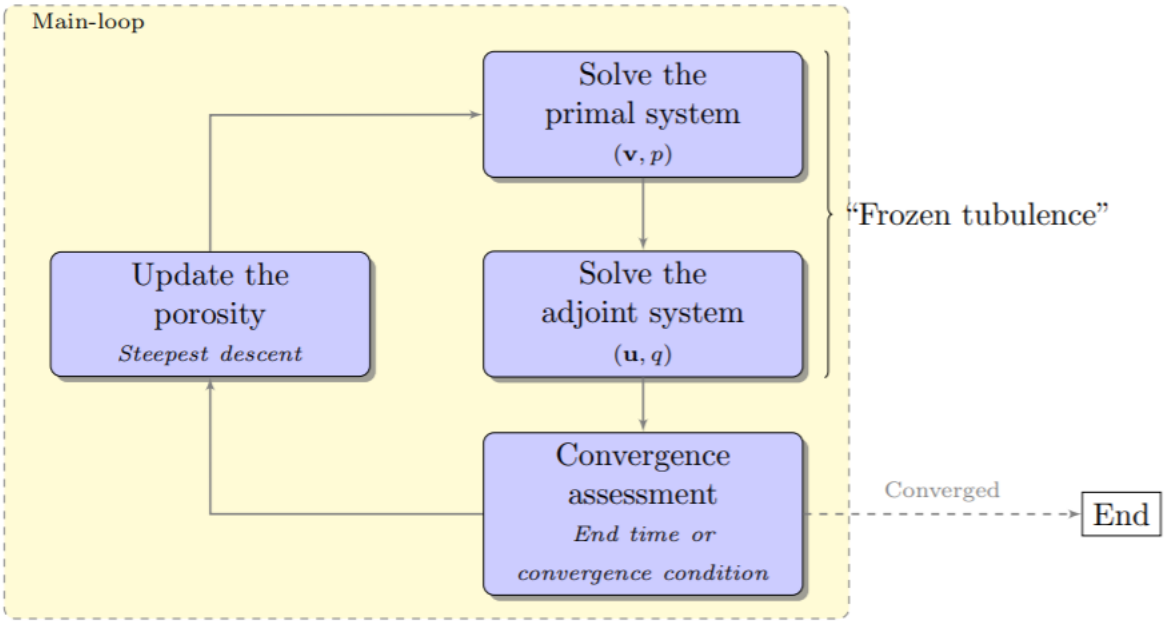

Figure 5.2: Solution procedure scheme used in adjointShapeOptimizationFoam.C [6]

5.1.6 Fluid Flow Optimization Numerical Results

In figure 5.3 the velocity field of the fluid flow problem without optimization is shown and the solver simpleFoam.C was used to perform this base case simulation. Large recirculation areas that cause local pressure drops are present inside the box collecting the upper and lower pipes.

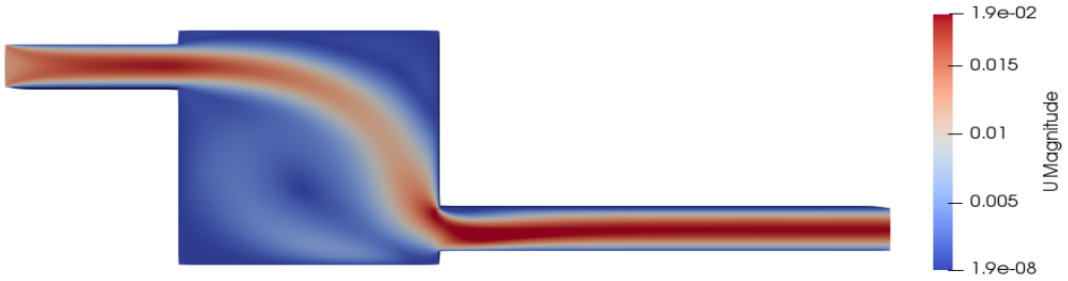

Figure 5.3: Base case velocity field

In figures 5.4 and 5.5 below the optimization results are shown. The recirculation areas were deleted by the introduction of the porous media that inhibited the fluid flow in that regions. As expected, the S-bend shape was obtained. The pressure drop in the system decreased from 0.4868 $[Pa]$ in the base case solution to 0.4386 $[Pa]$ in the optimized case. In this optimization test the reduction of the pressure drop resulted limited by the soft transition from solid region to liquid one. This inconvenience was solved in the other numerical test by the introduction of an interpolation scheme of the porosity field by a control variable.

Figure 5.4: Topology optimization result

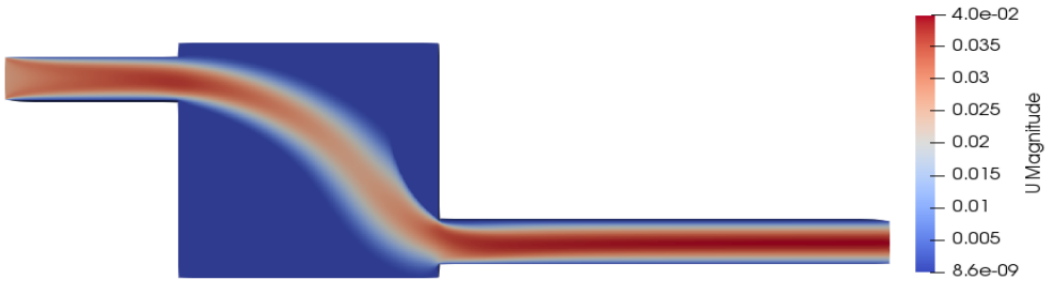

Figure 5.5: Optimizeed velocity fueld

5.2 Pure Heat Conduction Optimization

In this section the OpenfFOAM optimization of the pure heat conduction benchmark is presented. The same square geometry domain and boundary conditions of the case shown in 3.1 ,summarized below, were adopted.

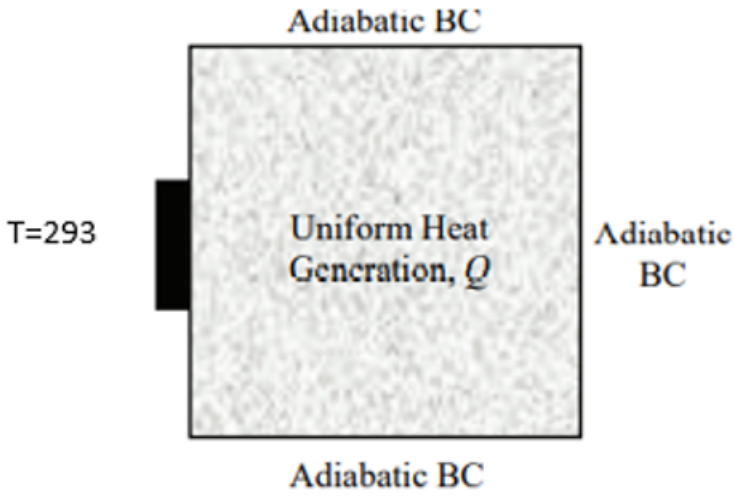

Figure 5.6: design domain and boundary conditions for pure heat conduction

The Fourier's governing equation for the steady state pure heat conduction was defined as follows:

$$-\nabla(k(\gamma)\nabla T) = Q \tag{5.17}$$

In this case the design domain is $\gamma : \Omega \rightarrow [0, 1]$ and is used to interpolate the conduction coefficient in the design domain of the problem with a SIMP like scheme as follows:

$$k(\gamma) = k_{min} + (k_{max} - k_{min})\gamma^p \tag{5.18}$$

Each cell was associated to a value of thermal conduction coefficient ranging from the minimum and maximum values according to:

$$\gamma = \begin{cases} 0 : \ k = k_{min} = 0.001 \left[\dfrac{W}{m\,K}\right] \\ 1 : \ k = k_{max} = 1 \left[\dfrac{W}{m\,K}\right] \end{cases} \tag{5.19}$$

The purpose of this optimization was the definition of the optimal conduction path to remove heat inside the domain. In this case a volume constrain was implemented as additional term in the definition of the cost function. Hence, this numerical test was a multi-objective optimization problem since the total objective function was the sum of a thermal contribution and a volume constrain. The former was aimed in minimizing the average temperature in the domain, while the latter provides a constrain of the more

conductive material, associated to $\gamma =$ as a fraction of the total volume as:

$$V_{target} = \frac{\int_{\Omega_d} \gamma \, d\Omega d}{V_{max}} \tag{5.20}$$

The total cost funtion was defined as the sum of the thermal and volume contribution:

$$J = J_t + J_v \tag{5.21}$$

where,

$$J_t = \int_{\Omega} (T - T^*)^2 \, d\Omega \tag{5.22}$$

$$J_v = L = -\lambda_k c_k + \omega c_k^2 \tag{5.23}$$

In equation 5.23 the Augmented Lagrange Multiplier (ALM) method was used. According to this method the Lagrangian function L was considered as J_v and λ_k was the k-th Lagrangian multiplier, ω a scalar weight factor and c_k was defined as follows:

$$c_k = \left[\frac{\int_{\Omega} \gamma \, d\Omega}{\int_{\Omega} d\Omega} - V_{target} \right]^2 \tag{5.24}$$

5.2.1 Adjoint equation and boundary conditions

The adjoint equation for this problem was derived from the results of the previous chapter neglecting the fluid flow terms:

$$\nabla \cdot (k(\gamma) \nabla T_a) = -\frac{\partial J}{\partial T} \tag{5.25}$$

where T_a was the adjoint temperature variable. Performing the derivative of the cost function with respect to the temperature, the final form of the adjoint equation was:

$$\nabla \cdot (k(\gamma) \nabla T_a) = -(T - T^*). \tag{5.26}$$

T^* was the objective temperature of the system and was set equal to the temperature of the heat sink.
The ajoint boundary conditions were:

$$k(\gamma) \nabla^2 T = 0 \qquad wall \tag{5.27}$$

$$T_a = 293[K] \qquad heatsink \tag{5.28}$$

5.2.2 Sensitivity Analysis

The sensitivity of the objective function with respect to the control variable can valuated as follows:

$$\begin{aligned} J'(\gamma)[\delta\gamma] = \partial_\gamma L[\delta\gamma] = \partial_\gamma J + \int_{\Omega} T_a R \\ \partial_\gamma J_v + \int_{\Omega} -T_a \nabla \cdot (H(\gamma) \nabla Y) \delta\gamma \end{aligned} \tag{5.29}$$

In this case a further term related to the derivative of the volume constrain cost function apperared formulation. $H(\gamma)$ was the derivative of $k(\gamma)$.Then the derivative by part led to:

$$J'(\gamma)[\delta\gamma] = \partial_\gamma J_v + \int_\Omega (\nabla T_a \cdot \nabla T H(\gamma))\delta\gamma - \int_\Gamma T_a H(\gamma)\nabla T \boldsymbol{n}\delta\gamma \tag{5.30}$$

Considering this particular study case, the boundary conditions were such that the integral on Γ disappeared. Hence, the discrete formulation of the sensitivity read:

$$J'_h(\gamma_h)[\delta\gamma_h] = J'_{v,h}(\gamma_h) + \sum_i (\nabla T_{ai} \cdot T_i H(\gamma_i))V_i\delta\gamma_i \nabla J_h \cdot \delta\gamma_h \tag{5.31}$$

The problem was wolved implementing the previous mathematical results in the solver *adjointHeatConduction* (appendix 8.1).

5.2.3 Pure Heat Conduction Numerical Results

The numerical results of the optimization with increasing volumetric fraction of conductive material are now presented. The red areas represent the more conductiove material ($\gamma = 1$), while the blue areas are the less conductive one ($\gamma = 0$).

- $V_{target} = \frac{\int_{\Omega_d} \gamma \, d\Omega d}{V_{max}} = 0.3$

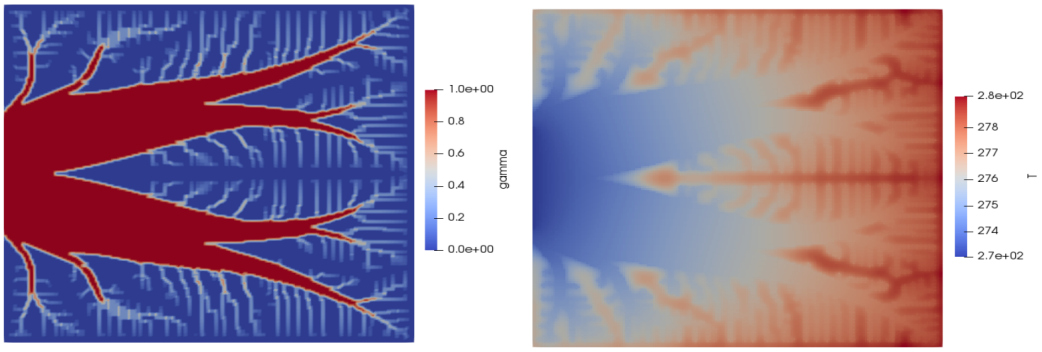

(a) *Topology Optimization* (b) *Temperature*

Figure 5.7: $V_{target} = 0.3$: topology optimization and temperature field

- $V_{target} = 0.4$

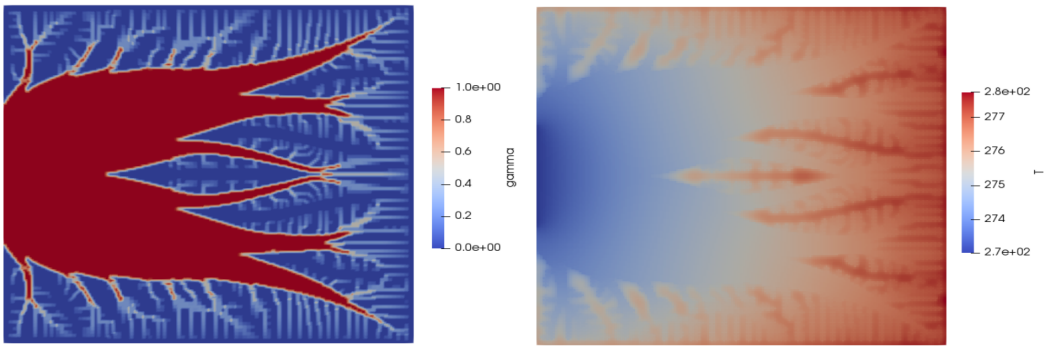

(a) *Topology Optimization* (b) *Temperature*

Figure 5.8: $V_{target} = 0.4$: topology optimization and temperature field

- $V_{target} = 0.5$

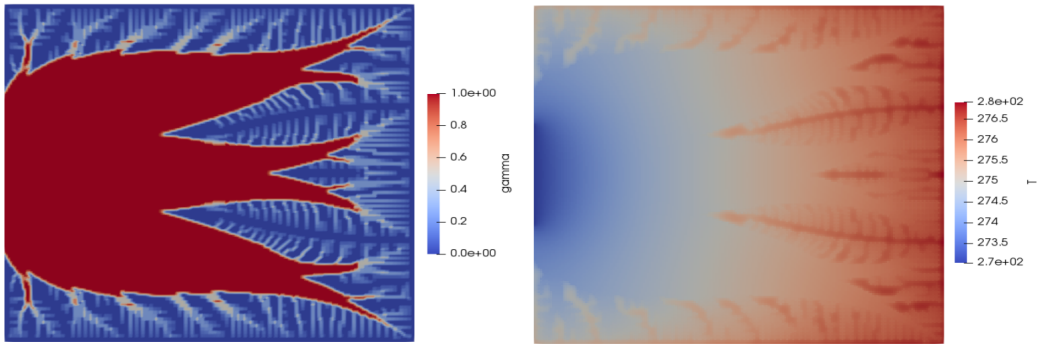

(a) *Topology Optimization* (b) *Temperature*

Figure 5.9: $V_{target} = 0.5$: topology optimization and temperature field

The OpenFOAM numerical tests showd results similar to those obtained with COMSOL optimization. The results are summerized below.

V_{target}	J	$T_{avg}[K]$	$\Delta T_{max} = T_{max} - T_{min}[K]$
0.3	6 675.57	276.4	7
0.4	3 941.63	275.62	5
0.5	2 789.43	275.22	4

Table 5.2: Pure heat conduction optimization results

In this case, the OpenFOAM adjoint optimization led to thermal improvement even bettere compare to the COMSOL one. The heat sink was better exploited to decrease the

average temperature of the system and gave a promising result for the further simulations.

5.3 Multiphysics Optimization

This section presents the optimal numerical design obtained for Multiphysics and multi-objective topology optimization of the model described in section 3.1.3. The design domain and boundary conditions are summarized below.

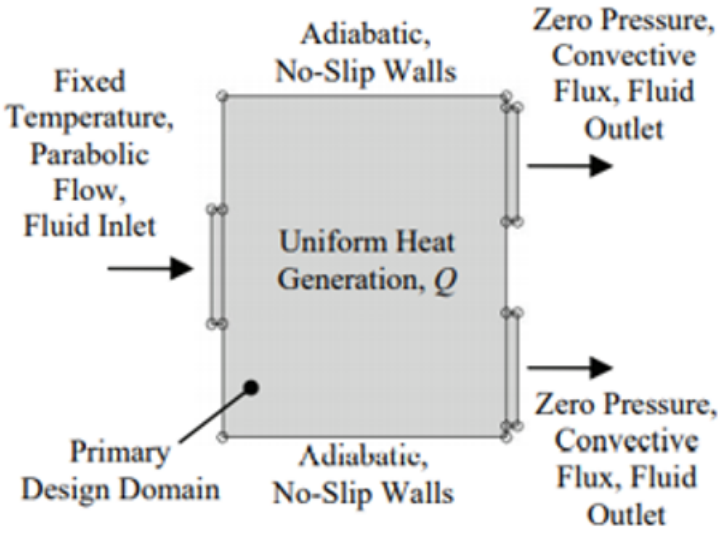

Figure 5.10: topology optimization design domain and boundary conditions for fluid flow and heat transfer

At the inlet of the devise, the average velocity was set equal to 0.01 $\left[\frac{m}{s}\right]$ and the temperature was 293$[K]$ while the central square domain was subjected to uniform heat generation $Q = 100\left[\frac{kW}{m^3}\right]$.

The problem was governed by the following state equations:

$$\begin{cases} \rho_{fl} \cdot (\boldsymbol{u} \cdot \nabla)\boldsymbol{u} = -\nabla p + \mu(\nabla^2 \boldsymbol{u}) + \alpha(\eta)\boldsymbol{v} \\ \rho_{fl}(\nabla \cdot \boldsymbol{v}) = 0 \\ \rho C(\boldsymbol{v} \cdot \nabla T) = \nabla \cdot (k \nabla T) + Q \end{cases} \tag{5.32}$$

The Darcy term $\alpha(\eta)\boldsymbol{v}$ still allows the porosity field to control the momentum equation. In this case the $\eta = (1 - \gamma)$ was used as design variable and the interpolation of the porosity filed was given by the following q-parametrized function:

$$\alpha(\eta) = \alpha_{max} - \alpha_{max}\frac{\eta(1+q)}{\eta+q} \tag{5.33}$$

Figure 5.11 shows how the parameter q affects the interpolation function for α. In the further numerical tests a value of 0.1 was imposed for q.

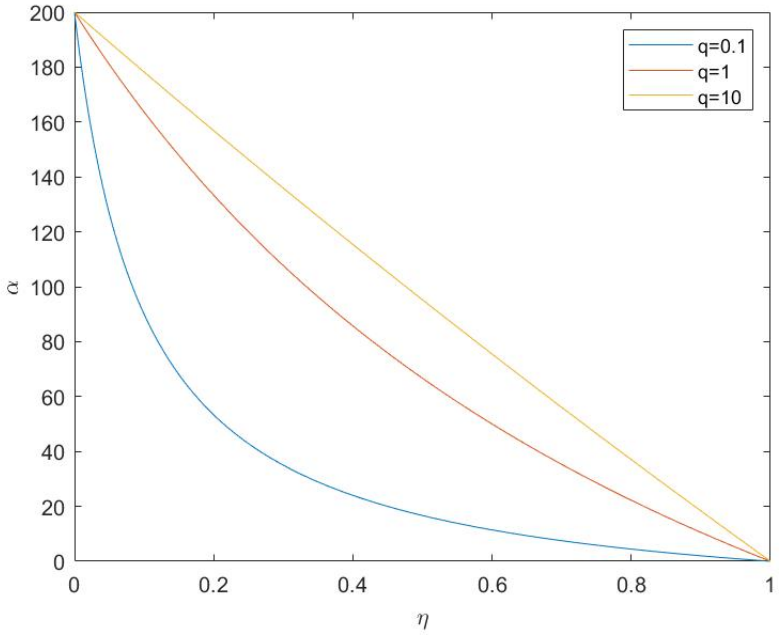

Figure 5.11: α interpolation scheme for differnt q values

Hence, the porosity field ranges from 0 to α_{max} according to:

$$\eta = \begin{cases} 0 : \alpha = \alpha_{max} \rightarrow \textit{solid domain} \\ 1 : \alpha = 0 \rightarrow \textit{liquid domain} \end{cases} \tag{5.34}$$

The multi-objective cost function was defined as the sum of two contributions in order to optimize both the heat transfer and fluid flow.

$$\begin{aligned} J &= J_f + J_t \\ &= \omega_1 \left(\int_{inlet} p \, d\Gamma - \int_{outlet} p \, d\Gamma \right) + \omega_2 \int_\Omega (T - T_{in})^2 \, d\Omega \end{aligned} \tag{5.35}$$

The first contribution was aimed in minimizing the pressure drop in the system while the second one was meant to minimize the mean temperature in the domain making the temperature distribution as close as possible to the inlet one. The two coefficients ω_1 and ω_2 were not only constants for unit consistency, but also weighting values that scaled the respective thermal and fluid portions of the objective function.

5.3.1 Adjoint equation and boundary conditions

The adjoint equations were derived from the integrals over the domain Ω in equation 4.9 including the cost function 5.35 obtaining:

$$\begin{cases} -(\nabla \boldsymbol{u})\boldsymbol{v} - (\boldsymbol{v}\cdot\nabla)\boldsymbol{u} - \nabla\cdot(2\nu D(\boldsymbol{u})) + \alpha(\gamma)\boldsymbol{u} + \nabla q + T_a\nabla T = 0 \\ \nabla\cdot\boldsymbol{u} = 0 \\ -\boldsymbol{v}\cdot\nabla T_a - \nabla\cdot(K\nabla T_a) + T - T_{in} = 0 \end{cases} \tag{5.36}$$

The adjoint boundary conditions of the current problem were derived from equation 4.12 as follows:
adjoint boundary conditions for inlet and walls :

$$\boldsymbol{u}_{at} = 0 \tag{5.37a}$$
$$u_{an} = -\frac{\partial J_\Gamma}{\partial p} \tag{5.37b}$$
$$\boldsymbol{n}\cdot\nabla p_a = 0 \tag{5.37c}$$
$$T_a = 0 \tag{5.37d}$$

adjoint boundary conditions for outlet :

$$\boldsymbol{u}_a\cdot\boldsymbol{v} + u_n v_n + \nu(\boldsymbol{n}\cdot\nabla)u_n + TT_a + \frac{\partial J_\Gamma}{\partial v_n} = p_a \tag{5.38a}$$
$$v_n\boldsymbol{u}_t + \nu(\boldsymbol{n}\cdot)\boldsymbol{u}_t + \frac{J_\Gamma}{\partial \boldsymbol{v}_t} = 0 \tag{5.38b}$$
$$v_n T_a + k(\boldsymbol{n}\cdot\nabla T_a) + \frac{J_\Gamma}{T} = 0 \tag{5.38c}$$

5.3.2 Sensitivity Analysis

According to the results obtained in section 4.4, the gardient of the cost function was defined as follows:

$$\begin{aligned} J'(\eta)\delta\eta] = \partial_\eta L[\delta\eta] &= \int_\Omega (\boldsymbol{u}, q, T_a)\partial_\eta \boldsymbol{R} \\ &= \int_\Omega (\boldsymbol{u}, q, T_a)\begin{bmatrix} \boldsymbol{v}h(\eta)\delta\eta \\ 0 \\ 0 \end{bmatrix} \\ &= \int_\Omega \boldsymbol{u}\cdot\boldsymbol{v}h(\eta)\delta\eta. \end{aligned} \tag{5.39}$$

Where $h(\eta)$ was defined as:

$$h(\eta)\delta\eta = \alpha'(\eta) = \alpha_{max}(1+q)\frac{q}{(\eta+q)^2}\delta\eta. \tag{5.40}$$

The discrete formulation of the sensitivity became:

$$\begin{aligned} J'_h(\eta_h)[\delta\eta_h] &= \sum_i ((\boldsymbol{u}_i \cdot \boldsymbol{v}_i h(\eta_i) V_i \delta\eta_i \\ &= \nabla J_h \cdot \delta\eta_h \end{aligned} \tag{5.41}$$

5.3.3 Multiphysics Optimization Numerical Results

In this section the numerical results of the multiphysics and multi-objective optimization are reported. First the base case simulation was perfomed to set the initial conditions for temperature, velocity and pressure as reported in figure 5.12. The simulations provided numerical results coherent with those obtained with COMSOL Multiphysics. The maximum and the average temperatures were respectively 321.84 [K] and 299.78 [K].
Then two different optimization tests were performed changing the weighting factor ω_2 of the thermal component of the cost function in equation 5.35. The solver *adjointSimpleFoam* (appendix 8.2) was used for the following nuemrical test.

Test 1
In the first optimization test ω_2 was set equal to 0.1. In figure 5.13 the results are shown. In the optimal topology the red areas are referred to solid regions, while the blue areas are associated to liquid regions. The solver created single a path for water aimed in increasing the cooling performance in the domain. The maximum temprature in the system decreased to 300 [K] and the average temperature was 294.3 [K].

Test 2
In the second optimization test the weighting factor ω_2 was set equal to 0.5. In this case, figure 5.14, the optimization was more focused toward the thermal component of the cost function. The maximum temperature was 297.6 [K] and the average temperature was 294.1 [K].

5.4 Conclusions

In this chapter, the OpenFOAM optimization benchmarks with the adjoint method were presented. The solver adjointShapeOptimization already implemented in the OpenFOAM library was exposed with the fluid flow optimization of a duct explaining the strengths and the weaknesses of the code that led to modifications in the other solvers. In particular, the linear distribution of the porosity field in the design domain induced coarse transition from solid to liquid regions and made it necessary the implementation of interpolation schemes for sharper transitions. Than the pure heat conduction case was studied implementing an optimization solver based on the Poisson's equations aimed in finding the optimal conduction path to for a heat remover. The results obtained were even better with respect to those obtained with the COMSOL module. Then the Multiphysics and multi-objective benchmark was considered. An optimization solver based on Navier-Stokes equations coupled with convection diffusion equation was developed. The solver exploited in the OpenFOAM optimization were based on the "one shot" approach in which

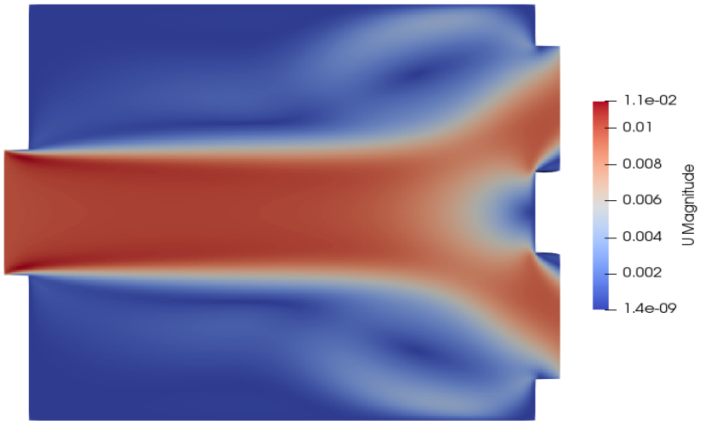

(a) *Velocity field*

(b) *Temperature field*

(c) *Velocity field*

Figure 5.12: OpenFOAM multiphysics optimization results BC

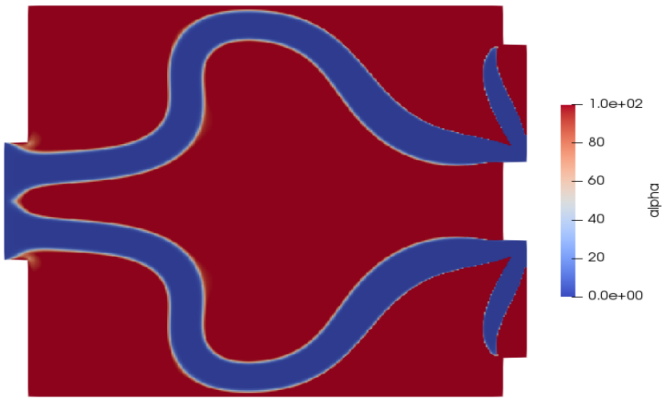

(a) *Topology optimization*

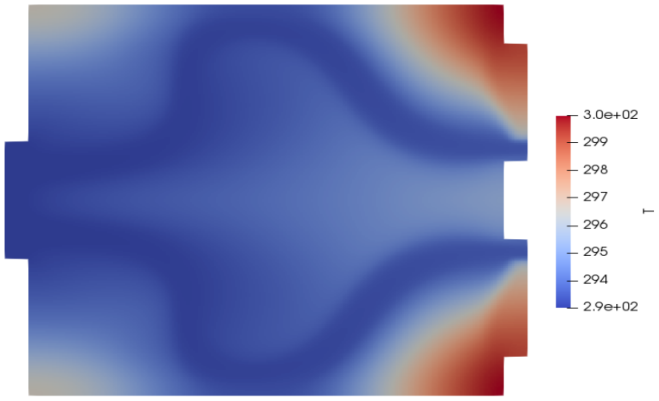

(b) *Final temperature field*

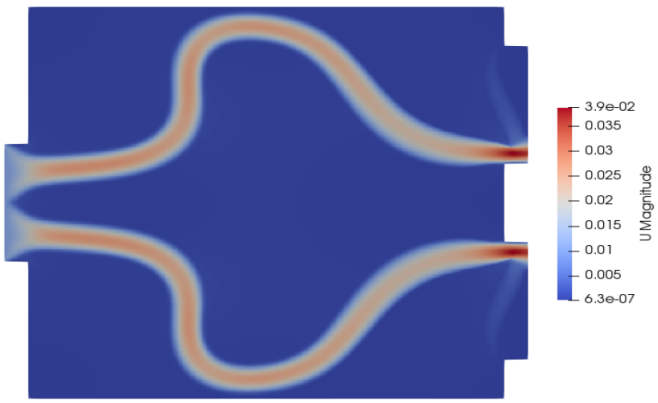

(c) *Final velocity field*

Figure 5.13: OpenFOAM multiphysics optimization results: $\omega_2 = 0.1$

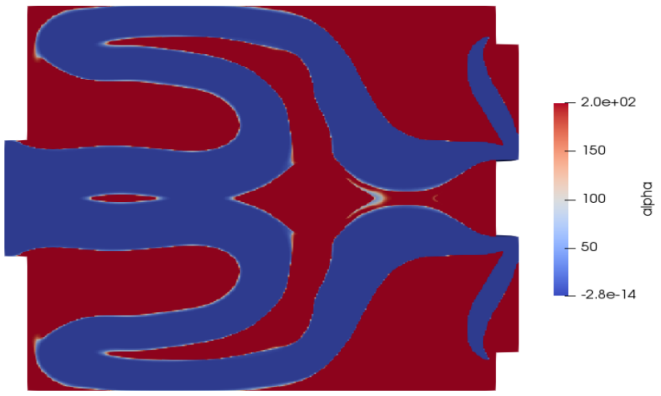

(a) *Topology optimization*

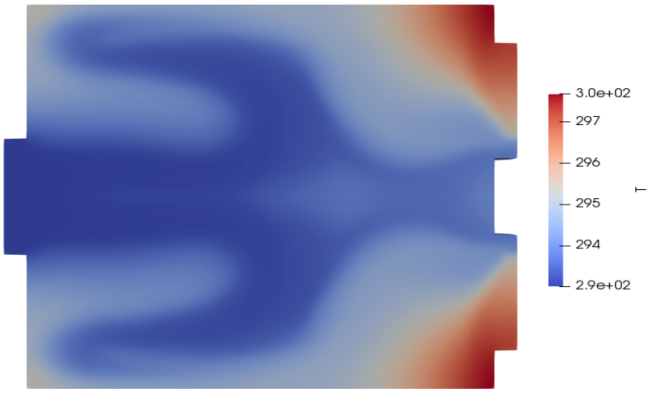

(b) *Final temperature field*

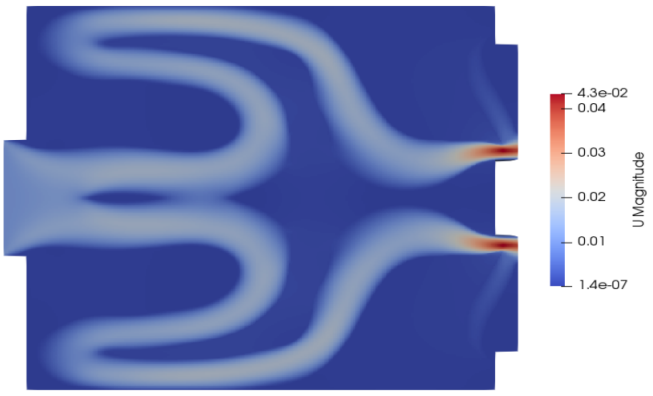

(c) *Final velocity field*

Figure 5.14: OpenFOAM multiphysics optimization results: $\omega_2 = 0.5$.

the sensitivity analysis were computed with the partially converged quantities. This led to simulation characterized by relatively high residuals placing the need for validation tests.

Molten Salt Fast Reactor Geometry Optimization

The Molten Salto Reactors (MSRs) concept was devised in 1950s and nowadays is acquiring interest among the nuclear engineering community as promising technology for sustainable energy production. The Generation-IV International Forum has identified the MSRs among the six reactor systems with encouraging potential concerning sustainability, economics, safety, reliability and proliferation resistance [23].
MSRs are circulating fuel reactors characterized by a nuclear fuel in liquid form acting also as coolant. Despite water and gas cooled reactors, molten salt coolant operates al low pressure decreasing stresses and failure risks. Furthermore, molten salt presents a lower chemical reactivity compared to liquid metal coolants of other generation IV reactors, decreasing the reactions with air and water.
In the following studies the Molten Salt Fast Reactor (MSFR) was considered. MSFR may play a key role in future nuclear energy systems presenting sustainability and economics advantages, peculiar of fast neutron reactors, like extended resource utilization and waste minimization. Moreover, the MSFR concept can provide large negative temperature and void coefficients, high burnup and high capacity factors that added to the benefits related to the use of molten salt as coolant, such as low operative pressure and high boiling temperature, make this reactor a competitive alternative to solid fueled fast neutron systems.
Nevertheless, MSFR is characterized by relevant engineering challenges which make it object of numerous research efforts. The primary circuit presents a corrosive environment with high temperatures and high neutron flux leading to the need of further compatible structural material studies. These drawbacks are enhanced by a not-optimal core shape. The core geometry was initially designed as a square cylinder for the neutron economy optimization. Computational Fluid Dynamics simulations evinced that this configuration leads to recirculation areas in the central part of the core, increasing not only the pressure drop of the system but also, and most important, the maximum temperature of the reactor.
This section of the thesis work was focused in the exploitation of the COMSOL Optimization tools to identify an optimal reactor shape improving both the fluid dynamics and the thermal aspect of the system. Starting from the square cylindrical shape, the Topology Optimization succeeded in defining a new design able to improve the reactor performances decreasing the maximum temperature reached but increasing the average temperature in the hot leg of the plant leading also to an increase of the power plant yield.

6.1 MSFR Introduction

6.1.1 Molten Salt Fast Reactor concept

The MSFR concept presents aspiring unconventional differences with the consolidated nuclear reactor technologies. The salt is used as fuel and coolant at the same time and operates on the Th/U^{233} fuel cycle with a fast and intermediate neutron spectrum and a nominal power of 3GW. A mixture of Li^7F and ThF_4 at the eutectic point is used as salt with a proportion of heavy nuclides fixed at $22.5mol.\%$. As shown in schematic 6.1 the fuel salt flow in the central part from the bottom to the top of the core cavity. After exiting the core, the return path is constituted by 16 groups of pumps and heat exchangers located around the core. The fuel circuit is surrounded by a reactor vessel for safety reasons.

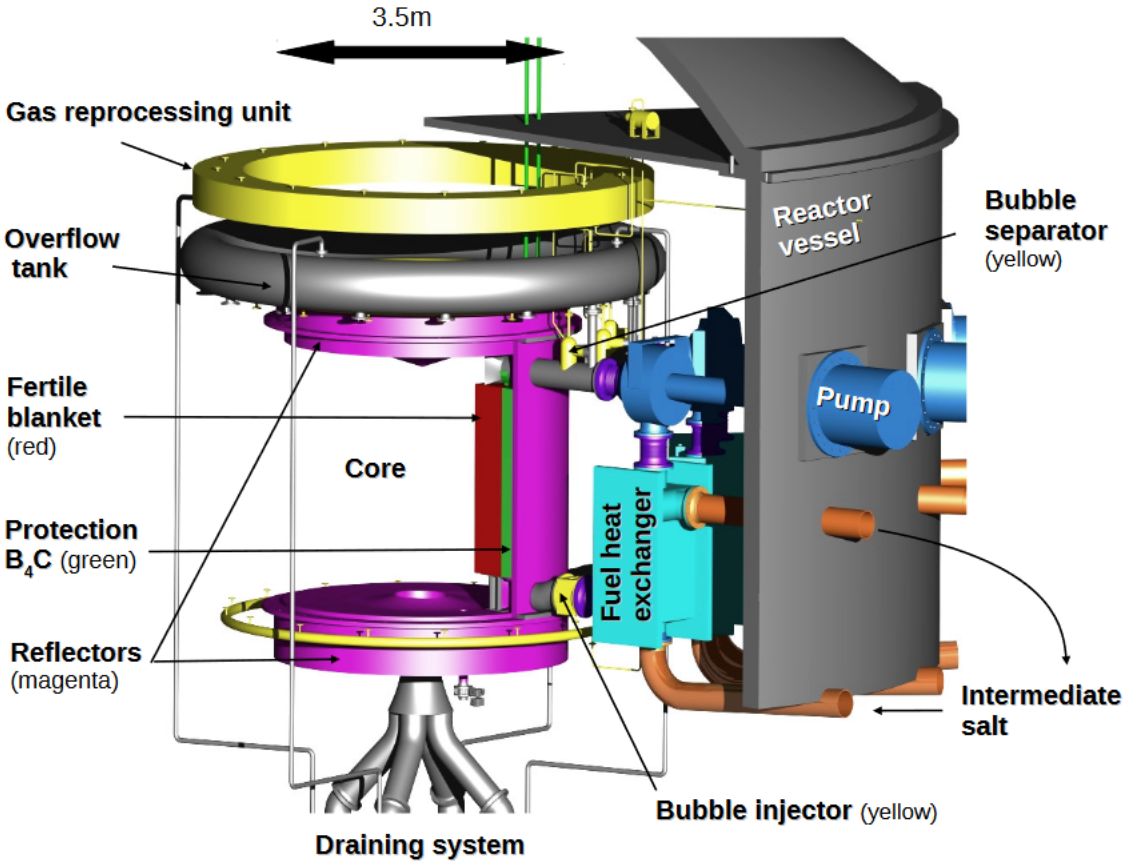

Figure 6.1: Schematic representation of the Molten Salt Fast Reactor fuel loop [7]

An online bubbling system inject gas in the fuel circuit after the heat exchanger in the lower part of the core and extract it from the liquid part at the outlet of the core. This system was designed with the purpose of removing gaseous fission products and metallic

particles dragged by fuel salt. The concentration increase of gaseous fission products like xenon and krypton can led to fuel saturation and consequent formation of gas bubbles that will escape via fuel's free surfaces. Furthermore, the bubble injection system has a reactivity control application independent from the fission product extraction. The reduction of the local fuel density induced by the injection of large bubbles and the consequent reactivity redaction is still an object of study.
The three important components of the core are the lower and upper nickel-based alloy reflectors and the radial fertile blankets which belong to the radial reflector. The top and bottom reflectors can absorb more than 99% of the leaking neutrons. The lower one is also connected to a drain system able to drain the reactor core in criticality-safe drain tank in case of incidental situations or planned shutdowns, avoiding the increase of temperatures. A fertile blanked of 50 [cm] in the radial reflector are designed to increase the breeding ratio.
MSFR concept is characterized by excellent safety coefficients, strong negative void and temperature coefficients, low fissile inventory and very good deployment capabilities.

6.1.2 EVOL Benchmark Geometry

The preliminary core shape design of the MSFR was conceived as a single compact cylinder (2.25 m high and 2.25 m diameter) for neutron economy optimization purposes. This first shape was selected as official geometry for neutronic benchmarks of the EVOL Project and has been used as reference configuration for numerous works (figure 6.2).

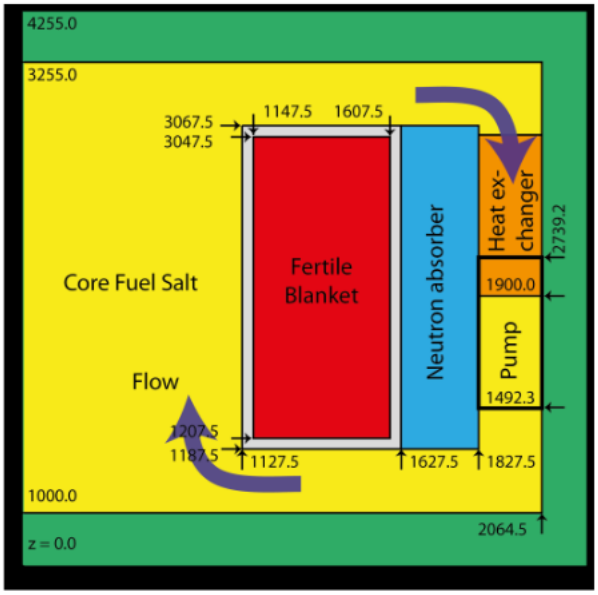

Figure 6.2: 2D MSFR benchmark geometry [8]

Computational Fluid Dynamics studies underlined thermal-hydraulics problems related to this configuration. In particular, the cylindrical configuration leads to the establishment of recirculation areas near the radial core wall of the reactor inducing high localized

pressure drop and excessive temperature increase. These represent unacceptable working conditions for the structural components of the core subjected to severe thermal, chemical and irradiation environment. Despite the mentioned disadvantages, the cylindrical configuration was selected as reference for numerous MSFR analysis and studies. This is mainly due the fact that MSFR design has still not been finalized and geometry changes can lead to different core configurations. Furthermore the EVOL Project simple geometry is best performing from the computational cost point of view avoiding the presence of details and complex structures.
In recent years, core optimization process have been proposed in literature aimed in obtaining a maximization of the overall flow mixing in the core cavity and reducing the temperature peaks in the salt and on the core walls. A revisited geometry is shown in figure 6.3.

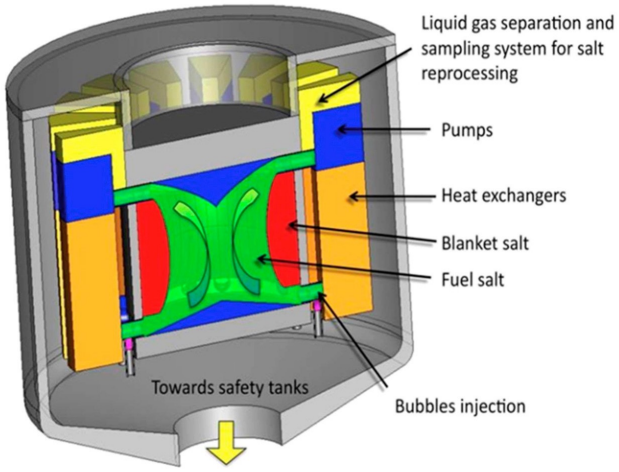

Figure 6.3: Revisited MSFR core design [9]

In the following sections, the optimization procedure fot the reactor core is presented. COMSOL Topology optimization was used to minimize recirculation areas, pressure drops and the temperature gradient of the salt helping the reduction of thermal stresses induced on the core wall structures. As shown in the previous chapters, a design variable γ was introduced in a selected design domain of the core and a porosity field was associated to it inducing a volume force associated to a the solid domain. A gradient based algorithm was selected for the optimization process.

6.2 MSFR Optimization

In this section the COMSOL optimization of the EVOL benchmark geometry is presented. First, a numerical simulation without optimization is shown, highlining the disadvantages of the cylindrical geometry. Than the topology optimization was applied showing promising thermal-hydraulic improvements. As for the 3D fin Optimization, a validation procedure was performed since the optimization results couldn't produce a design variable transition sharp enough to guarantee physical coherent results. The validation procedure passed through the extraction of the filtered topology result and the reconstruction of the geometry. Than the same operative condition were applied to the new system. The final numerical results sowed promising improvements. The large reduction of recirculation zones led to an important decrease of maximum temperature of the salt. Moreover the average temperature in the hot leg resulted increased respect to the base case allowing an improvement also in the power plant yield.

6.2.1 Base Case Model

The model (6.4) was constituted by a cylindrical core connected to the heat exchanger, linked to the secondary loop and the pump through the hot leg and the cold leg of the reactor. Fixed temperature values were imposed on the heat exchanger walls and the pump was modelled with a volume force. In the cylindrical core a homogeneous heat production of about 3 000 [MW] was imposed.

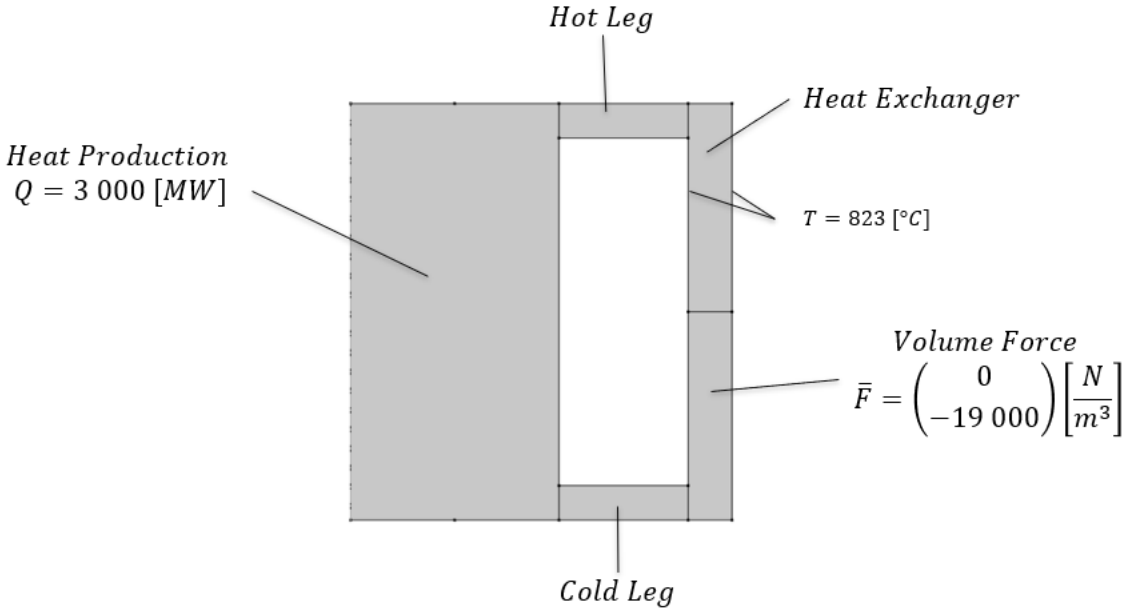

Figure 6.4: MSFR initial geometry and boundary conditions

The fuel salt properties, summarized in table 6.1, were averaged in order to simplify the computational cost required by the simulation. The fluid flow was modelled with

RANS equations and $\kappa - \epsilon$ turbulence model.

Properties	Symbol	Unit	Value
$Density$	ρ	$\left[\frac{kg}{m^3}\right]$	4286
$DynamicViscosity$	μ	$[Pa \cdot s]$	$1.7 \cdot 10^{-2}$
$SpecificHeatCapacity$	C_p	$\left[\frac{J}{kg \cdot K}\right]$	1010
$ThermalConductivity$	k_{iso}	$\left[\frac{W}{m \cdot K}\right]$	1.7

Table 6.1: MSFR fuel salt properties

6.2.2 Base Case Numerical Results

The numerical results regarding velocity and temperature field are shown in figure 6.5 and 6.6.

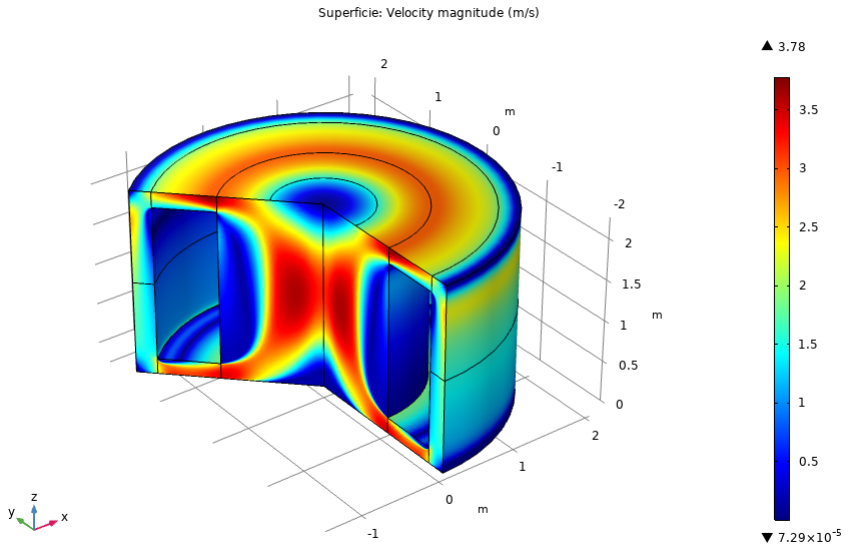

Figure 6.5: MSFR initial velocity field

As discussed before, the numerical results of the core cylinder geometry showed large recirculation areas mainly close to the radial core wall but also in the upper and lower walls. In those areas the fuel salt is characterized by a higher residence time in the core. The consequent overheating leads to a maximum temperature in the system equal to 1730 [K]. This temperature field defines an unallowable operative condition for the reactor core material and mostly for the reflectors and container structures subjected to severe conditions from both chemical and radiation point of view.

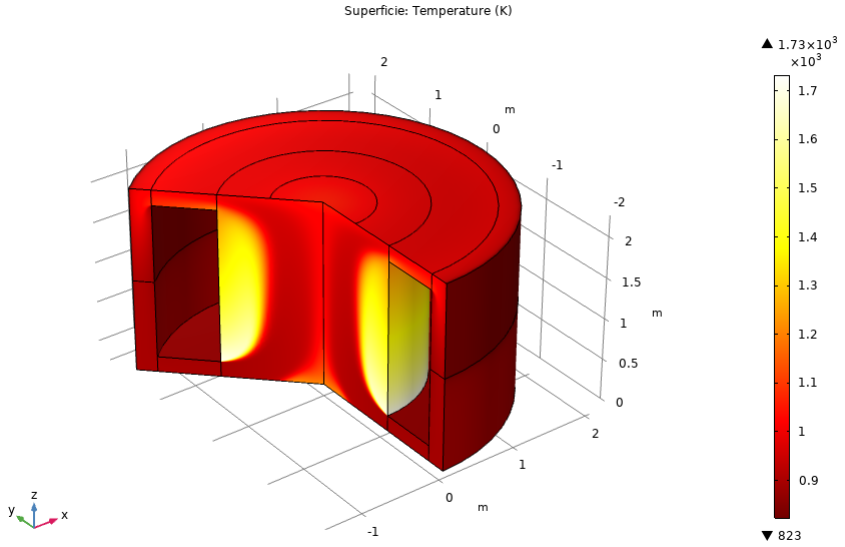

Figure 6.6: MSFR initial temperature field

6.2.3 Optimization Numerical Test

The design domain selected for the topology optimization was constituted by the cylindrical core, the hot leg and the cold leg. This domain was characterized by the presence of volumetric force $\boldsymbol{F}$ producing a penalization of the fluid velocities in the porous material introduced with the topology optimization.

$$\boldsymbol{F} = \alpha(\gamma) \cdot \boldsymbol{u}$$

α is again the inverse permeability of porous medium and was defined as function of the control variable γ through the Darcy interpolation scheme (equation 3.9).

The definition of the optimization problem proceeded with the determination of an objective function to be minimized. The most effective function resulted to be the difference between average inlet pressure in the heat exchanger and the average outlet pressure from the pump system:

$$J = p_{avg,inlet-heatexchanger} - p_{avg,out-pump} \tag{6.1}$$

Defining Vol as the total volume of the design domain, the following volume constrain was imposed:

$$V_{target} = \int_{\Omega_d} \frac{\gamma}{Vol}\, d\Omega = 0.98 \tag{6.2}$$

The topology optimization result obtained with MMA solver algorithm is shown in figure 6.7.

Nevertheless, a validation numerical test on the topology optimization result was mandatory due to unphysical aspects related to the design variable field. First, the portion of design domain related to solid porous media were still associated to power production. Moreover, the design variable smooth transition from values associated to solid region to

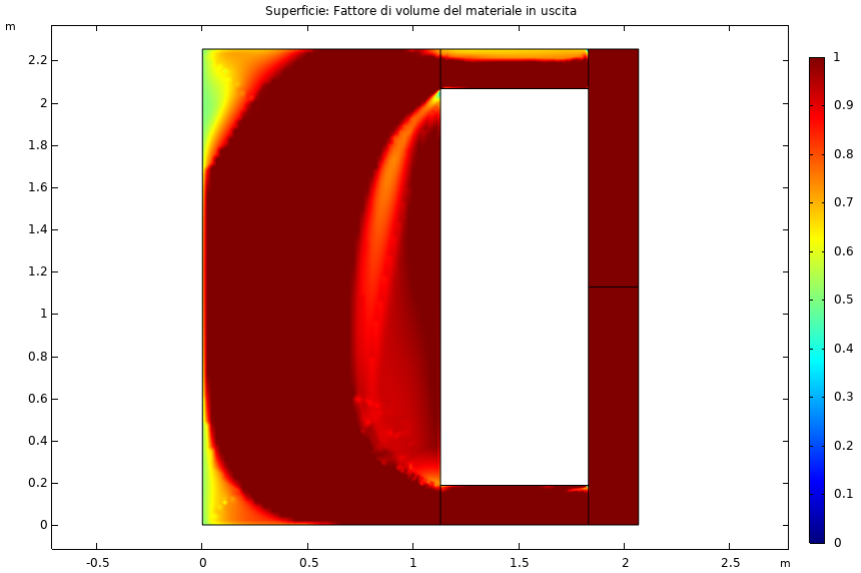

Figure 6.7: MSFR topology optimization result

fluid one introduced a velocity field different from zero also in solid region.

6.2.4 Validation Numerical Test

In this section the numerical validation of the core shape obtained in the optimization is performed. First, a filter equal to 0.8 was applied to the design variable in the topology optimization result.

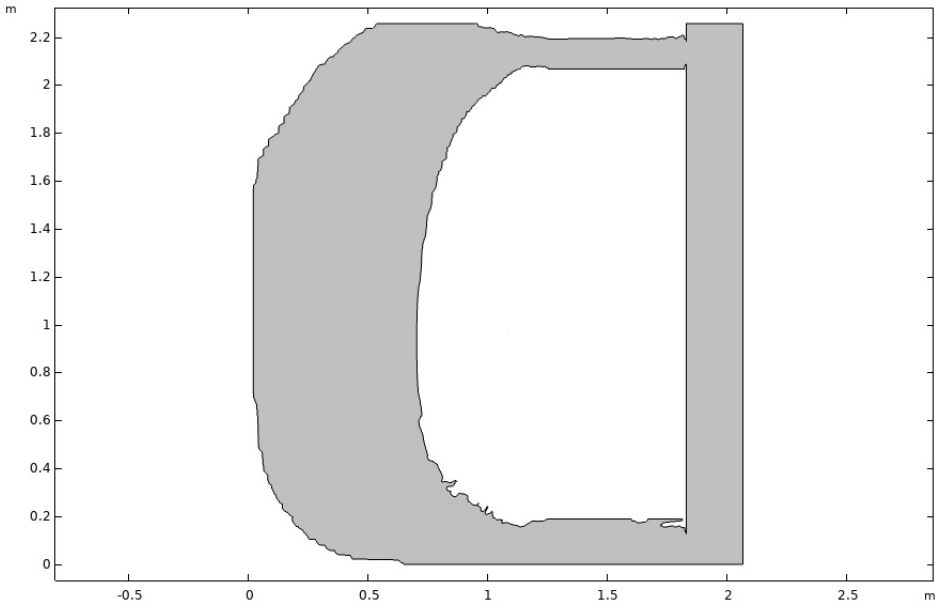

Figure 6.8: MSFR filtered topology optimization result

As shown in figure 6.8, the geometry obtained through the filter application presented numerous superficial defects typical of optimization processes. Since these imperfection caused excessive viscous friction contribution, the point of the curves in the optimized design were interpolated with quadratic Bézier functions in order to obtain perfectly smoothed surfaces as shown in figure 6.9.

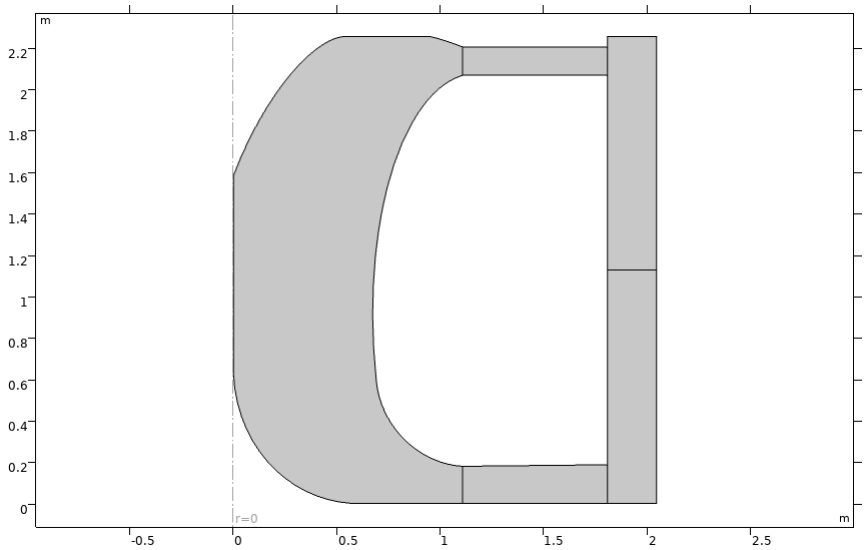

Figure 6.9: MSFR refined geometry

The same boundary conditions and operative condition of the base case were applied to the new geometry in order to validate the improved thermo-hydraulic performances. The results are shown in figures 6.10 and 6.11.

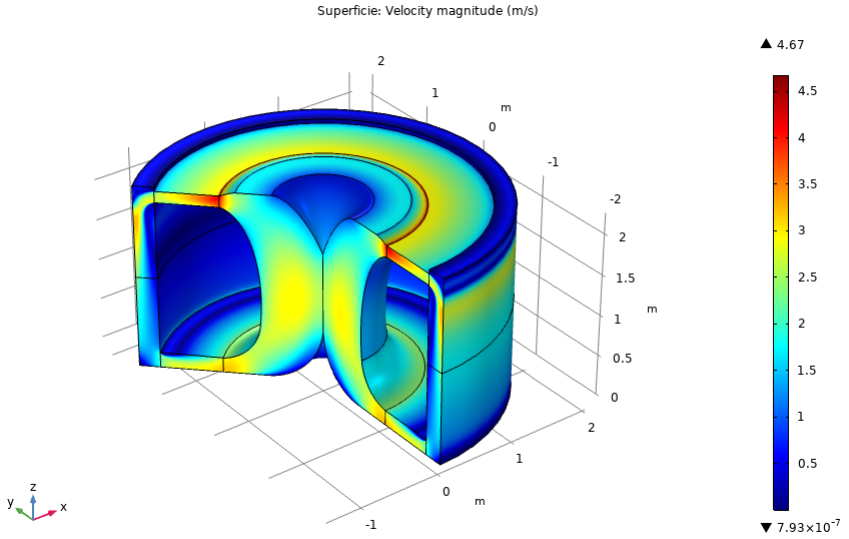

Figure 6.10: MSFR velocity field

The optimized geometry led to promising improvements regarding the thermal aspect of the reactor. The absence of recirculation areas decreased the maximum temperature

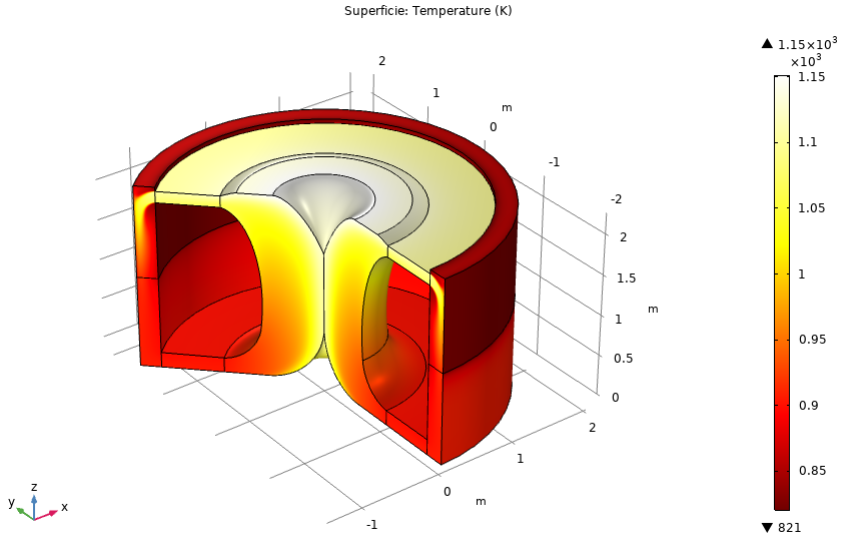

Figure 6.11: MSFR temperature field

reached by the system from 1730 [K] to 1150 [K]. This represent a very important results for the material aspect of the reactor since the excessive thermal gradient represented the most limiting factor for the life of components.
Another important improvement introduced was that despite the average core temperature decreased from 1137.5 [K] in the base case to 991.2 [K] in the optimized geometry, the average temperature in the hot leg increased. This parameter represent a crucial aspect in a nuclear power plant. The steam cycle related to the nuclear plant is defined as power cycle with heat source at constant temperature. In this case the power yields of first and second thermodynamics principle are defined as:

$$\eta_I = \frac{W}{Q_h} \tag{6.3}$$

$$\eta_{II} = \frac{W}{Q_h \cdot (1 - \frac{T_0}{T_h})} = \frac{\eta_I}{1 - \frac{T_0}{T_h}} = \frac{\eta_I}{\eta_{rev}} \tag{6.4}$$

Where W [W] is the electric or mechanical power, Q_h [W] is the thermal power entering the cycle while T_h and T_0 are the temperature of the heat source and the minimum temperature of the power cycle.

η_I and η_{II} are related through η_{rev} that represents the yield of a Carnot cycle operating between T_h and T_0. The difference between η_I and η_{II} increases with the decrease of T_h making more thermodynamically poor the heat source. In this case the average temperature of the hot leg, that is T_h of the power cycle, increased from 1050.7 [K] to 1082.2 [K].

An important aspect that must be taken into account is that the new core design presents a reduced volume respect the base case while the total power production (3000 $[MW_{th}]$) and the volume force due to the pump (19 000 $[\frac{N}{m^3}]$) were kept equal to the base

case. This led to increased power density and average velocity of the reactor. Further studies must consider also the enlargement of the core keeping the same curves shape.

6.2.5 MSFR Optimization Conclusions

This chapter of the thesis work was aimed at facing with some engineering challenges typical of a nuclear power plant and in particular of the MSFR. This reactor represents one of the most encouraging concept for a sustainable energy production competitive also from the economics, safety, reliability and proliferation resistance points of view. However, the unconventional aspects that give the MSFR such potentiality are characterized by drawbacks regarding the severe operative conditions which the structural core material are subject. The COMSOL Topology Optimization was used to design an optimized core shape of the reactor improving the thermal aspect. The results showed that the optimized geometry led to a decrease of the maximum temperature of about 580 [K] and an increased temperature in the hot leg of the system. Further studies must take into account not only the reduction of the core volume but also the neutronic aspect of the optimization. A multi-objective optimization regarding the thermal-hydraulic aspect with the reduction of the neutronic leakages can introduce additional improvements in the reactor design.

Conclusions and Future Works

In the first two parts of the present work, topology optimization was investigated through two different software, respectively COMSOL Multiphysics and OpenFOAM. The former includes an established optimization module and was initially used for a better understanding of the gradient based optimization algorithms and porosity interpolation schemes. First three 2D benchmarks were used as preliminary study of the solvers and the control variable interpolation schemes which gave promising optimization results regarding fluid flow and heat transfer. The gradient based algorithms did not show particular limitations regarding fluid flow instabilities or computational efforts and seemed to lent itself well for more complex problems. Hence, a 3D Multiphysics and multi-objective heat transfer optimization was investigated. COMSOL Multiphysics succeeded in defining an optimized shape for a heat transfer fin in cooling system governed by forced convection. The result of the optimization was fist validated through the exportation of the filtered geometry, in order to avoid errors introduced by intermediate porosity regions, then was compared with a standard rectangular fin with the same volume and width. The results showed that the optimized geometry leads to a better heat transfer and fluid flow performances. However, since the computational effort required by the tridimensional simulation resulted to be the most limiting factor of this topology optimization approach, the second part of the thesis work focused on an alternative method for topology optimization.

In the second part, a Multiphysics optimization solver based on the adjoint approach was implemented in OpenFOAM. The adjoint optimization was tested with the same 2D benchmarks of the previous section. The comparison between the results obtained with the two software was limited by the fact that the adjoint algorithm implemented the "one-shot" approach. This involve a sensitivity analysis calculated with only partially converged quantities and resulted in numerical tests with high residual values. Nonetheless, the adjoint optimization showed remarkable results.

In the laminar flow optimization, the two software converged to a similar S-bend shape of the design domain. In this case the OpenFOAM simulation was performed with the solver *adjointShapeOptimizationFoam* already implemented in the software. The forementioned solver provides a linear porosity interpolation which induced the formation of intermediate porosity regions affecting the velocity and pressure fields making it necessary a validation test for a better analysis. In the further tests, this problem was effectively mitigated with the use of suitable interpolation schemes. Furthemore, the solver showed instabilities induced by increasing fluid flow velocities that represented a computational

limitation.

The pure heat conduction optimization problems converged to very similar topology and temperature results for both the software. The numerical results regarding the average temperature of the systems for the two software are summarized in table 7.1 with different target volumes defined as volume fraction of the most conductive material.

V_{target}	COMSOL: $T_{avg}[K]$	OpenFOAM: $T_{avg}[K]$
0.3	278.23	276.39
0.4	276.93	275.62
0.5	376.18	275.22

Table 7.1: Comparison between COMSOL and OpenFOAM numerical results in pure heat conduction optimization

In the last benchmark, the Multiphysics and multi-objective problem aimed at minimizing the temperature in a heated domain was presented. Both the software defined optimal coolant paths able to reduce the average temperature of the system with different values of the thermal cost function weighting factors. The "one-shot" approach adopted by the adjoint method succeeded in improving the computational effort of the solver with respect to the traditional procedures used in COMSOL. For this reason the adjoint topology optimization is a promising tool for further tridimensional studies regarding thermal-hydraulic problems of engineering interest. However, it induced high residual values which introduced the need of further validation test and the computational instabilities induced by turbulences limited it applicability to low Reynolds numbers.

In the final part of the thesis work, topology optimization was applied to the MSFR. The cylindrical symmetry of the problem allowed the use of COMSOL optimization module which showed to be a more performing tool for 2D multiphysics systems. Starting from the cylindrical geometry approved by the EVOL Project, the topology optimization was used for the improvement of the thermal-hydraulic aspect of the reactor. The cylindrical core shape in fact, induces large recirculation areas leading to high temperature gradients. The topology optimization succeeded in reducing the maximum temperature in the system of about 580 [K] and the average temperature in the core decreased from 1137.5 [K] to 991.20 [K]. This resulting operative conditions of the system represents an important improvement for the structural material point of view which are subject not only to high temperature gradient but also to severe chemical attacks and neutronic radiations.
The promising thermal-hydraulic optimization results obtained with MSFR can be extended on more complex systems. In particular, the stability of the COMSOL gradient based algorithms represents a promising starting point for multiphysics optimizations including the neutronic economy in the reactor defining an additional contribution in the cost function aimed at minimzing the neutron leakages from the core.

Appendix

8.1 adjointHeatConduction.C

```
*---------------------------------------------------------------------------*\
  =========                 |
  \\      /  F ield         | OpenFOAM: The Open Source CFD Toolbox
   \\    /   O peration     | Website:  https://openfoam.org
    \\  /    A nd           | Copyright (C) 2011-2018 OpenFOAM Foundation
     \\/     M anipulation  |
-------------------------------------------------------------------------------
License
    This file is part of OpenFOAM.

    OpenFOAM is free software: you can redistribute it and/or modify it
    under the terms of the GNU General Public License as published by
    the Free Software Foundation, either version 3 of the License, or
    (at your option) any later version.

    OpenFOAM is distributed in the hope that it will be useful, but WITHOUT
    ANY WARRANTY; without even the implied warranty of MERCHANTABILITY or
    FITNESS FOR A PARTICULAR PURPOSE.  See the GNU General Public License
    for more details.

    You should have received a copy of the GNU General Public License
    along with OpenFOAM.  If not, see <http://www.gnu.org/licenses/>.

Application
    laplacianFoam

Description
    Solves a simple Laplace equation, e.g. for thermal diffusion in a solid.

\*---------------------------------------------------------------------------*/

#include "fvCFD.H"
#include "fvOptions.H"
#include "simpleControl.H"

// * * * * * * * * * * * * * * * * * * * * * * * * * * * * * * * * * * * * //

int main(int argc, char *argv[])
{
    #include "setRootCaseLists.H"
```

```
    #include "createTime.H"
    #include "createMesh.H"

    simpleControl simple(mesh);

    #include "createFields.H"

    // * * * * * * * * * * * * * * * * * * * * * * * * * * * * * * * * * * * * //

    Info<< "\nCalculating temperature distribution\n" << endl;

    while (simple.loop(runTime))
    {
        Info<< "Time = " << runTime.timeName() << nl << endl;
transportProperties.lookup("lambda") >> lambda;
transportProperties.lookup("Vtarget") >> Vtarget;

        while (simple.correctNonOrthogonal())
        {
K=(ks-kf)*(0.001+0.999*gamma*gamma*gamma);
scalar objFunction (0.0);
scalar volFraction (0.0);
scalar volTotal (0.0);

forAll(mesh.cells(),celli)
{
 volFraction +=
(ref.value()-K[celli])*mesh.V()[celli];
 volTotal +=mesh.V()[celli];
 objFunction += (T[celli]-273)*(T[celli]-273);
}

Info<< "\ total volume=\n" << volTotal;
Info<< "\ volFraction=\n" << volFraction;

scalar costFunctionTotal = objFunction*volTotal/2;

scalar ck= Foam::sqr(volFraction/volTotal-Vtarget.value());

scalar stepInt = -lambdaVol.value() + iki.value()*weightFactor.value()*ck;

scalar ckDer = -iki.value()/(volTotal)*(volFraction/volTotal-Vtarget.value());
scalar Jv = stepInt*ckDer;

        gamma +=
            mesh.fieldRelaxationFactor("gamma")
           *(min(max(gamma + (scal1*Coeff*gamma*gamma*(ks-kf)*(fvc::grad(T) & fvc::grad(Ta))-scal2*J

lambdaVol += -iki.value()*weightFactor.value()*ck;


        fvScalarMatrix TEqn
        (
       -fvm::laplacian(K, T) - Q
```

```
        );
  TEqn.solve();

fvScalarMatrix TaEqn
     (
       -fvm::laplacian(K, Ta) - (T - Tin)
     );
        TaEqn.solve();


        }

        // #include "write.H"
        runTime.write();

        Info<< "ExecutionTime = " << runTime.elapsedCpuTime() << " s"
            << "  ClockTime = " << runTime.elapsedClockTime() << " s"
            << nl << endl;
    }

    Info<< "End\n" << endl;

    return 0;
}


// ************************************************************************* //
```

8.2 adjointSimpleFoam.C

```
/*---------------------------------------------------------------------------*\
  =========                 |
  \\      /  F ield         | OpenFOAM: The Open Source CFD Toolbox
   \\    /   O peration     | Website:  https://openfoam.org
    \\  /    A nd           | Copyright (C) 2011-2018 OpenFOAM Foundation
     \\/     M anipulation  |
-------------------------------------------------------------------------------
License
    This file is part of OpenFOAM.

    OpenFOAM is free software: you can redistribute it and/or modify it
    under the terms of the GNU General Public License as published by
    the Free Software Foundation, either version 3 of the License, or
    (at your option) any later version.

    OpenFOAM is distributed in the hope that it will be useful, but WITHOUT
    ANY WARRANTY; without even the implied warranty of MERCHANTABILITY or
    FITNESS FOR A PARTICULAR PURPOSE.  See the GNU General Public License
    for more details.

    You should have received a copy of the GNU General Public License
    along with OpenFOAM.  If not, see <http://www.gnu.org/licenses/>.

Application
```

```
    ajointShapeOptimizationFoam

Description
    Steady-state solver for incompressible, turbulent flow of non-Newtonian
    fluids with optimisation of duct shape by applying "blockage" in regions
    causing pressure loss as estimated using an adjoint formulation.

    References:
    \verbatim
        "Implementation of a continuous adjoint for topology optimization of
         ducted flows"
        C. Othmer,
        E. de Villiers,
        H.G. Weller
        AIAA-2007-3947
        http://pdf.aiaa.org/preview/CDReadyMCFD07_1379/PV2007_3947.pdf
    \endverbatim

    Note that this solver optimises for total pressure loss whereas the
    above paper describes the method for optimising power-loss.

\*---------------------------------------------------------------------------*/

#include "fvCFD.H"
#include "singlePhaseTransportModel.H"
#include "turbulentTransportModel.H"
#include "simpleControl.H"
#include "fvOptions.H"


template<class Type>
void zeroCells
(
    GeometricField<Type, fvPatchField, volMesh>& vf,
    const labelList& cells
)
{
    forAll(cells, i)
    {
        vf[cells[i]] = Zero;
    }
}


// * * * * * * * * * * * * * * * * * * * * * * * * * * * * * * * * * * * * //

int main(int argc, char *argv[])
{
    #include "postProcess.H"
    #include "setRootCaseLists.H"
    #include "createTime.H"
    #include "createMesh.H"
    #include "createControl.H"
    #include "createFields.H"
    #include "initContinuityErrs.H"
```

```
    #include "initAdjointContinuityErrs.H"


    turbulence->validate();

    // * * * * * * * * * * * * * * * * * * * * * * * * * * * * * * * * * * * * //

    Info<< "\nStarting time loop\n" << endl;


    while (simple.loop(runTime))
    {
simpleControl directSimple(mesh, "DSIMPLE");
simpleControl adjSimple(mesh, "ASIMPLE");

        Info<< "Time = " << runTime.timeName() << nl << endl;

        laminarTransport.lookup("lambda") >> lambda;
laminarTransport.lookup("Vtarget") >> Vtarget;

scalar objFunction (0.0);
        scalar volFrac (0.0);
scalar volTotal (0.0);


forAll(mesh.cells(),celli)
{
 volFrac +=
(ref.value()-alpha[celli]/alphaMax.value())*mesh.V()[celli];
 volTotal +=mesh.V()[celli];
}

Info<< "\ total volume=\n" << volTotal;
Info<< "\ volFrac=\n" << volFrac;

scalar ck = Foam::sqr(volFrac/volTotal-Vtarget.value());

scalar stepInt = -lambdaVol.value() + iki.value()*weightFactor.value()*ck ;

scalar ckDer = -iki.value()/(alphaMax.value()*volTotal)*(volFrac/volTotal-Vtarget.value());
scalar Jv = stepInt*ckDer;

thermalK = turbulence -> nu()/Pr;

eta +=
mesh.fieldRelaxationFactor("eta")
*(min(max(eta - ll*q * (1+q)* (alphaMax)/(eta+q)/(eta+q)* (Ua & U ) , zeroEta), etaMax)- eta);



alpha = (alphaMax -alphaMax * eta * (1+q)/(eta+q)) ;
zeroCells(alpha, inletCells);


        // Pressure-velocity SIMPLE corrector
```

```
        {
            // Momentum predictor

            #include "UEqn.H"
     #include "pEqn.H"
     #include "TEqn.H"

        }

        // Adjoint Pressure-velocity SIMPLE corrector
        {
            // Adjoint Momentum predictor

            #include "UaEqn.H"
     #include "paEqn.H"
     #include "TaEqn.H"

        }

        laminarTransport.correct();
        turbulence->correct();


      //  }
        runTime.write();

        Info<< "ExecutionTime = "
            << runTime.elapsedCpuTime()
            << " s\n\n" << endl;
    }

    Info<< "End\n" << endl;

    return 0;
}


// ************************************************************************* //
```

8.2.1 UaEqn.H

```
volVectorField adjointTransposeConvection((fvc::grad(Ua) & U));

    zeroCells(adjointTransposeConvection, inletCells);

    tmp<fvVectorMatrix> tUaEqn
     (
        fvm::div(-phi, Ua)
        - adjointTransposeConvection
        + turbulence->divDevReff(Ua)
        + fvm::Sp(alpha, Ua)
        + scal2*Ta*fvc::grad(T)
       - T*fvc::grad(Ta)
         ==
```

```
        fvOptions(Ua)
      );

         fvVectorMatrix& UaEqn = tUaEqn.ref();

         UaEqn.relax();

         fvOptions.constrain(UaEqn);

         solve(UaEqn == -fvc::grad(pa));

         fvOptions.correct(Ua);
```

8.2.2 PaEqn.H

```
volScalarField rAUa(1.0/UaEqn.A());
    volVectorField HbyAa("HbyAa", Ua);
    HbyAa = rAUa*UaEqn.H();
    tUaEqn.clear();
    surfaceScalarField phiHbyAa("phiHbyAa", fvc::flux(HbyAa));
    adjustPhi(phiHbyAa, Ua, pa);

    // Non-orthogonal pressure corrector loop
    while (simple.correctNonOrthogonal())
            {
                fvScalarMatrix paEqn
                (
                    fvm::laplacian(rAUa, pa) == fvc::div(phiHbyAa)
                );

                paEqn.setReference(paRefCell, paRefValue);
                paEqn.solve();

                if (simple.finalNonOrthogonalIter())
                {
                    phia = phiHbyAa - paEqn.flux();
                }
            }

            #include "adjointContinuityErrs.H"

            // Explicitly relax pressure for adjoint momentum corrector
            pa.relax();

            // Adjoint momentum corrector
            Ua = HbyAa - rAUa*fvc::grad(pa);
            Ua.correctBoundaryConditions();
            fvOptions.correct(Ua);
```

8.2.3 TaEqn.H

```
{
```

```
    fvScalarMatrix TaEqn
    (
         fvm::div(phi, Ta)
        -fvm::laplacian(thermalK*qqq, Ta)
        +scal2*(T - Ttarget)
     ==
       fvOptions(Ta)
    );

    TaEqn.relax();

    fvOptions.constrain(TaEqn);

    TaEqn.solve();

    fvOptions.correct(Ta);


}
```

Bibliography

[1] E. M. Dede, "Multiphysics topology optimization of heat transfer and fluid flow systems," *Excerpt from the Proceedings of the COMSOL Conference 2009 Boston*, 2009.

[2] M. Fesanghary, "Topology and shape optimization of hydrodynamically–lubricated bearings for enhanced load-carrying capacity," *Materials Science*, 2013.

[3] H. Jan, "Design of thermal systems using topology optimization," *THES*, 2017/12/28.

[4] M. J. Tomlin M, "Proceeding of the 7th altair cae technology conference," pp. 1–9, 2011.

[5] G. G. W. Endashaw Tesfaye Woldemariam, Hirpa G. Lemu, "Cfd-driven valve shape optimization forperformance improvement of a microcross-flow turbine," *energies*, 2018.

[6] U. Nilsson, "Description of adjointshapeoptimizationfoam and how to implement new objective functions," *A course at Chalmers University of Technology Taught by Hakan Nilsson*, 2014.

[7] M.-L. e. a. Brovchenko M., Heuer D., "Designrelated studies for the preliminary safety assessment of the molten salt fast reactor," *Tesi di laurea Magistrale*, vol. 175(3), pp. 329–339, 2013.

[8] E. van der Linden, "Coupled neutronics and computational fluid dynamics for the molten salt fast reactor," *Master's thesis*, 2012.

[9] O. B. e. a. Jérôme Serp, Michel Allibert, "The molten salt reactor (msr) in generation iv: Overview and perspectives," *Progress in Nuclear Energy*, vol. 77, pp. 308–319, 2014.

[10] M. D. S. e. a. John Nicklow, F.ASCE; Patrick Reed, "State of the art for genetic algorithms and beyond in waterresources planning and management," *JOURNAL OF WATER RESOURCES PLANNING AND MANAGEMENT*, vol. 136(4), pp. 412–432, 2010.

[11] W. Z. D. Q. e. a. Liang Meng, "From topology optimization design to additive manufacturing: Today's success and tomorrow's roadmap," *Archives of Computational Methods in Engineering*, vol. 27, pp. 805–830, 2020.

[12] J.-L. H. V. Subramaniam, T. Dbouk, "Topology optimization of conjugate heat transfer systems: A competition between heat transfer enhancement and pressure drop reduction," *International Journal of Heat and Fluid Flow*, vol. 75, pp. 165–184, 2019.

[13] G. X. e. a. Bin ZHANG, Jihong ZHU, "Design of nanofluid-cooled heat sink using topology optimization," *Chinese Journal of Aeronautics*, 2020.

[14] T. Dbouk, "A review about the engineering design of optimal heat transfer systems using topology optimization," *Applied Thermal Engineering*, vol. 112, pp. 841–854, 2017.

[15] G. F. N. Jan H.K. Haertel, "A fully developed flow thermofluid model for topology optimization of 3d-printed air-cooled heat exchangers," *Applied Thermal Engineering*, vol. 119, pp. 10–24, 2017.

[16] J. Y. M. Ajay Vadakkepatt, Sanjay R. Mathur, "Efficient automatic discrete adjoint sensitivity computation for topology optimization – heat conduction applications," *International Journal of Numerical Methods for Heat and Fluid Flow*, vol. 28 No.2, pp. 439–471, 2018.

[17] O. S. e. a. Janus Asmussen, Janus Asmussen, "A "poor man's" approach to topology optimization of natural convection problems," *arXiv:1809.01900v2 [cs.CE] 19 Feb 2019*.

[18] B. S. L. J. H. K. Haertel, K. Engelbrecht and O. Sigmund, "Topology optimization of thermal heat sinks," *Excerpt from the Proceedings of the 2015 COMSOL Conference in Grenoble*, 2015.

[19] "Optimization module user's guide," 2018.

[20] A. Neofytou, "Topology optimization for heat flow manipulation," *Master of Science thesis*, 2016.

[21] E. Ruberto, "An adjoint based topology optimization for flows including heat transfer," *Tesi di laurea Magistrale*, 2017.

[22] N. ¸SENOL, "Development of computational fluid dynamics (cfd) based topology optimization codes in openfoam," *A thesis submitted to the graduate school of natural and applied sciences of Middle East Technical University*, 2019.

[23] P. Bajpai, "Modelling and analysis of inert gas bubbles in molten salt fast reactor," *Nuclear Science and Engineering*, 2018.